

Asphaltene deposition simulation in porous media during CO₂ injection using
Lattice Boltzmann Method

by
© Navid Eskandari

A Thesis Submitted to the
School of Graduate Studies
in partial fulfillment of the requirements for the degree of

Master of Engineering

Department of Engineering and Applied Science
Memorial University of Newfoundland

May 2020
St. John's, Newfoundland and Labrador, Canada

Abstract

Carbon dioxide (CO₂) injection in oil reservoirs is a potential means of Enhanced Oil Recovery (EOR) and reducing greenhouse gas. Change in the thermodynamic condition and composition due to the CO₂ injection process may trigger the asphaltene precipitation and deposition which directly affects the efficiency of the EOR process. Predicting the possibility of the asphaltene issue under different operating conditions can help the oil industry for better process design, handle the potential operational problems and estimate the production cost. In spite of, the existence of different modeling approaches based on conventional numerical methods, the lack of a flexible and more comprehensive modeling approach is inevitable. The new and advanced numerical method, called the Lattice Boltzmann Method (LBM) covers the limitations of the conventional numerical methods in dealing with complex boundary conditions and incorporating the microscopic interactions. This study is aiming at the modeling of the Asphaltene deposition, and it's effect on the fluid flow in porous media during an immiscible injection of CO₂ with applying the LBM as the main simulator engine that gets fed by the given phase behavior to take the asphaltene deposition into account as well. Porosity and CO₂ injection velocity are the changing factors in this study. Applying the same condition on two mediums, it has been seen that the recovery factor is 22.5% higher and deposited asphaltene is 2.56% lower in a more porous medium that is attributed to uniform pore size distribution and higher absolute permeability of the more porous case. Furthermore, the fingering phenomena seem to be high in a less porous medium which causes an early breakthrough. Studies on the CO₂ injection velocity effect showed that by increasing CO₂ injection velocity by 2 times and 3 times, the recovery factor increases 4% and decreases 6%, respectively. A decrease in recovery factor is attributed to the asphaltene deposition at which the deposited asphaltene is two times higher at injection velocity of $3 \frac{cm}{h}$ in compare to injection velocity of $2 \frac{cm}{h}$. Furthermore, it is seen that the asphaltene deposition is highly potential in the near-surface area of the grain domain due to the higher number of the flash calculations in that area, particularly when the injection velocity increases.

Acknowledgments

I would like to express my deepest gratitude to Dr. Greg Naterer and Dr. Faisal Khan for their great help and supports in the way of graduation.

I would also like to thank my brother, Dr. Saeid Eskandari, who was always there for me under all circumstances.

Special appreciation is given to the Equinor, Natural Sciences and Engineering Research Council of Canada (NSERC), the School of Graduate Studies and Memorial University of Newfoundland for providing financial support throughout my master's program

Last but not least, I would like to deeply thank my parents and my beautiful wife Nazila for their unconditional support and love, Specially my wife, for her endless patience and understanding of my absence.

Table of Contents

Abstract	ii
Acknowledgments	iii
List of Tables	vi
List of Figures.....	vi
Chapter 1: Introduction	1
1.1. Research Motivation	1
1.2. Objectives	1
1.3. Thesis Structure	2
Chapter 2: Comprehensive Review of COA Systems	3
2.1. Introduction	3
2.2. Multiphase flow properties of COA systems	6
2.2.1. Chemical Structure	6
2.2.2 Density	7
2.2.3. Molecular Weight	8
2.2.4. Viscosity	9
2.2.5. Solubility Parameter	10
2.3. Asphaltene phenomena during CO ₂ injection in porous media	11
2.3.1 Important factors in asphaltene precipitation	13
2.3.2 Asphaltene Precipitation Mechanisms	15
2.3.3. Formation Damage Caused by Asphaltene phenomena	16
2.3.4. Asphaltene Deposition Mechanisms	18
2.4. Modeling studies on the multiphase flow of COA systems in porous media.....	20
2.4.1. Model's Assumptions	20
2.4.2. Mathematical Solvers	21
2.4.3. Asphaltene Precipitation Models	23
2.4.4. Asphaltene Deposition Models	35
2.4.5. Porosity and Absolute Permeability Reduction Models.....	36
2.4.6. Review on the Modelling Studies of COA systems	37
Chapter 3: Methodology	48
3.1. General Assumptions.....	48
3.2. Simulation Modules.....	49

3.2.1. Porous Medium Generator.....	50
3.2.2. Fluid Characterization.....	54
3.2.3. Lattice Boltzmann Method Module.....	55
3.2.4. Thermodynamic Module	60
3.2.5. Deposition Module	62
Chapter 4: Results and Discussions	64
4.1. Changing Factors	64
4.2. Asphaltene deposition.....	65
4.2.1. Porous medium properties effect	65
4.2.2. CO ₂ Injection Velocity Effect.....	67
4.3. Recovery Factor	69
4.3.1. Porous medium properties effect	69
4.3.2. CO ₂ Injection Velocity Effect.....	70
4.4. Relative Permeability Reduction	72
4.4.1. Porous medium properties effect	72
4.4.2. CO ₂ Injection Velocity Effect.....	73
Chapter 5: Conclusion	75
References	77

List of Tables

Table 2- 1: Typical elemental composition for heavy crude oils [17]	7
Table 2- 2: Oil Classification based on density and API gravity [20]	7
Table 2- 3: Overview of the modeling studies on CAO systems categorized by different factors effect	14
Table 2- 4: Comparison of different scales of simulation.....	21
Table 2- 5: Comparison of the simulators.....	39
Table 2- 6: Summary of modeling studies on COA systems.....	46
Table 3- 1: Case 1 Properties	52
Table 3- 2: Case 2 properties	53
Table 3- 3: Assumed oil phase composition	55
Table 3- 4: Assumed oil properties	55
Table 3- 5: Model properties.....	58
Table 4- 1: Changing factors and studied responses.....	64
Table 4- 2: Designated level for the injection velocity	64

List of Figures

Figure 2- 1: Asphaltene chemical structure: “Island” (A),”Archipelago” (B) [19].	6
--	---

Figure 2- 2: Schematic of asphaltene precipitation/aggregation process during CO ₂ injection.....	12
Figure 2- 3: Permeability reduction due to asphaltene deposition during CO ₂ injection	17
Figure 2- 4: Comparison of the permeability reduction and asphaltene deposition amount of miscible and immiscible CO ₂ injection.	18
Figure 2- 5: Surface adsorption and mechanical plugging mechanisms: a) adsorption, b) pore-throat bridging, c) internal cake-formation, d) external- cake formation.....	20
Figure 2- 6: The modeling procedure of COA system.....	20
Figure 2- 7: Asphaltene precipitation models	24
Figure 2- 8: Solubility model [10]	25
Figure 2- 9: Contribution terms in SAFT-EOS [137].....	31
Figure 2- 10: Description of contribution terms in SAFT-EOS.....	32
Figure 2- 11: Colloids model [10].....	34
Figure 2- 12: P-X diagram of the asphaltene deposition during CO ₂ injection [85].....	42
Figure 2- 13: Deposition profile from a micromodel experiment (left), LBM (right): white points are obstacles, dark points are deposited asphaltene [92]	43
Figure 2- 14: Pore structure (38% porosity): a) ideal sphere pack, b) simplified structure [39]	43
Figure 2- 15: Relative permeability curves of oil (k_{rw}) and CO ₂ (k_{rnw}) under different: capillary number (Top), pore structure (Bottom) (1: simple, 2: ideal sphere pack) [39].....	44
Figure 2- 16: The comparison between the relative permeability obtained from LBM and experimental study [39]	45

Figure 2- 17: The 3D pore structure of medium used in LBM modeling [105]	45
Figure 2- 18: Distribution of CO ₂ in oil using LBM: near miscible condition (left), miscible condition (right) [105].....	46
Figure 3- 1: Simulator engine	50
Figure 3- 2: Generated pattern and for case 1 (53% porosity).....	51
Figure 3- 3: Pore Size Distribution (PSD) for case 1 (53% porosity).....	52
Figure 3- 4: Generated pattern and for case 2, 28% porosity	53
Figure 3- 5: Pore Size Distribution (PSD) for case 2 (28% porosity).....	53
Figure 3- 6: Selected ROI for case 2.....	54
Figure 3- 7: Selected ROI's gridding.....	54
Figure 3- 8: The D2Q9 lattice structure	57
Figure 3- 9: Lattice Boltzmann Method procedure.....	59
Figure 3- 10: The stability analysis procedure for each timestep	62
Figure 4- 1: Deposited Asphaltene in case 1(porosity=53%) and case 2 (porosity=28%), both at the same injection velocity.....	66
Figure 4- 2: Asphaltene deposition at 3 cm/h injection velocity and 1 IPA, case 1 (Top), ROI in case 2 (bottom), (blue is deposited asphaltene)	66
Figure 4- 3: CO ₂ velocity profile at 3 cm/h injection velocity an 1 IPA. Case 1 (top), ROI of case 2 (bottom).....	67

Figure 4- 4: Deposited asphaltene of different injection velocities at different IPA	68
Figure 4- 5: Differential pressure from inlet and outlet at each IPA for different injection velocities...	69
Figure 4- 6: Oil recovery of case 1 and 2 at injection velocity of 3 cm/h.....	70
Figure 4- 7: Effect of injection velocity on oil recovery.....	71
Figure 4- 8: Particles vectors distribution before breakthrough (top) and after breakthrough (bottom) for ROI.....	72
Figure 4- 9: Oil relative permeability using Yiotis's model for case 1 and case 2.....	73
Figure 4- 10: Oil relative permeability using Yiotis's model for different injection velocities	74
Figure 4- 11: Oil Saturation for different injection velocities	74

Chapter 1: Introduction

1.1. Research Motivation

Asphaltene is the heaviest, most aromatic and polar fraction of the oil with a complex structure known as the most troublesome component of crude oil, Asphaltene precipitation and deposition on the surfaces of reservoir rock pores, near-wellbore area, and whole pipelines and surface facilities are inevitable issues that fall in to place during natural pressure depletion and CO₂ injection. Asphaltene causes huge and severe problems both for upstream and downstream areas that can considerably reduce process efficiency. In the upstream zone, the asphaltene phenomena cause porosity and permeability reduction, wettability alteration and oil viscosity reduction. Subsequently, the crude oil rheology changes. On the other hand, the downstream equipment including pipelines, heat exchangers, separators and storage tanks are affected by the presence of asphaltene, which reduces the well deliverability and makes the flow thicken and more intricate. Therefore, a mathematical predictive tool that can evaluate “When” and “How” does the asphaltene phenomena becomes a serious problem is required.

In this research, instead of conventional numerical methods, a Lattice Boltzmann Method (LBM) which can handle heterogeneous porous medium with complex boundaries is used. Due to the parallelable skills of LBM, different modules for the main simulator engine are defined which increased the possibility of the model convergence.

1.2. Objectives

In this study, it is aimed to develop a mathematical model to simulate asphaltene deposition in porous media during immiscible CO₂ injection using LBM.

The followings are the main objectives of this study:

- Provide a comprehensive understanding of CO₂/Oil/Asphaltene (COA) systems in porous media
- Model a fluid flow through porous media using LBM
- Assess the effect of asphaltene deposition on the permeability reduction

- Assess the effect of CO₂ injection velocity on the asphaltene deposition, relative permeability reduction, and the recovery factor
- Assess the effect of porous medium properties (porosity and pore size distribution) on the asphaltene deposition, relative permeability and recovery factor
- Assess the parallelable property of the LBM and it's the capability in handling the complex physics

1.3. Thesis Structure

This study includes five chapters:

- Chapter 1 provides an overview of the topic along with research motivations and objectives
- Chapter 2 provides a comprehensive review of COA systems including COA flow properties, asphaltene phenomena during CO₂ injection, multiphase flow characterization of COA systems, experimental studies on COA system and modeling studies on COA systems
- Chapter 3 presents a methodology of this study which includes pattern generator and properties, fluid properties, LBM module, thermodynamic module and the deposition module
- Chapter 4 provides the results of this study by considering the CO₂ injection velocity and porous medium properties as changing factors and their effect on asphaltene deposition, permeability variation and the recovery factor
- Chapter 5 provides a brief review on the important conclusions of the thesis

After the mentioned chapters, the references are provided.

Chapter 2: Comprehensive

Review of COA Systems

2.1. Introduction

There are three main steps in the oil industry; production, processing, and transportation. At each step, asphaltene deposition is a major concern. Thus, understanding the asphaltene and its behavior under different thermodynamic and physical conditions help the oil industry to avoid the considerable cost associated with this issue due to production loss and remediation methods.

Asphaltene is the heaviest and the most polarizable fraction of the oil which can cause severe problems when it becomes unstable. The instability of the asphaltene is referred to the different processes such as natural pressure depletion, solvent injection and gas injection but the asphaltene issue becomes more destructive and considerable during CO₂ injection process [1,17].

Depending on the Minimum Miscibility Pressure (MMP) and CO₂ injection pressure values, the CO₂ flooding process can be categorized into two miscible and immiscible CO₂ injections. When the CO₂ injection pressure is less than the MMP, the injection is called immiscible which is mostly applicable to the heavy crude oils. On the other hand, When the CO₂ injection pressure is more than the MMP value, the injection is called miscible which is more efficient and applicable for light and medium crude oils. In miscible CO₂ injection, when CO₂ contacts the oil, a complete dissolution of CO₂ in oil takes place that leads to oil composition change, oil swelling, oil viscosity reduction, and oil density increase. Consequently, the mutual dissolution process causes light hydrocarbon vaporization from oil and forms CO₂-rich and CO₂-lean phases. As a result, the solubility parameter of the oil's heavy components changes which leads to asphaltene instability and finally asphaltene-phase formation. On the other hand, in the immiscible scenario when the CO₂ contacts the oil, viscosity reduction, oil swelling, and the interfacial tension reduction happen which lower the drag forces in the medium and push the residual oil towards the producing well. In contrary to the miscible process, the mass transfer is negligible in this

process, instead, the viscous forces and capillary pressure are dominant. In the immiscible process, the high capillary pressure and variations in the thermodynamic condition of the system cause a reduction in the solubility parameter of the asphaltene in oil which ends with asphaltene precipitation and deposition [4-6].

Upstream and downstream zones can be affected by the asphaltene problem. Plugging pipelines for downstream and permeability impairment, wettability alteration, oil viscosity reduction and water-in-oil emulsion formation for upstream are technical problems caused by asphaltene deposition [55]. Asphaltene deposition and its remediation strategies in flowlines are widely studied both experimentally and using modeling approaches [55]. Unlike the pipelines, for a reservoir, although there is a number of investigations about asphaltene deposition, the problem is much less sensible due to a lack of reliable experimental approaches and modeling techniques with too many adjustable parameters that lower the credibility [93].

Experimental studies on CO₂/Oil/Asphaltene (COA) systems can be categorized into two sub-groups of precipitation experiment and deposition experiment. Precipitation experiment deals with assessing the effect of temperature, pressure, and precipitant (CO₂) concentration on precipitation step [51,94-96]. Deposition experiments for pipelines are usually conducted using capillary tubes or Taylor-Couette cells. On the other hand, for porous media, microfluidics devices, and core-flooding experiments are utilized. Deposition experiments evaluate the damage formation caused by the asphaltene deposition [40,43,48,59,82,99,101-105]. In addition to these two major types of experiments, there are some studies based on devices such as FTIR, NMR, SDS,.. which analyze and compare the chemical structure and morphology of the asphaltene induced by miscible CO₂ injection, immiscible CO₂ injection and n-alkane addition [83,85,108].

The modeling investigations on the COA system in porous media are classified into two groups of studies based on advanced software (Eclipse, CMG, ..) [70,100,106,142] or developed computer programs [44,69,99,101,107]. The literature review of modeling approaches for the COA system in porous media indicates that the model's structure is build up from three main steps. The first step is selecting a mathematical solver to solve the fluid transport equation to find the velocity and density profiles of the system. Mathematical solvers include continuum approaches such as Finite Element Method (FEM), Finite Volume Method (FVM) and Finite Difference Method (FDM) and probabilistic methods such as Lattice Boltzmann Method (LBM). COA system is a complicated system due to three reasons: Firstly, the occurrence of phenomena such as asphaltene precipitation and deposition, interphase

diffusion/solution, swelling, coalescence and gas phase dissolution; Secondly, the intricacy of pore structures, which leads to complex boundary conditions; Finally, the evolution of porous media during operation [7-9] so accurate and stable solver due to a long time of simulation is required. The bold advantage of LBM over conventional numerical methods is its capability in dealing with complicated boundary conditions. The second step is introducing the asphaltene precipitation model to find the phase behavior and evaluate the thermodynamic aspect of the COA system. Asphaltene precipitation models are divided into two capital groups of Colloidal and Solubility models. The colloidal approach is originated in collide theory and considers the asphaltene as a suspended solid particle which is stabilized with the aid of resins. Colloidal models consider the asphaltene precipitation as an irreversible process. On the other hand, the solubility model is based on considering the system in a real solution mode. When the solubility comes under a threshold value, the asphaltene precipitation happens either in Solid-Liquid Equilibrium (SLE) state or in Liquid-Liquid Equilibrium (LLE) condition. The solubility model is divided into two subdivisions of solution theory and equation of state (EOS) models. Solution theory models are based on Regular solution theory, Flory-Huggins theory, and Scott Magat theory. On the other hand, the EOS models involve the Solid model, Cubic Equation Of State (CEOS), Perturbed Chain Association Fluid Theory Equation Of State (PCSAFT-EOS) and Cubic Plus Association Equation Of State (CPA-EOS). Studies show that CPA-EOS, PCSAFT-EOS, and Peng-Robinson Equation Of State (PR-EOS) are the best candidates for presenting the precipitation step in COA systems [44,69,99,101,107]. The third step is dealing with the deposition stage. Technically there are five mechanisms for asphaltene deposition in porous media which are adsorption, surface deposition, entrainment, pore-throat plugging, and pore-throat opening. Depending on the number of considered deposition mechanisms in a model, the number of adjustable parameters varies. Models developed by Nghiem [129], Leontaritis [55], Kord et al [37], Behbahani [83] and Ali and Islam [71] have 3,4,6,10 and 16 adjustable parameters respectively. But the well-known model with a reasonable number of adjustable parameters is Deep Bed Filtration (DBF) model which is introduced by Wang and Civan [90].

Assessing the risk of asphaltene precipitation in a way whether it is a real problem or not can be made by advanced models that can treat the complex fluid dynamics like the one that occurs in a real porous medium. In this research, the Lattice Boltzmann Method (LBM) is utilized to find the effect of pore properties and CO₂ injection velocity on the fluid flow and formation damage due to asphaltene deposition during the immiscible CO₂ injection process.

2.2. Multiphase flow properties of COA systems

2.2.1. Chemical Structure

Crude oil components are divided into two groups: C_6- and C_{6+} . C_6- group consists of light hydrocarbons with an atom number less than six, which are straight-chain normal alkanes (n-alkanes) and their branched isomers (i-alkanes). The C_{6+} group can be subdivided into four main constituents, which are saturates, aromatics, resins and asphaltene (known as SARA components). The chemical structure of saturates is mainly formed of nonpolar hydrocarbons along with aliphatic cyclic paraffins. Aromatic rings connected to aliphatic chains make the Aromatics chemical formation [16]. Between these four heavy components of crude oil, resins have the second heaviest molecular weight. The shape of the resins range from heavy liquids to sticky solids and are formed by polar polycyclic aromatic rings which make the resin relatively volatile and soluble in oil [16,17]. Finally, the heaviest component of the crude oil, Asphaltene, is a dark black substance which is non-volatile and soluble in aromatic solvents but insoluble in light n-alkanes solvents [18]. Many researchers have noticed the structural complexity of asphaltene. Generally, its basic structure is formed by carbon, hydrogen, oxygen, nitrogen, sulfur and small amounts of metals. Table 2-1 represents the typical elemental composition for heavy crude oils [17]. Different ways of linking these atoms in asphaltene lead to the presence of various heteroatom functional groups such as amine, amide, pyridine, pyrrole, phenol, carboxyl, ketone, benzothiophene, thiophene and porphyrin groups. Several chemical structure models such as Island, Archipelago, Continental, Mullins-Yen, etc. have been proposed for asphaltene [2]. The two well-known asphaltene structures are Island and Archipelago which are presented in Figure 2-1.

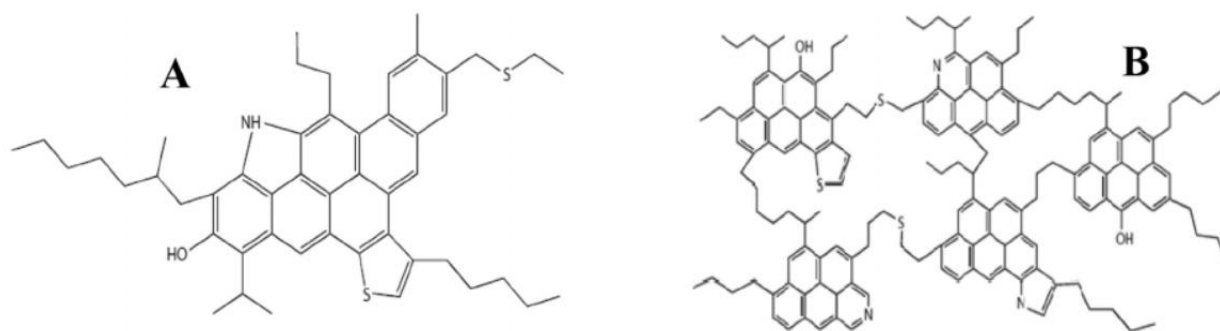


Figure 2- 1: Asphaltene chemical structure: “Island” (A),”Archipelago” (B) [19].

Table 2- 1: Typical elemental composition for heavy crude oils [17]

Fraction	Weight (%)	Carbon	Hydrogen	Nitrogen	Oxygen	Sulfur
Asphaltene	14.1	83.8	7.5	1.3	1.7	4.8
Resin	37.3	82.8	8.9	1.5	2.0	4.3
Aromatic	37.2	84.3	10.0	< 0.3	1.1	4.0
Saturates	11.4	86.6	13.0	< 0.3	< 0.2	< 0.1

2.2.2 Density

It is proven that, the heavier the crude oil, the more asphaltene content in the sample. Heavier oil is less prone to asphaltene precipitation due to the higher solubility parameter of the asphaltene in heavy oils. On the other hand, despite the low content of asphaltene in light and medium oils, they are the best candidates for asphaltene issues [15]. Using Oil density and API gravity, crude oil can be categorized into four different groups as presented in Table 2-2 [20].

Table 2- 2: Oil Classification based on density and API gravity [20]

Oil	Density ($\frac{Kg}{m^3}$)	API Gravity ($^{\circ}$)
Light	$\rho_o < 870$	$API > 31.1$
Medium	$870 < \rho_o < 920$	$22.3 < API < 31.1$
Heavy	$920 < \rho_o < 1000$	$10 < API < 22.3$
Extra Heavy	$\rho_o > 1000$	$API < 10$

In addition to the oil density, the asphaltene density is a key parameter for evaluating the asphaltene nature. It is proven that the direct measurement of asphaltene density is infeasible, so the only technique is calculating the asphaltene density in solution. Yarranton and Masliyah [21] used an Anton Paar device to measure the asphaltene density experimentally. Barrera et al [22], measured asphaltene density in toluene by varying the solution ratio and dividing the asphaltene into light (soluble) and heavy (insoluble) cuts. Regular and excess volume mixing rules are utilized. In regular mixing rule, the density of the mixture of asphaltene and toluene can be calculated using the following equation:

$$\frac{1}{\rho_{mix}} = \frac{w_A}{\rho_A} + \frac{w_T}{\rho_T} \quad (1)$$

Where ρ_{mix} , ρ_A , ρ_T , w_A and w_T are mixture density, asphaltene density, toluene density, the mass fraction of the asphaltene and mass fraction of the toluene respectively. Now plotting $\frac{1}{\rho_{mix}}$ versus w_A , the asphaltene density can be evaluated using the slope and intercept of the plot as follows:

$$\rho_A = \frac{1}{\text{Slope} + \text{Intercept}} \quad (2)$$

The results for the density of the lightest and heaviest cuts of asphaltene using regular mixing rule were 1078.4 and 1189.6 ($\frac{Kg}{m^3}$), respectively. On the other hand, Barrera et al used a different approach, the so-called excess volume mixing rule by considering the binary interaction term for density calculation:

$$\frac{1}{\rho_{mix}} = \frac{w_A}{\rho_A} + \frac{w_T}{\rho_T} - w_A w_T \left(\frac{1}{\rho_A} + \frac{1}{\rho_T} \right) \beta_{12} \quad (3)$$

Where β_{12} is the asphaltene and solvent binary interaction parameter which is assumed 0.015 for the calculation. The results of lightest and heaviest cuts of asphaltene using excess volume mixing rule were 1044.1 and 1150.4 ($\frac{Kg}{m^3}$), respectively. A difference of approximately 3% is detected between the results of regular and excess volume mixing rule. They concluded that the lower the asphaltene mass fraction in the solution, the lesser the difference between two mixing rule approaches [22]. There were some studies based on molecular dynamics simulation conducted by Diallo et al [13] and Rogel and Carbognani [14] which found that the asphaltene density correlates well with the H/C ratio of asphaltene. Rogeland and Carbognani developed the equation for this relationship as follows:

$$\rho_A = 1.3447 \frac{H}{C} - 0.5396 \quad (4)$$

2.2.3. Molecular Weight

Crude oil is a mixture of various hydrocarbons and chemical compounds with different molecular weights. Each compound or hydrocarbon plays a role in the mixture's molecular weight based on their fraction. There are three well-known methods of determining the oil molecular weight of a mixture which is a mole, mass, and ln averaging [23].

The largest molecular weight between the crude oil components belongs to the asphaltene. The fraction of asphaltene varies from one crude oil to another. Several experiments have been performed to find the molecular weight, but no limited range is reported. This instability in results comes from two causes, asphaltene polydispersity in composition and the different aggregation degree of asphaltene. Unlike the other oil components, asphaltenes have an affinity to aggregate because of pressure, temperature and oil composition variation. Furthermore, the degree of aggregation depends on the type of utilized solvent for characterization [18]. Early research by Waller et al. showed a range of 500-1200 g/mole for asphaltene molecular weight. Speight and Plancher et al. utilized polar solvents for asphaltene dissolution to find

the asphaltene molecular weight using vapor pressure osmometry with results showing a value around $2000 \frac{g}{mol}$ [16]. The same procedure with odichlorobenzene solvent is used by Wiehe et al. Results were considerably different and showed 500 and $4000 \frac{g}{mol}$. Mullins et al. used mass spectral techniques and determined the molecular weight of 750 gr/mole [24]. Yarranton used VPO and SAXS techniques and reported 850 g/mole and 8000 gr/mole, respectively [1].

2.2.4. Viscosity

Oil viscosity directly impacts the recovery and productivity of the reservoir, since it is a controller parameter of the oil's rheology and mobility [25]. Oil viscosity is a function of oil composition, temperature, dissolved gas, and pressure. The lesser the API gravity, the higher the oil viscosity due to the higher density. As pressure declines, the oil viscosity decreases and reaches a minimum at the bubble point pressure. A further decline in pressure leads to an increase in the oil viscosity due to gas liberation and oil shrinkage. Increase in temperature decreases the oil viscosity and eases fluid flow. Heavy oils have viscosities ranging from a couple of hundred to tens of millions of centipoises under store conditions [16]. Thus, as the viscosity of crude oil increases, the need for employing external forces, heat or diluents for moving the fluid from pores toward wellbore and pipelines increases.

There is a bold difference between the dead oil and live oil which is the presence of dissolved gas in live oils. This distinction is a starting point to divide the oil viscosity correlations into three groups of below bubble point, at bubble point and above bubble point oil viscosity models.

Ikiensikimama and Ogboja [26] assessed the most well-known viscosity correlations published before 2009. The evaluation encompassed the models of dead oil viscosity, viscosity at the bubble point and unsaturated oil viscosities. This comparison has been made on the data obtained from Niger Delta crude. They used different statistical parameters such as percent mean absolute relative error which indicates the percent of absolute relative deviation from experimental data as follows:

$$E_a = \frac{1}{n} \sum_{i=1}^n |E_i| \quad (5)$$

$$E_i = \left(\frac{X_{exp} - X_{pred}}{X_{exp}} \right) \times 100 \quad (6)$$

Where E_a , E_i , X_{exp} , X_{pred} and n is the percent of absolute relative deviation from experimental data, relative deviation of predicted value from experimental data, experimental value, predicted value and number of data, respectively. Results of this comparison study revealed that:

- Beal's [27] correlation ($E_a=6.7291$) is the best for unsaturated oil viscosity

- Beggs and Robinson's [28] ($E_a=24.4174$) correlation is the best for bubble point oil viscosity
- Labedi's correlation [29] ($E_a=31.2628$) is the best for dead oil viscosity

When asphaltene precipitation takes place, the viscosity of the oil increases, on the other hand when asphaltene deposition happens, the asphaltene particles completely separate from the oil which makes the oil lighter and a viscosity reduction happens. Generally, in the asphaltene-contained system the viscosity change can be modeled using two following equations [30]:

- ✓ Generalized Einstein Model:

$$\frac{\mu}{\mu_0} = 1 + aC_p \quad (7)$$

- ✓ Krieger and Dougherty Model:

$$\frac{\mu}{\mu_0} = \left(1 - C_p \frac{C_p}{C_{p0}}\right)^{-\xi C_{p0}} \quad (8)$$

Where μ =oil viscosity after precipitation, μ_0 =initial oil viscosity, $a=2.5$ (default value), C_p = Volume concentration of precipitate, C_{p0} =volume concentration for maximum packing (0.65 for spheres packing), ξ =intrinsic viscosity (2.5 for spherical colloids).

2.2.5. Solubility Parameter

Solubility parameter can be easily defined as a degree of solubility which at first applied for liquid state substances and originated in the findings of Hildebrand et al [31]. This parameter acts as an indicator of the molecular interaction to evaluate the cohesive and adhesive properties of materials. Liquid solubility parameter can be calculated easily using vaporization energy and liquid molar volume and expresses the amount of required energy to evaporate one unit of liquid volume as follow:

$$\delta = \left(\frac{\Delta E}{V}\right)_T^{0.5} \quad (9)$$

Where $\frac{\Delta E}{V}$ defined as a cohesive energy density. Further works of Hildebrand et al. led to important result for nonpolar liquids, where the equality of internal pressure and cohesive energy density is suggested, which made the calculations of the solubility parameter of liquids and gases easy with the aid of Equation Of State (EOS) models [32,33]:

$$\delta^2 = \left(\frac{\Delta E}{V}\right)_T \approx \left(\frac{\partial E}{\partial V}\right)_T = T \left(\frac{\partial P}{\partial T}\right)_V - P \quad (10)$$

Where $\frac{\partial E}{\partial V}$ is internal pressure, and pressure profile can be studied by different EOS's [34].

It has been reported that the solubility parameter of crude oils encompasses the range of 16 to 21 MPa^{0.5}. Nowadays, the applicability range of the solubility parameter is extended to supercritical fluids like CO₂ and solids such as asphaltene. For supercritical fluids, the concept of “internal energy isothermally expanded to zero pressure” is used instead of vaporization energy. The Allada equations at different thermodynamic conditions are the best reference for CO₂ solubility parameter estimation [35]. As mentioned above, the base and reference concept of the solubility parameter belongs to liquids; therefore, calculating the solubility parameter of solids is not straightforward and needs to consider the substance as a hypothetical liquid at which it is cooled below its melting point. Due to the complexity of the asphaltene solubility parameter calculations, different techniques such as Heithaus titration, dilution experiments, molecular modeling, and IR-NIR analysis are developed. Different studies showed the range of 19 to 21 MPa^{0.5} for the asphaltene solubility parameter and it has been proven that the origin of asphaltene either coal, petroleum or shale does not have a considerable effect on solubility parameter value [34]. The temperature effect on the solubility parameter of the asphaltene has been detected by Hirschberg et al [36]. It has been reported that by increasing the temperature, the solubility of oil decreases that in turn, the oil can not keep the particles in the suspension. Leontaritis and Mansoori [10] studied the pressure effect on asphaltene solubility parameter and reached to the statement that the pressure keeps the dissolved gas and light hydrocarbons in the solution, moreover keep the temperature constant, so by pressure depletion, the gas expansion happens, and the temperature decreases and asphaltene precipitate.

2.3. Asphaltene phenomena during CO₂ injection in porous media

CO₂ is a greenhouse gas with a molecular weight of 44 g/mole which is solid at low temperatures and pressures and in a gas phase at pressures and temperatures above the critical point (reservoir condition). The last decade in EOR history is mostly devoted to CO₂ injection due to its high efficiency and reduction in emissions of greenhouse gas [37]. The first step in experimental and modeling projects of CO₂ injection is determining the Minimum Miscibility Pressure (MMP). This value indicates the miscibility condition of the CO₂/Oil system, also helps to appoint the CO₂ injection pressure. Based on the MMP value, the CO₂ injection can be categorized into two types of immiscible and miscible injections. When the CO₂ injection pressure is less than the MMP, the injection is called immiscible which is mostly applied for the heavy crude oils. On the other hand, When the CO₂ injection pressure is more than the MMP value, the injection is called miscible which is more efficient and applicable for light and medium

crude oils [5,6,38]. It is proven that to perform the miscible CO₂ injection, the depth of the reservoir and the oil API gravity should be greater than 800 m and °27, respectively [38,39].

In the miscible scenario when CO₂ contacts the oil, complete dissolution of CO₂ in oil takes place that leads to oil composition change, oil swelling, oil viscosity reduction and increases in oil density. This miscible injection which is an example of a high mass transfer process causes light hydrocarbons vaporization from the oil and dissolution in CO₂ and forms the CO₂-rich phase, on the other hand, the remained heavier hydrocarbons make the CO₂-lean phase. This mutual dissolution process causes a change in the solubility parameter of the oil heavy components that end with equilibrium disturbance at which a large number of CO₂ molecules occupy the surfaces of asphaltene molecules and decreases the asphaltene stabilizer concentration and prevent from micelle formation. As a result, asphaltene instability occurs and the third solid phase which is asphaltene-phase is formed. With time evolution, the asphaltene particles precipitate, aggregate and finally deposit [4-6].

In the immiscible scenario when the CO₂ contacts the oil, viscosity reduction, oil swelling, and the interfacial tension reduction happen which lower the drag forces in the medium and push the residual oil towards the producing well. In contrary to the miscible process, the mass transfer is negligible in this process, instead, the viscous forces and capillary pressure are dominant. In the immiscible process, the high capillary pressure and variations in the thermodynamic condition of the system cause a reduction in the solubility parameter of the asphaltene in oil which ends with asphaltene precipitation and deposition [4,5]. The schematic of the asphaltene precipitation/aggregation process during CO₂ injection is presented in figure 2-2.

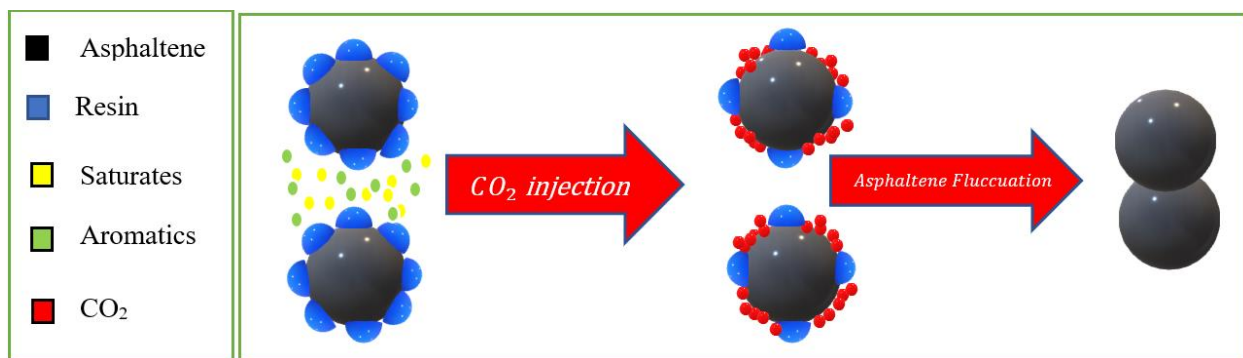


Figure 2- 2: Schematic of asphaltene precipitation/aggregation process during CO₂ injection

Asphaltene phenomena involve three steps which are asphaltene precipitation, flocculation, and deposition. These three steps of asphaltene problems are different but connected concepts. The asphaltene precipitation takes place prior to other phenomena and is defined as a process which little amount of micron size asphaltene particles suspend but not dissolve in a liquid phase and can be shown as a

separated solid phase. Several factors such as temperature, pressure and crude oil composition affect the asphaltene precipitation initiation. In the next step, the asphaltene particles start to aggregate and become bigger particles called flocs with the size of hundred microns which are still in a suspended form. Finally, by increasing the molecular weight of aggregates and flocs, they fall, stick and attach to the different surfaces which are considered as a deposition step. The system starts to get damaged by asphaltene deposition. Asphaltene size, surface type, surface-asphaltene interactions, and flow rate are determinative elements in asphaltene deposition [2,40,41]. Several studies have been published about asphaltene deposition during CO₂ injection. Gholoum et al, [42] compared the severity of the asphaltene deposition during CO₂ injection and n-alkane addition. Results revealed that CO₂ has the lowest asphaltene onset pressure which makes it the most effective precipitant. Another comparison is made by Monger and Fu [42] which states that asphaltene deposition during CO₂ injection is more extensive and less abrupt in comparison with n-alkane addition. Srivastava and Huang [43] named CO₂ concentration and pore topography as the most important factors in asphaltene deposition during CO₂ injection. Gonzalez et al, [44] expressed a different vision on COA system and defined two reverse roles of asphaltene precipitant or inhibitor for CO₂ depending on temperature and pressure.

2.3.1 Important factors in asphaltene precipitation

Asphaltene precipitation is the first step of asphaltene phenomena and it is generally affected by four parameters as follows:

- **Pressure:** At pressures above bubble point, with increasing pressure, the solubility parameter of the asphaltene in oil increases which lead to less asphaltene precipitation, on the other hand, at pressures below the bubble point, with decreasing pressure, the light hydrocarbons are extracted which lead to increase in asphaltene solubility parameter and decrease in asphaltene precipitation. It is proven that, the maximum amount of asphaltene precipitation occurs at and around bubble point pressure [45].
- **Temperature:** There is a number of contradicting statements about temperature effect on asphaltene precipitation. When the experiment temperature is less than reservoir temperature, increasing temperature leads to an increase in asphaltene solubility which in turn, asphaltene precipitation decreases. On the other hand, at temperatures above reservoir temperature, asphaltene solubility parameter decreases with an increase in temperature [46-49]. It is also stated that, at higher temperatures, the oil viscosity decreases which leads to higher diffusivity of asphaltene particles and faster aggregation, also the light hydrocarbons come out of the solution

and make the oil poor solvent for the asphaltene. It is noted that the temperature effect on asphaltene precipitation of light oils is more severe than heavy crudes and at the earlier stages of the precipitation, the viscosity variation is more important than solubility changes [50]. So, when considering the temperature effect, a number of side elements should be considered to make a final statement.

- **Oil Composition:** This factor involves several subfactors such as the amount of dissolved gas, asphaltene content, resin content, saturates content and aromatic content. With increasing the amount of dissolved gas in oil, the asphaltene solubility parameter decreases which leads to more asphaltene precipitation. In fact, the higher the GOR, the higher the asphaltene precipitation. Additionally, with an increase in the ratio of $\frac{\text{Asphaltene content}}{\text{Resin content}}$, the number of peptizing agents decreases that ends with asphaltene instability and precipitation [45]. Furthermore, the asphaltene is stable in oil if it contains high hydrogen content and low aromaticity. Oil composition may experience changes due to CO₂ injection at which the light hydrocarbons extract from the oil and cause a decrease in asphaltene solubility.
- **CO₂ Concentration:** In CO₂ flooding systems, the mass fraction of CO₂ is one of the substantial elements at which when the CO₂ concentration increases and reaches the critical value, a large number of small molecular size CO₂ reside at the asphaltene surface (presented at figure 2-2). In this case the concentration of resins decreases which leads to asphaltene instability and precipitation [6,51].

Besides these factors, Zekri et al [52] conducted an experiment on heavy oils and considered flow rate as another key factor in asphaltene phenomena. They showed that by reducing the flow rate, the formation damage caused by asphaltene may decrease. Table 2-3 presents a summary of studies on COA systems categorized by different factors.

Table 2- 3: Overview of the modeling studies on CAO systems categorized by different factors effect

Factor	Modeling Studies	Highlights of studies
Temperature effect	Gonzalez et al ⁴⁴ , Zendeboudi et al ⁴⁰ , Zanganeh et al ⁹⁶	<ul style="list-style-type: none"> • Light oils: increase in T leads to an increase in AP • Heavy oils: increase in T leads to a decrease in AP • Increase in T leads to a decrease in AOP • When T increases, P_{BBP} and P_{onset} increases slightly • When T increases, P_{BBP}, P_{MMP}, P_{FCM} increase drastically • When P_{injection} > P_{MMP}, the higher T, leads to higher RF • To avoid asphaltene precipitation, Secure temperature range: 50°C < T < 100°C
Pressure effect	Sanchez & Repsol ⁷⁰ , Gonzalez et al ⁴⁴ , Lei et al ¹⁰⁷ ,	<ul style="list-style-type: none"> • Highest asphaltene deposition occurs at pressures near and above P_b

	Al-Qasim ¹⁰⁰ , Zendejboudi et al ⁴⁰ , Khamehchi et al ⁹⁹ , Zanganeh et al ⁹⁶	<ul style="list-style-type: none"> • At $P > P_b$, increasing pressure leads to a decrease in asphaltene deposition • At $P < P_b$, the effect of pressure is not significant • the oil recovery and permeability reduction increases with an increase in injection pressure which is attributed to the CO_2 viscosity and solubility enhancement, reduction in the equilibrium IFT of the light oil-CO_2 system and asphaltene deposition • $P_{BBP} < P_{onset} < P_{extraction} < P_{MMP} < P_{FCM}$ • At $P < MMP$, the immiscible CO_2 flooding happens and the main reason for permeability reduction is gas trapping in the pores • At $P > MMP$, the miscible CO_2 flooding happens and the main reason for permeability reduction is asphaltene precipitation and deposition • asphaltene precipitation at lower pressures are reversible • asphaltene precipitation at higher pressures are immediate, more severe and irreversible
CO ₂ concentration effect	Vafaei & Dehghani ¹⁰¹ , Gonzalez et al ⁴⁴ , Lei et al ¹⁰⁷ , Zendejboudi et al ⁴⁰ , Zanganeh et al ⁹⁶ , Nasrabadi et al ⁶⁸	<ul style="list-style-type: none"> • Increasing CO_2 concentration leads to an increase in asphaltene deposition • Light oils ($P > P_b$): increase in CO_2 mole% leads to a decrease in AP • Light oils ($P < P_b$): increase in CO_2 mole% leads to an increase in AP • Heavy oils ($P > P_b$): increase in CO_2 mole% leads to an increase in AP • Heavy oils ($P < P_b$): increase in CO_2 mole% leads to a decrease in AP • To avoid asphaltene precipitation, Secure CO_2 mass fraction: $< 35\%$
CO ₂ injection rate effect	Behbahani et al ⁸³	<ul style="list-style-type: none"> • AP has a straight relationship with CO_2 flow rate, the lower the rate the higher CO_2 solubility and lower AP • Increase in CO_2 injection flow rate leads to an increase in recovery factor, pressure drop and permeability reduction • Mechanical plugging has more contribution in comparison with adsorption to permeability reduction.
Pore topography and rock properties effect	-	<ul style="list-style-type: none"> • Pore topography plays a key role in asphaltene precipitation/deposition • The bigger the grain size, the higher the asphaltene precipitation

2.3.2 Asphaltene Precipitation Mechanisms

In this section, technical aspects and reasons for asphaltene phenomena are elaborated which can be categorized in a sequence as follows [53]:

- **Polydispersity (Solubility) Effect:** A polydisperse oil is stable when the ratio of polar/nonpolar molecules is in balance, so any variation in temperature, pressure and oil composition affects this

equilibrium and destabilizes the oil. The result of the polydispersity effect is Asphaltene-phase formation.

- **Steric Colloidal Effect:** This term is connected to the self-association tendency of asphaltene at which the separated asphaltene particles fluctuate and form collides. These formed steric collides are stable with the aid of peptizing agents on their surface such as resins. Enough resins on the surface of asphaltenes make it stable, but the migration of peptizing agents into the oil phase leads to an increase in surface energy and makes the asphaltene to precipitate.
- **Aggregation Effect:** Concentration of peptizing agents play an important role in this step. Aggregation is a result of a continuous decrease in the peptizing agent concentration that makes the asphaltene to be full of free active sites which leads to irreversible aggregation of asphaltene particles.
- **Electrokinetic Effect:** This term causes a collide deposition which is due to the movement of charged colloidal particles that make an electrical potential difference through the porous media. This difference cause instability in asphaltene micelles and highly depend on the fluid velocity. The electro-kinetic effect is the highest in the near-wellbore regions due to higher fluid velocity in this area [54].

2.3.3. Formation Damage Caused by Asphaltene phenomena

The displacement process in CO₂ injection is determined by the medium properties such as porosity, permeability, and heterogeneity, the fluid properties such as oil composition and viscosity, also the thermodynamic condition of the system such as pressure and temperature. When asphaltene precipitates and deposits as a result of CO₂ injection, both rock, and fluid properties are affected in a way that leads to a decrease in process efficiency and increases in production cost. Leontaritis et al [55] categorized the formation damage caused by asphaltene deposition into four forms:

- Permeability impairment
- Wettability alteration
- Oil viscosity reduction
- Water in oil emulsion formation

Permeability reduction is the dominant form of the formation damage which directly affects the recovery factor. When asphaltene deposits on the rock as a result of CO₂ injection, it plugs the pores and reduce permeability which is visualized in figure 2-3.

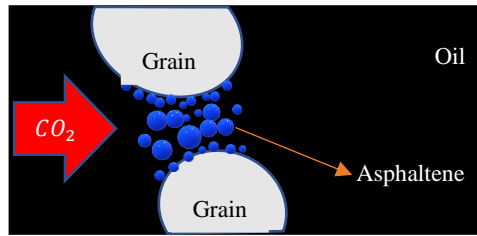


Figure 2- 3: Permeability reduction due to asphaltene deposition during CO₂ injection

In the water-wet pores, the water covers the rock surface and forms a film on it, when asphaltene deposition happens, heavy and positive charge asphaltene particles penetrate through the water film and interact with negative charge mineral particles which in turn, the asphaltene resides at the rock surface and changes the rock wettability. Wettability alteration from water-wet to oil-wet or mixed-wet due to asphaltene adsorption mechanism can affect the capillary pressure, relative permeabilities, irreducible water saturation, residual oil saturation and dispersion [56,57]. After the CO₂ flooding process, the surfaces with asphaltene will be yellow and the surfaces without asphaltene will be colorless. The yellow surface is a representative of oil-wet regions which shows the oil film that did not remove by CO₂ injection [58]. Simply speaking, When the wettability alteration takes place, the oil-grain interaction increases and the oil covers the rock surface which makes it harder to push out of the pore and reduces the sweep efficiency. On the other hand, the wettability alteration can be beneficial for the waterflood or WAG processes as it increases the chance of Solvent-Oil contact and decreases the residual oil saturation [25,59]. Besides, despite the relative permeability reduction, Kamath et al accredited the sweep efficiency enhancement in some cases due to the adsorption process because of the relative permeability curve alteration and flow diverting effects. The positive effects of wettability alteration on CO₂ injection processes are still subject to many kinds of research. It is proven that the residual oil saturation increases with the wettability alteration [54]. The formation of the emulsion is another potential damage caused by asphaltene which directly increases the fluid viscosity and reduces mobility. The severity of the formation damage caused by CO₂ injection is expressed schematically in figure 2-4, which permeability reduction (%) is a ratio of permeability at a desired injection pressure to initial permeability. As can be seen, with increasing CO₂ injection pressure, the permeability reduction and the number of deposited asphaltene increases. The slope of the enhancement for permeability reduction and the amount of deposited asphaltene at pressures above minimum miscibility pressure is much lower than the immiscible case. Near wellbore, regions are more prone and experience sever asphaltene deposition problems than other regions, this formation damage area can be extended over considerable distances from the wellbore in miscible CO₂ injection than immiscible injection [32,60,61].

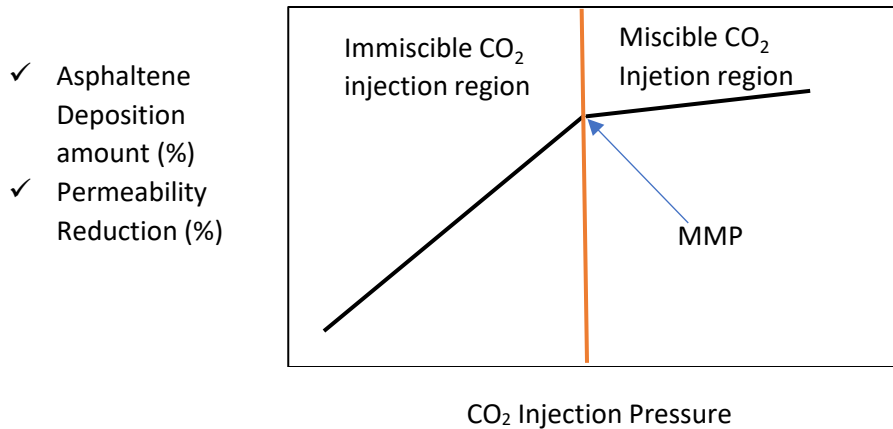


Figure 2- 4: Comparison of the permeability reduction and asphaltene deposition amount of miscible and immiscible CO₂ injection.

2.3.4. Asphaltene Deposition Mechanisms

Considering the COA system, when the asphaltene starts to precipitate and fluctuate, there will be two options for a separated asphaltene solid phase which are:

- Remaining as a suspended solid in oil and being in a flowing stream
- Depositing on the medium

It has been proven that the probability of the first option is low, so most of the precipitated asphaltenes, deposit on the rock surfaces. Permeability impairment and wettability alteration which are two definite consequences of asphaltene deposition, vary for different areas of porous media and depend on “How”, “Where” and “What Amount” of asphaltene are deposited. So studying the different asphaltene deposition mechanisms are inevitable. There are three different deposition mechanisms that are as follows:

- **Surface adsorption:** It is the first stage of the asphaltene deposition which is the dominant factor in wettability alteration and mostly modeled using Langmuir, Freundlich, Temkin, and Dubinin-Redushkevich isotherm models. The interaction between functional groups of asphaltene and surface causes the adsorption occurrence. Dominant forces in surface adsorption of asphaltenes are electrostatic, Van der Waals, charge transfer interactions, repulsion, and hydrogen bonding. The amount of the adsorption varies for different rock types and depend on the contribution values of the mentioned forces, also ions present in the brine is one of the determinant factors at which the more ion valency indicates the more adsorption degree. Besides, the PH and composition of brine in the rock are important parameters in surface adsorption determination. It is proven that shale rocks are more prone to a higher degree of adsorption. Depending on the attractive and

repulsive forces between particles, this deposition mechanism can be monolayer or multilayer. In this mechanism, the total amount of deposited asphaltene is not important, instead, the place where asphaltene surface deposition takes place is a matter of interest. The closer to the pore throat areas, the more severe the permeability reduction is [62-64].

- **Mechanical plugging:** After a surface deposition or sometimes simultaneously, a fraction of fluctuated asphaltene may fall down further and start to plug and block the pore throat and body. This deposition mechanism highly depends on the pore size distribution and asphaltene particle sizes and play the most important role in the permeability reduction. Depending on the mentioned factors, the mechanical plugging process is formed by three sub-processes which are: pore-throat bridging, internal cake formation, and external cake formation. When the asphaltene particle size is larger than pore throat size, the single-particle bridging takes place which can plug whole throat, on the other hand when the asphaltene particle size is smaller than the pore throat size, the particles can pass through the throat and enter to the pore body. Then number of particles may attach and make a bridge and block the throat-body pathway. When the number of formed bridges reaches the critical value, the internal cake formation takes place at which, the new incoming particles start to reside at the immediate pore throat and available pore body. After an internal cake formation step, the asphaltene particles reside at the porous medium inlet and make the external cake formation [64-66]. Each of these mentioned steps is showed schematically in figure 2-5.
- **Mechanical entrainment:** when the high-velocity fluid flows through a medium, the fluid passage may become narrow and the shear rate value may prevail the critical value, in this case the deposits sweep away and entrained by a liquid phase.

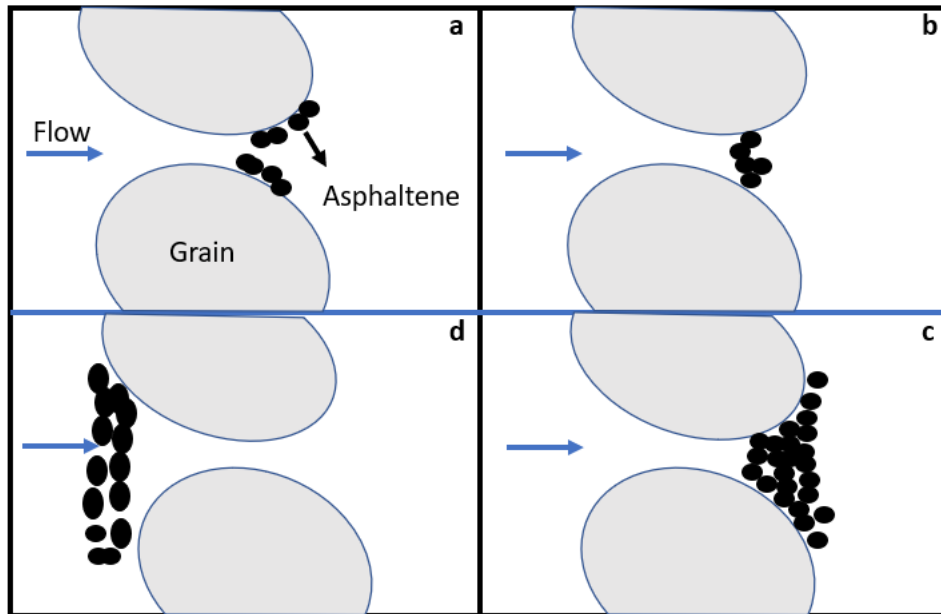


Figure 2- 5: Surface adsorption and mechanical plugging mechanisms: a) adsorption, b) pore-throat bridging, c) internal cake-formation, d) external- cake formation.

2.4. Modeling studies on the multiphase flow of COA systems in porous media

In the case of COA flow through porous media, to build up a model, there are few steps that need to be taken carefully to develop a reliable approach. This procedure is summarized in figure 2-6.

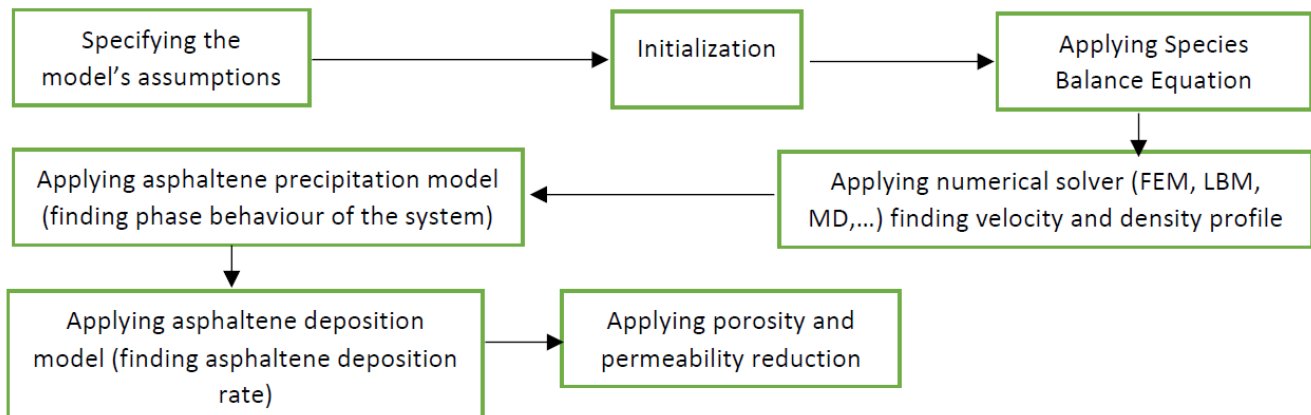


Figure 2- 6: The modeling procedure of COA system

2.4.1. Model's Assumptions

The first step in the mathematical model development is specifying the assumptions and conditions of the system. Specifically, In COA flow through porous media, there are several questions that come in to the mind which should be answered to build the foundation of the model which are:

- What is the dimension of the model? 1D, 2D, 3D?

- What fluids are in porous media? Oil, water, hydrocarbon gas, CO₂?
- What is the type of oil? Black oil, Volatile, Condensate, etc?
- Is CO₂ soluble in oil and water? Is it a miscible flow or an Immiscible flow?
- Is there a water component in the oil or oil component in the water?
- Is the compressibility of medium and fluids considered?
- What is the type of flow? Laminar or turbulent? Is Darcy's law applicable for flow in porous media?
- What forces are considered? Capillary, Gravity, Viscous?
- Are the Fickian diffusion and mechanical dispersion considered?
- Is the flow iso-thermal? or non-isothermal?

2.4.2. Mathematical Solvers

There are three different scales for representing the fluid flow through porous media using modeling and simulation which are: microscopic, mesoscopic and macroscopic scales [109]. A comparison of these different scales is shown in table 2-4.

Table 2- 4: Comparison of different scales of simulation

Scale	Microscale	Mesoscale	Macroscale
Time scale (seconds)	10 ⁻⁹ -10 ⁻⁶	10 ⁻⁶ -10 ⁻³	10 ⁻³ -10 ⁰
Length scale (meters)	10 ⁻¹² -10 ⁻⁹	10 ⁻⁹ -10 ⁻³	10 ⁻³ -10 ⁰
Model type	Particle model	Collection of particles	Continuum Model
Model Basis	Newtonian Mechanics	Kinetic Theory	Conservation laws
Governing Equation	Hamilton's Equation	Boltzmann transport Equation	Navier-Stokes Equation
Equation type	Ordinary differential equation	Partial Differential equation	Partial Differential equation
Simulation method	Monte-Carlo Molecular Dynamics	Lattice Boltzmann Method	Finite Difference Method Finite Element Method Finite Volume Method

In COA systems, solvers apply on the flow transport equation to assess the flow velocity field and density profile. On a microscopic scale, the system is studied by evaluating the particle position and momentum using Molecular Dynamic or Monte-Carlo methods [63,110]. Hamilton's equation is the governing equation in this scale. The macroscopic scale is based on the Navier-Stokes equation and deals with average field properties such as density, pressure, velocity and stress tensor. In the last five decades, a

notable number of modeling studies based on numerical techniques based on Finite Difference (FD), Finite Volume (FV) and Finite Element (FE) methods have been developed to solve the governing equations of fluid flows in macro scale [111-112]. The FEM is the most well-known numerical technique which divides the medium into a certain number of non-overlapping sub-domains called finite elements. Then set of algebraic element equations will be gathered and solved to obtain the variables. Every aspect of the FE method has been investigated by a large number of researchers which revealed that FE is based on a strict mathematical foundation and has intrinsic mesh flexibility, but it is not mass conservative and needs high numerical effort [113-114]. The FVM is one of the powerful numerical methods which discretizes the domain to the number of arbitrary polyhedral sub-domains so-called control volume. Studies on FV methods verified that this method is mass conservative and flexible which means that it can be applied for both structured and unstructured grids [115,116]. The FDM is the first numerical simulator that has been used for multiphase flow in porous media and mostly applicable for simple geometries and structured grids [117]. In this method, the approximation and simplification of the main equation accomplished by replacing the derivatives of the differential form of the governing equations with backward, forward and central difference equations. Several researchers found this method simple which can easily get to the high order approximation, on the other hand, the complicated boundary conditions and geometry is hard to handle with this method.

Mesoscopic Scale fills the gap between micro and macro scales and studies the behavior of the collection of particles as a unit. Dissipative Particle Dynamics (DPD), Smoothed Particle Hydrodynamics (SPH), Stochastic Rotation Dynamics (SRD) and the most well-known method which is Lattice Boltzmann Method (LBM) are methods of interest for mesoscale. LBM is a new and advanced numerical technique. In contrast to conventional numerical methods that directly use the Navier-Stokes equation, LBM is based on kinetic theory and molecular distribution function which discretize the positions and moment of particles by setting them predefined values. The fluid flow in porous media can be modeled with LBM in two scales. REV scale (Representative elementary volume) and Pore-scale. REV-scale does not need details about the microstructure of the porous media and a number of assumptions and simplifications to make it easier to examine the media. It just depends on porosity and permeability. On the other hand, pore-scale is the smallest available level, so it highly depends on the detailed pore characteristics and also different boundary conditions. Moreover, complex geometries can be analyzed with LBM at this scale [25]. Despite being versatile method with a wide range of applicability and capabilities such as parallel implementing and applying on complex boundary conditions, there are some drawbacks and challenges in the simulation of multiphase flow through porous media using several models of LBM. In

LB models, the lack of precise knowledge of the location of the pore/solid interface is a potential source of error. In addition, the handling of interfaces between solid and fluid in the LBM can be tedious and computing-intensive due to its rigid lattice structure [104,118]. Although several algorithms have been developed to optimize the streaming step but LBMs are yet typically limited by memory bandwidth [119]. In the lattice Boltzmann method, the macroscopic boundary conditions and variables such as velocity and pressure can not be used directly, so the microscopic distribution functions should be built from available macroscopic quantities on the boundary. One of the major challenges in the LBM is converting and connecting the macroscopic variables to kinetic variables [120].

2.4.3. Asphaltene Precipitation Models

Asphaltene Precipitation models are applied to assess the phase behavior of the COA system. Asphaltene precipitation models are divided into two capital groups of Colloidal and Solubility models. The colloidal approach is originated in collide theory and considers the asphaltene as a suspended solid particle which is stabilized with the aid of resins. Colloidal models consider the asphaltene precipitation as an irreversible process. On the other hand, the Solubility model is based on a simple concept which in the first place considers asphaltene as a completely dissolved component in the oil, then describes the asphaltene precipitation by changes in the solubility. The asphaltene precipitation in the solubility model is considered a reversible process. Figure 2-7 presents the different asphaltene precipitation models.

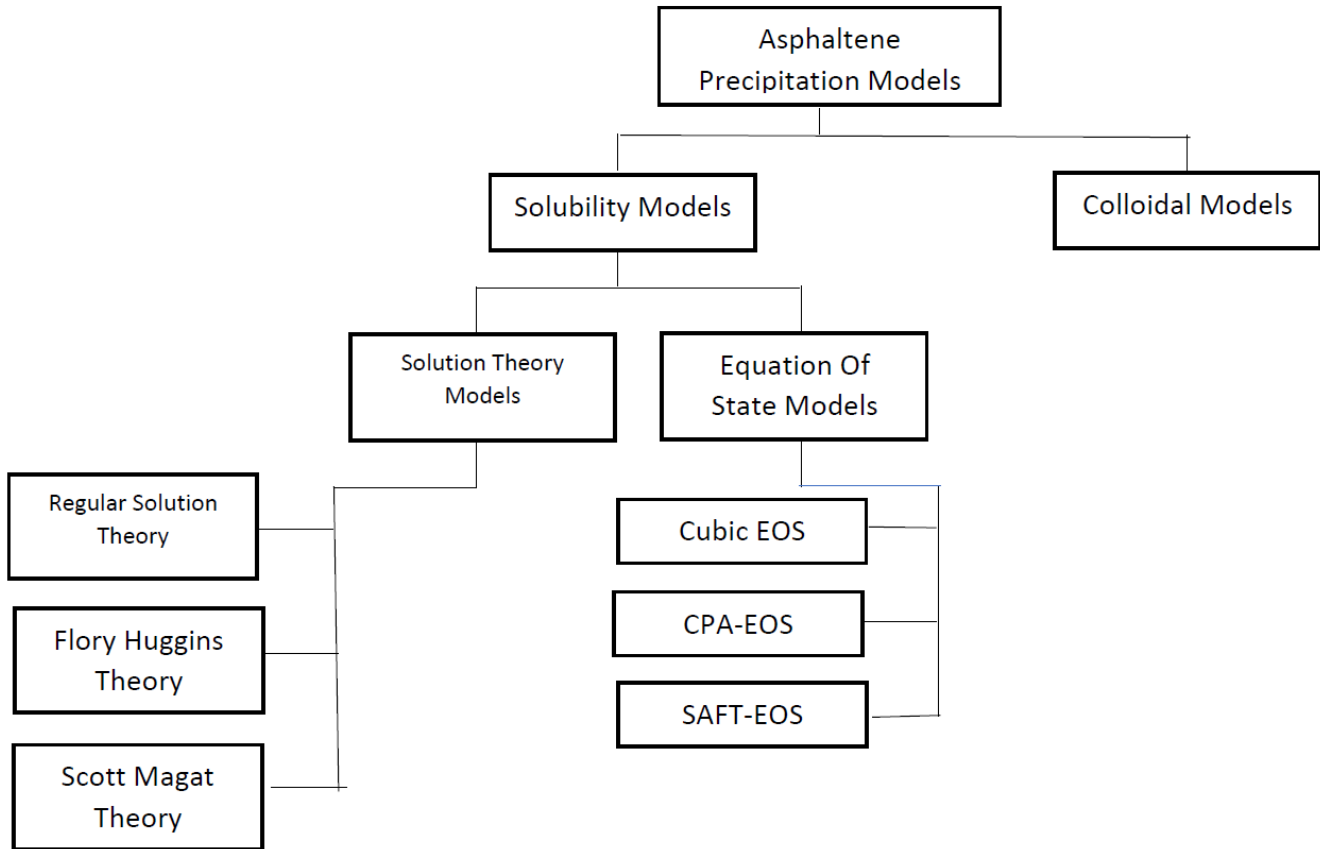
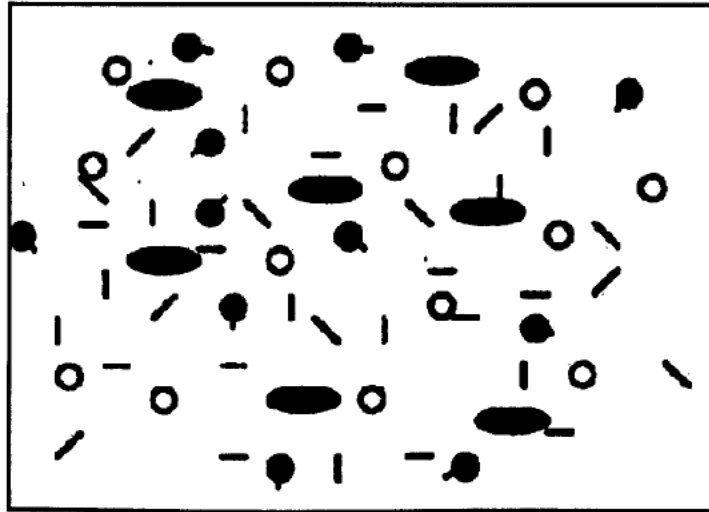


Figure 2- 7: Asphaltene precipitation models

I. Solubility Models

The solubility model is based on considering the system in a real solution mode as presented in figure 2-8. When the solubility comes under a threshold value, the asphaltene precipitation happens either in Solid-Liquid Equilibrium (SLE) state or in Liquid-Liquid Equilibrium (LLE) condition. The solubility model is divided into two subdivisions of Solution theory and Equation of State (EOS) models. Solution theory models are based on Regular solution theory, Flory-Huggins theory, and Scott Magat theory. On the other hand, the EOS models involve Cubic EOS, CPA EOS, and SAFT-EOS models.



-  Paraffinic, olefinic, and naphthenic molecules
-  Aromatics molecules
-  Resin (polar, aromatic/heteroatom) molecules
-  Asphaltenic molecules

Figure 2- 8: Solubility model [10]

I-1: Solution Theory Models

The solution theory model involves Regular Solution Theory, Flory-Huggins Theory, and Scott-Magat Theory. One of the first studies on describing the wax and asphaltene based on regular solution theory is done by Won [121]. He developed a theoretical approach to examine the solid-liquid thermodynamic equilibrium of wax-contained mixtures with the key assumption of the equality of Gibbs free energy and internal energy of the solution. Based on this assumption, the solid-liquid equilibrium ratio (K_i^s) is defined as follows:

$$\ln K_i^s = \ln \left(\frac{x_i^s}{x_i^l} \right) = \frac{1}{RT} \left[V_{mol-i}^l \delta^l - \delta_i^{l2} - V_{mol-i}^s \delta^s - \delta_i^{s2} \right] + \frac{\Delta H_f}{RT} \left[1 - \frac{T}{T_f} \right] + \frac{\Delta C_p}{R} \left[1 - \frac{T_f}{T} + \ln \frac{T_f}{T} \right] + \frac{1}{RT} \int_0^P (V_{mol-i}^l - V_{mol-i}^s) dp \quad (11)$$

Where superscripts s and l refer to solid and liquid respectively. x_i , δ_i and V_{mol-i} is mole fraction, molar volume and solubility parameter of i^{th} fraction respectively. δ , ΔH_f , ΔC_p and T_f are average solubility parameters, the heat of fusion, heat capacity and fusion temperature, respectively. Thomas and his coworkers [48] extended the Won's model for predicting the start point of asphaltene precipitation and found it appropriate.

Flory-Huggins theory is originally defined for polymer and solvent mixtures. In this theory, the polymer structure is made of many segments, in a way that each polymer segment and solvent molecules are equal

in size. Extending this theory to the asphaltene contained system leads to an assumption that asphaltenes and solvent have a homogenous and uniform structure in Flory-Huggins based models.

The Hirschberg solubility model [36] is based on the Flory-Huggins model. For developing this model, at first, the crude oil is split into the liquid and vapor phases using SRK EOS. Then the liquid phase is divided into two phases of pure liquid solvent phase and asphaltene phase (as a pure liquid state component) which are in liquid-liquid equilibrium. In this model, the amount of precipitated asphaltene is calculated using the Flory-Huggins Theory. This model is based on the following equation:

$$\frac{\mu_i - \mu_i^0}{RT} = \ln\Phi_i + 1 - \frac{V_i}{V_{mix}} + \frac{V_i}{RT} (\delta_i - \delta_{mix})^2 \quad (12)$$

Where μ_i , μ_i^0 , Φ_i , V_i , V_{mix} , δ_i and δ_{mix} are the chemical potential of component i in solution, the chemical potential of component i in solution at standard condition, the volume fraction of component i, the molar volume of component i, the molar volume of the mixture, the solubility parameter of component i and solubility parameter of the mixture, respectively.

Rewriting equation (12) for asphaltene, Hirschberg defined three regions for asphaltene as follows:

- *Unstable*: $\ln\Phi_{asp} + 1 - \frac{V_{asp}}{V_{mix}} + \frac{V_{asp}}{RT} (\delta_{asp} - \delta_{mix})^2 > 0$
- *Onset*: $\ln\Phi_{asp} + 1 - \frac{V_{asp}}{V_{mix}} + \frac{V_{asp}}{RT} (\delta_{asp} - \delta_{mix})^2 = 0$
- *Stable*: $\ln\Phi_{asp} + 1 - \frac{V_{asp}}{V_{mix}} + \frac{V_{asp}}{RT} (\delta_{asp} - \delta_{mix})^2 < 0$

From the Onset condition, the maximum volume fraction of asphaltene soluble in crude oil can be obtained. Ignoring the asphaltene aggregation and interaction with resins, along with considering the asphaltene as a homogenous substance make the Hirschberg's model, a simple model with limited applications [36].

Yang et al [95] referred to the shortcomings of the Hirschberg model such as unreliable results of the solubility parameter for the oil phase and incapability in handling the gas-injected oil reservoirs and proposed their modified version of Hirschberg model. In contrary to Hirschberg's model, they considered the oil phase as a multicomponent mixture and introduced binary interaction coefficient and new correlation for the solubility parameter as follows:

$$\ln\Phi_{asp} + 1 - \frac{V_{asp}}{V_{mix}} + \frac{V_{asp}}{RT} \sum_i \sum_j (D_{iasp} - 0.5 D_{ij}) = 0 \quad (13)$$

$$D_{ij} = (\delta_i - \delta_j)^2 + 2I_{ij}\delta_i\delta_j \quad (14)$$

$$\delta = 0.500765 \times (T_B)^{0.982382} \times \left(\frac{\Upsilon}{MW}\right)^{0.482472} \quad (15)$$

Where T_B , γ and MW are average boiling temperature (K), specific gravity at 20 °C and molecular weight ($\frac{g}{mole}$). Yang et al compared the new correlation with the data obtained from experimental work, Peng - Robinson EOS and Chung correlation. Results revealed a very good agreement.

Another modification on Hirschberg's model is made by Cimino et al [122]. In this model, the pure phase (asphaltene-free solvent) and the impure phase (asphaltene+solvent) is introduced. A cloud point data which can be obtained by spectrophotometer are used for deriving the governing equation of the asphaltene precipitation as follows:

$$\ln(1 - \varphi_{asp}^*) + \left(1 - \frac{V_{mix}}{V_{asp}}\right) \varphi_{asp}^* + \frac{V_{mix}}{RT} (\delta_{asp} - \delta_{mix})^2 \varphi_{asp}^{*2} = 0 \quad (16)$$

Where φ_{asp}^* is the asphaltene volume fraction of the nucleating phase at the cloud point of the oil. A comparison study between the original Hirschberg's model and Cimino's model exhibited better accuracy for Cimino's model.

Treating asphaltene as a single component is the main deficiency of Hirschberg's and Cimino's model, which leads to the incapability of both models in calculating the asphaltene precipitation amount. To overcome this problem and predict the asphaltene precipitation onset along with the amount of precipitated asphaltene, Yarranton and Masliyah [21] considered asphaltene as a mixture of a number of sub-fractions and proposed the following solid-liquid equilibrium ratio (K_i) equation:

$$K_i = \frac{x_i^s}{x_i^l} = \exp \left[\frac{\Delta H_{f-i}}{RT} \left(1 - \frac{T}{T_{f-i}}\right) + \left(1 - \frac{V_{mol-i}^l}{V_{mol-sol}}\right) + \left(\ln \frac{V_{mol-i}^l}{V_{mol-sol}}\right) + \left(\frac{V_{mol-i}^l}{RT} (\delta_{sol} - \delta_i^l)^2\right) \right] \quad (17)$$

Where superscripts s and l refer to solid and liquid respectively. x_i , δ_i and V_{mol-i} is a mole fraction, solubility parameter and molar volume of i^{th} fraction respectively. δ_{sol} , $V_{mol-sol}$, ΔH_{f-i} and T_{f-i} are solvent solubility parameter, the molar volume of solvent, the heat of fusion of i^{th} fraction and fusion temperature of i^{th} fraction, respectively.

De Boer [123] used Hirschberg's model as a basis and introduced his own model by defining the degree of supersaturation of the crude oil to predict the instability of asphaltene as follows:

$$\frac{\Delta S}{S} = \int_{P_{bub}}^{P_{res}} \left(\frac{\partial S}{S \partial P}\right)_T dp \cong \left(\frac{\partial S}{S \partial P}\right)_T (P_{res} - P_{bub}) \quad (18)$$

It is stated that the asphaltene precipitation takes place when the supersaturation degree comes below the threshold value. The supersaturation term can be simply calculated using De Boer's plot as a function of

the asphaltene solubility parameter, oil density, and the difference in reservoir and bubble point pressure. According to De Boer's plot, higher bubble point pressure, higher compressibility and lighter crude oil lead to more asphaltene precipitation. Although, the supersaturation degree worked as a good indicator of asphaltene stability in some cases but considering the oil completely saturated with asphaltene along with incapability in measuring the precipitated asphaltene amount are drawbacks of this model.

Further improvement on Hirschberg's model is also made by Novosad and Costain [124] for precipitation prediction in the COA system. The heavy components interaction with each other was heeded. Results showed the ability of the Novosad and Costain model in asphaltene phase behavior calculation for a high range of thermodynamic conditions.

There are some other models based on Flory-Huggins theory which is used for gas-injection systems such as Burke et al [45] and n-alkane addition systems like Nor-Azlan and Adewumi [125], Rassamdana et al [126]. The latter models showed poor performance and high deviation from experimental data which is attributed to considering the complete asphaltene reversibility and dealing with C_{7+} as a single pseudo-component.

Scott-Magat theory is an improved version of the Flory-Huggins theory. In contrary to Flory-Huggins theory, which assumes a homogenous structure for asphaltene, Scott and Magat overcame the shortcomings and considered a heterogeneous structure for asphaltene, at which the asphaltene is formed by different chain length molecules. Due to the diversity of molecules, the asphaltene molecular weight distribution comes under consideration. A new parameter which is the solvent partial molal free energy of mixing (ΔF_0) is defined as follows:

$$\frac{\Delta F_0}{RT} = \ln \varphi_{sol} + (1 - \varphi_{sol}) \left(1 - \frac{1}{m_N}\right) + \mathcal{E}(1 - \varphi_{sol})^2 \quad (19)$$

Where φ_{sol} , m_N and \mathcal{E} are volume fraction of the solvent, a function of number average molecular weight and characteristic constant of the solvent respectively. In 1985, Mansouri and Jiang [127] became the first researchers who studied the asphaltene phase behavior using Scott and Magat model. Based on Mansouri and Jiang's investigation, Kawanka et al [128] sub-fractionated the asphaltene into number of the components and utilized gamma distribution function to obtain the asphaltene properties. Considering a Liquid-Solid equilibrium condition, the volume fraction of asphaltene (φ_{asp}^l) is derived as follows:

$$\varphi_{asp}^l = \int d\varphi_{asp-i}^l = \int_0^\infty \left(\frac{\left(\frac{M_{asp-i}}{M_{asp-avg}}\right) V_{asp}^{cr}}{V_{asp}^l + V_{asp}^s e^{-N_{asp-i}\theta}} M_{dis} \right) dM_{asp-i} \quad (20)$$

Where superscripts s, l and cr refer to solid, liquid and crude oil respectively. M_{asp-i} , N_{asp-i} and ϕ_{asp-i}^l are Asphaltene molecular weight, segment number and volume fraction of i^{th} fraction, respectively. $M_{asp-avg}$ is the average molecular weight of asphaltene, M_{dis} is the molecular weight distribution function which can be expressed by gamma distribution function and θ is a complicated variable which is a function of co-ordination number between two segments, interaction parameter, solubility parameter, the molar volume of solvent and volume fraction of asphaltene in a solvent. The efficiency of the model in CO₂ injection systems is not evaluated, on the other hand, n-alkane addition systems are modeled which showed a reasonable result except for n-heptane addition in comparison with experimental data.

I-2: Equation Of State (EOS) Models

- Cubic-EOS

Cubic Equation Of State (CEOS) is an easy, simple and almost accurate tool for determining the phase behavior of the light hydrocarbon mixtures. CEOS parameters are based on the critical properties of the mixture. Peng-Robinson (PR) and Soave-Redlich-Kwong (SRK) are two popular cubic EOS in the oil industry:

PR:

$$P = \frac{RT}{v-b} - \frac{a}{v(v+b) + b(v-b)} \quad (21)$$

SRK:

$$P = \frac{RT}{v-b} - \frac{a}{v(v+b)} \quad (22)$$

Where a,b are EOS parameters and v is molar volume.

The first CEOS-based modeling of asphaltene fluctuation is done by Gupta [128]. He treated the asphaltene as a pure solid phase and used PR-EOS along with solid fugacity equations to study the phase equilibrium. Thomas et al assessed Gupta's model and stated the poor predictive capability of this model when dealing with asphaltene [48].

Nghiem et al [129] introduced a solid model which is actually an SLE solubility model and it is categorized as a CEOS model. In this model, heavy components of oil (C₃₁₊) split into the non-precipitating and precipitating components with the same critical properties but different interaction parameters. Fugacity of oil, gas, solid and also interaction parameters should be calculated. The fugacity of the solid phase can be obtained using the following equation:

$$\ln f_{asp} = \ln f_{asp}^r + \frac{V_{m-asp}(P - P^r)}{RT} \quad (23)$$

Where f_s , f_s^r , V_s , P , P^r , R and T are solid fugacities, reference solid fugacity, solid molar volume, pressure, reference pressure, gas constant, and temperature, respectively.

Different CEOS can be used to calculate the non-precipitating phases (gaseous and oleic) fugacity such as Peng-Robinson as follows:

$$\ln f_i^{jv} = \ln f_i^j + \frac{s_i b_i P}{RT} \quad (24)$$

Where i denotes to the component and j denotes to the phase and f_i^{jv} , f_i^j , s_i and b_i are fugacity of component i in phase j with volume shift, fugacity of component i in phase j without volume shift, volume shift and EOS's parameter b for component i , respectively.

After fugacity calculation, the thermodynamic equilibrium definition for a system containing n components at which the n^{th} one is asphaltene can be applied when liquid, gas and solid phases coexist:

$$\ln f_{ig} = \ln f_{io} \quad (i = 1, 2, 3, \dots, n) \quad (25)$$

$$\ln f_{no} = \ln f_s \quad (26)$$

As mentioned above, in solid models, precipitating and non-precipitating components have different interaction coefficients with light hydrocarbons which can be calculated using the following equation:

$$d_{ik} = 1 - \left[\frac{2v_{ci}^{0.166} v_{ck}^{0.166}}{v_{ci}^{0.333} + v_{ck}^{0.333}} \right]^e \quad (27)$$

Where d_{ik} , v_{ci} , v_{ck} and e are interaction coefficient of component i and k , the critical volume of component i , the critical volume of component k and adjustable parameter. Comparison of Nghiem's model with experimental data showed a good agreement, however, suitable heavy components splitting and characterization of each subfraction are two important marks of this model. In spite of acceptable achievements of solid models but this model suffers from the complex structure along with intense dependency on the adjustable parameters which cause a limitation in covering a high operational range in means of temperature and pressure.

Nghiem's study attracted attention toward solid models so that researchers tried to extend and generalize this model [130,131]. Kohse et al [131] considered the effect of pressure and temperature and proposed their model for a flexible range of thermodynamic condition as follows:

$$\ln f_{asp} = \ln f_{asp}^r + \frac{V_{m-asp}}{R} \left[\frac{P - P^{tp}}{T} + \frac{P^r - P^{tp}}{T^r} \right] - \frac{\Delta H^{tp}}{R} \left[\frac{1}{T} - \frac{1}{T^r} \right] - \frac{\Delta C_p}{R} \left[\ln \frac{T}{T^r} - T^{tp} \left[\frac{1}{T} - \frac{1}{T^r} \right] \right] \quad (28)$$

Where f_{asp} is asphaltene fugacity at pressure P, f_{asp}^r is asphaltene fugacity at a reference pressure P^r , V_{m-asp} is asphaltene molar volume, ΔC_p is heat capacity difference and P^{tp} , T^{tp} and ΔH^{tp} are pressure, temperature and fusion enthalpy at the triple point, respectively.

In COA systems, in addition to physical interaction between different components, there exist chemical bondings which are known as asphaltene self-association and asphaltene-resin cross association. Unmodified CEOSs ignore the chemical interaction and study the state of the system by taking into account the physical interactions only. It is proven that CEOS is not appropriate to approach for modeling the asphaltene precipitation of heavy crudes. Oil composition changes during CO₂ injection, a poor database of the asphaltene critical properties and ignoring the association effects such as hydrogen bonding make the CEOS an inaccurate approach for asphaltene precipitation modeling [132]. But, the modifications on CEOS can make it reliable for asphaltene-contained systems. Du et al [133] and Sabbagh et al [134] added chemical contribution term and asphaltene self-association term to CEOS, respectively. The former found reasonable results, on the other hand, the latter model's performance was poor for n-pentane and n-heptane dilution.

- Statistical Association Fluid Theory (SAFT)-EOS

The thermodynamic perturbation theory of Wertheim [135] is the foundation of the Statistical Association Fluid Theory (SAFT) developed by Chapman et al [136]. SAFT is a statistical mechanics-based EOS which is a widely used EOS for asphaltene phase behavior description. The first step in SAFT EOS is defining a reference fluid that acts as a representative for the original fluid. The reference fluid in SAFT is in the form of spherical segments that bond with each other and form chains. Furthermore, the interaction and association of chains can occur which clearly visualized in Figure 2-9.

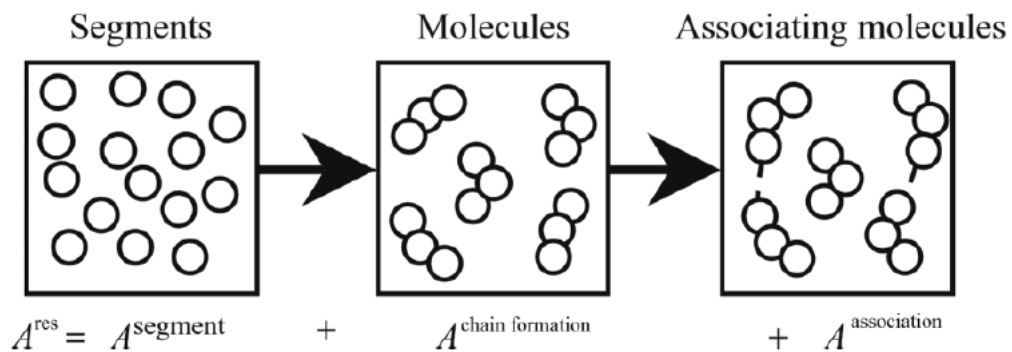


Figure 2- 9: Contribution terms in SAFT-EOS [137]

All contribution terms to calculate the Residual Helmholtz free energy (A^{res}) in SAFT-EOS is presented in Figure 2-10.

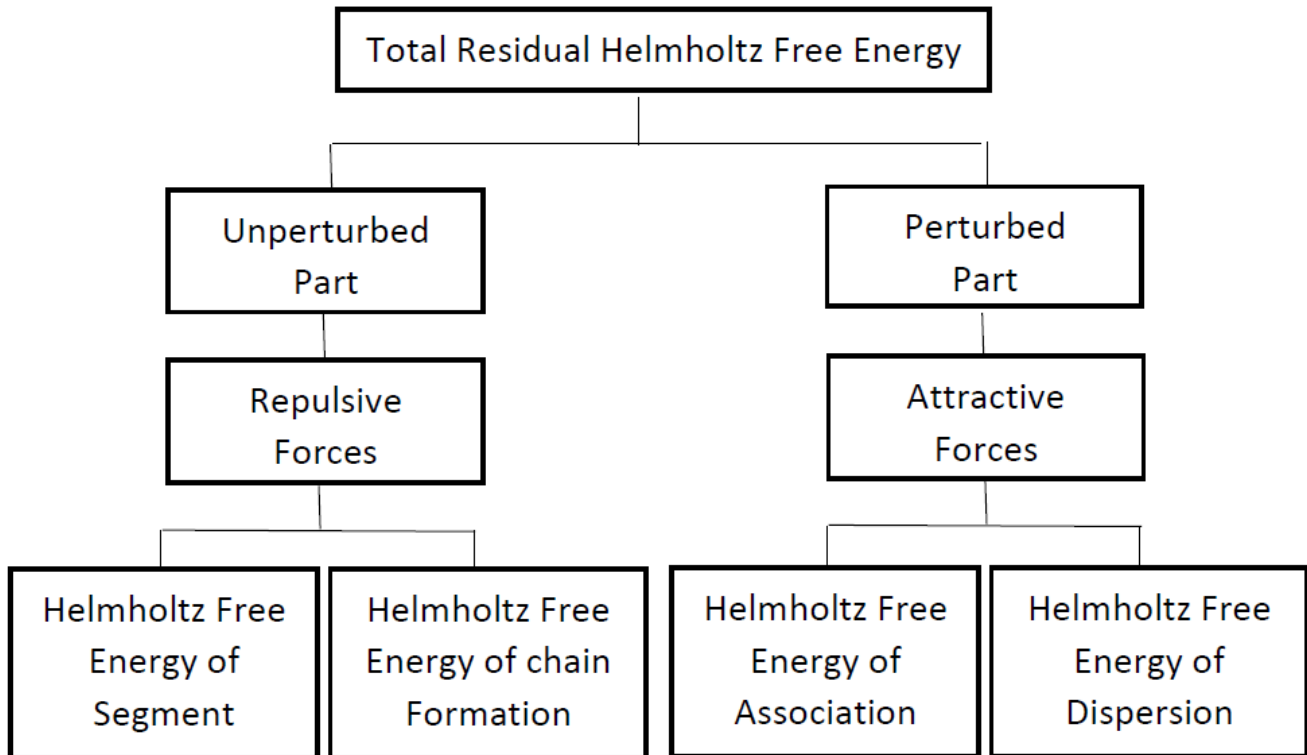


Figure 2- 10: Description of contribution terms in SAFT-EOS

Different derivatives of SAFT-EOS have been published such as LJ-EOS [138], CK-EOS [139], EOS-VR [140] and the most well-known version, especially in the case of COA systems, is PC-SAFT [141]. These derivatives of SAFT-EOS vary in the shape of segments.

Gross and Sadowski [141] changed the shape of the reference fluid in SAFT and considered that as a Perturbed Chain (PC) and developed a PC-SAFT EOS. Utilizing hard chain segments instead of spherical shape segments make the model more accurate and realistic. In this model, the chain length effect on the dispersion of the segments is considered. All detailed information about the equations of residual Helmholtz energy can be found in Mohebbinia et al [142].

Gonzalez et al [44] used PC-SAFT to assess the asphaltene problem during gas injection. It has been reported that the Onset of asphaltene can be precisely predicted. Furthermore, the Upper Critical Solution Temperature and Lower Critical Solution Temperature regions for asphaltene precipitation is successfully predicted using PC-SAFT. Further studies on SAFT-EOS are done by Panuganti et al [132], Punnapala [143] and Vargas, Zunigahinojosa et al [144] at which different lumping ways and distribution functions are used for better estimations of SAFT inputs.

Beside all satisfactory results of SAFT-EOS in predicting the asphaltene behavior especially in COA systems, the notably higher computational time of this model is not negligible. This problem is attributed to complex thermodynamic equations of SAFT-EOS.

- Cubic Plus Association (CPA)-EOS

The concept of the Cubic Plus Association (CPA) EOS can be easily derived from its name. The cubic part of the name refers to the CEOS, which describes the physical interactions (dispersion and short-range repulsion) of the system. On the other hand, Association term which is described by thermodynamic perturbation theory is added to express the chemical and polar interactions (self-association) between the heavy components. Governing equation of CPA model consists of physical and chemical terms as follows:

$$A_{excess} = A_{physical} + A_{association} \quad (29)$$

Where detailed equations of each term can be found in [145].

Studies of Li and Firoozabadi [58,146] on CPA-EOS for predicting the asphaltene behavior under different thermodynamic conditions showed the reliability of this model in evaluating the progression of asphaltene precipitation under temperature and pressure variation. However, they could not recognize the exact point of asphaltene onset. Shirani and his coworkers [108] tried to reduce the error of the CPA-EOS model by changing the adjustable parameters and number of association sites. Results were still unsatisfactory and showed a 55% deviation from the experimental data. But it is worth to mention that, the CPA-EOS model results are in a way better agreement with experimental data in comparison with the colloidal model and CEOS models. Cruz et al applied the CPA-EOS model for CO₂ contained systems and found this model reliable and in good agreement in comparison with experimental data [78].

II. Colloidal Models

Nellenstyn was the founder of collide theory. Leontaritis and Mansoori [10] are the first researchers who used that theory to develop a colloidal model for asphaltene precipitation prediction. They stated that crude oil is a system consisting of dispersion medium and dispersed phase. The dispersed phase includes resins and asphaltene, the resin plays a protector role for asphaltene, in a way that resins adsorbed at the surfaces of asphaltene colloid molecules and form a border layer which protects the asphaltene from interaction with other asphaltene molecules and other components as presented in figure 2-11. On the other hand, the dispersion medium encompasses the remained resin molecules along with other lighter components. Leontaritis and Mansoori [10] started to build up their model by implementing Vapour-Liquid Equilibrium (VLE) calculation to find the liquid phase composition. After distributing the resin in to the dispersion medium and dispersed phase by equating the chemical potential of resin in two

phases, the term “critical resin concentration” is defined. It is a threshold value at which, when the resin concentration in dispersion medium comes below the critical resin concentration, the asphaltene fluctuation occurs. This model is not recommended for gas injection systems, but the obtained results for n-alkane addition systems were acceptable except for n-heptane addition.

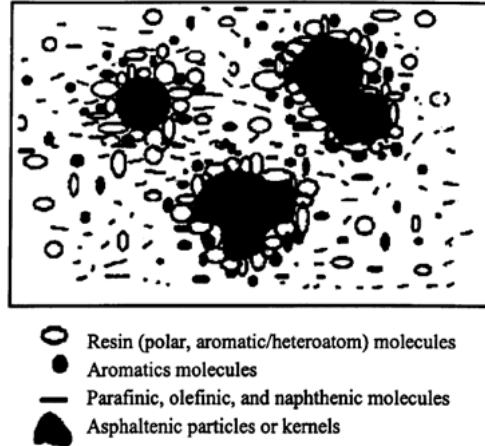


Figure 2- 11: Colloids model [10]

The thermodynamic micellization model is based on findings of Victorov and Firoozabadi [80] which considered the asphaltene precipitation as a micellization process. In the colloidal system, a combination of n_2 resins as a crust and n_1 asphaltene as a nucleus forms a micelle. These micelles are stable until the time that a change in solution and equilibrium disturbance takes place by processes such as CO_2 injection. As a result, CO_2 molecules reside at the asphaltene surface and cause a decrease in resin concentration and thickness of the layer on the surface which leads to the instability of micelles. To compensate these variations and getting back to the equilibrium condition, the asphaltene molecules get together, become bigger and start to precipitate, fluctuate and deposit [82]. The chemical potential of the micelle is related to the asphaltene and resin chemical potential as follows:

$$\mu_{micelle} = n_1\mu_{asphaltene} + n_2\mu_{resin} \quad (30)$$

Where:

$$\mu_{asphaltene} = \mu_{asp}^* + kT\ln x_{asp} \quad (31)$$

$$\mu_{resin} = \mu_{res}^* + kT\ln x_{res} \quad (32)$$

$$\mu_{micelle} = \mu_m^* + kT\ln x_m \quad (33)$$

Where μ_{asp}^* , μ_{res}^* and μ_m^* are a standard chemical potential of asphaltene, resin, and micelle respectively. x_{asp} , x_{res} and x_m are mole fractions of asphaltene, resin, and micelle respectively. Besides the ability of the thermodynamic micellization model in specifying the asphaltene precipitation during n-alkane

addition, it is proven that this model suffers from inaccurate predictions of asphaltene precipitation during the gas titration.

There is a number of studies that compared different asphaltene precipitation models. Tavakkoli et al [81] compared thermodynamic micellization and solid models. Results revealed that the micellization model is highly dependent and sensitive on resin content, interaction parameter, desorption energy, interfacial tension and asphaltene concentration in the liquid phase. The accuracy of both models can be affected by a chosen technique for critical properties and acentric factor calculations. Both models can predict the asphaltene precipitation trend well but their weakness in the prediction of maximum precipitation is not negligible. Overall, the micellization model is complex and time-consuming but on the other hand, leads to a more accurate and robust description of asphaltene precipitation. Behbahani et al [83] evaluated the performance of the Solid model, Flory-Huggins model and PC-SAFT EOS model during n-alkane addition which confirmed the more accuracy of PC-SAFT model.

2.4.4. Asphaltene Deposition Models

Three different asphaltene deposition mechanisms are introduced in previous sections which are, surface adsorption, mechanical plugging, and entrainment. The purpose of introducing the deposition model is finding the asphaltene deposition rate which plays a vital role in formation damage calculation. The first deposition model is proposed by Gruesbeck and Collins [84] at which the porous medium is divided into pluggable and non-pluggable pathways. non-pluggable type pores consist of small pores which only surface adsorption and entrainment take place. The deposition rate is formulated as follows:

$$\frac{\partial E_{AD-np}}{\partial t} = \alpha E_{AL} - \beta E_{AD-np} (v_l - v_{lc}) \quad (34)$$

Where E_{AD-np} = volume fraction of deposited asphaltene in non-pluggable pathways, α =surface adsorption coefficient, E_{AL} = volume fraction of suspended asphaltene in a liquid phase, β = entrainment coefficient, $v_l = \frac{u_l}{\phi}$ =interstitial velocity, v_{lc} = critical interstitial velocity and u_l is the liquid phase velocity. On the other hand, in pluggable type pore, the pores are large enough that can be a host of the mechanical plugging mechanism which is equated as follows:

$$\frac{\partial E_{AD-p}}{\partial t} = (\Omega + \chi E_{AD-p}) u_l E_{AL} \quad (35)$$

Where E_{AD-p} = volume fraction of deposited asphaltene in pluggable pathways, Ω and χ are constants. Different models are developed after the Gruesbeck and Collins [84] model such as Wojtanowicz et al [85,87], Pang and Sharma model [88], Ring Model [89] and Wang model [88,90]. One of the most

popular deposition models for net deposition rate calculation especially in COA systems are developed by Wang which is known as Deep Bed Filtration (DBF) model as follows:

$$\frac{\partial E_{AD}}{\partial t} = \alpha E_{AL} \varphi - \beta E_{AD} (v_l - v_{lc}) + Y u_l E_{AL} \quad (36)$$

Where E_{AD} = volume fraction of deposited asphaltene, α =surface adsorption coefficient, E_{AL} = volume fraction of suspended asphaltene in a liquid phase, φ = porosity, β = entrainment coefficient, $v_l = \frac{u_l}{\varphi}$ =interstitial velocity, v_{lc} = critical interstitial velocity, Y = mechanical plugging coefficient and u_l is the liquid phase velocity.

In equation 36, $\alpha E_{AL} \varphi$ is the surface adsorption rate which is proportional to the concentration of suspended asphaltene particles in a liquid phase. The second term, $\beta E_{AD} (v_l - v_{lc})$ indicates the particle entrainment rate by liquid phase which depends on interstitial velocity. Once the interstitial velocity passes the critical value, the entrainment mechanism becomes dominant and proportional to the amount of deposited asphaltene. When $v_l < v_{lc}$, β is considered zero. Finally, the third term, $Y u_l E_{AL}$ expresses the mechanical plugging rate which depends on the fluid velocity and the amount of suspended asphaltene in the liquid phase. For plugging coefficient (Y) determination, Wang defined a critical pore throat diameter (D_{ptc}) at which when average pore throat diameter is greater than a critical value, the plugging coefficient is zero, otherwise:

$$Y = Y_i (1 + \sigma E_{AD}) \quad (37)$$

Where σ is deposition constant.

Kord et al extended the works of Wang and Civan and introduced a new mechanism called pore throat opening which occurs when high-velocity fluid opens the previously plugged pore throats. According to this model, the adsorption and entrainment mechanisms govern the deposition process until the steady-state condition is reached. After that, the mechanical plugging will be dominant.

2.4.5. Porosity and Absolute Permeability Reduction Models

The most important formation damage caused by asphaltene deposition in porous media is porosity and permeability reduction. Gruesbeck and Collins [84] were the first researchers that developed an equation for permeability impairment as a result of asphaltene deposition. As same as the deposition model, they divided the medium to pluggable and non-pluggable portions and developed equations as follows:

$$K_p = K_{p0} e^{-\alpha E_{AD}^4 - p} \quad (38)$$

$$K_{np} = \frac{K_{np0}}{1 + b E_{AD}^{-np}} \quad (39)$$

Where K_p = Absolute permeability of pluggable portion, K_{np} = absolute permeability of non-pluggable portion, K_{p0} = initial Absolute permeability of pluggable portion, K_{np0} = initial absolute permeability of non-pluggable portion, a and b are phenomenological constants.

Several other theories were developed for permeability impairment calculation. Minssieux [94] developed a qualitative method using curve matching based on experimental data. The simplest equation for porosity determination is proposed by Wang and Civan [90] as follows:

$$\varphi = \varphi_0 - E_{AD} \quad (40)$$

Where φ_0 , φ and E_A are initial porosity, local porosity and volume fraction of deposited asphaltene.

Using the fact that the permeability is a function of porosity, Civan [65,66] and Wang [97] developed a power-law relationship for local permeability as follows:

$$K = K_0 \left(\frac{\varphi}{\varphi_0} \right)^3 \quad (41)$$

Where K_0 and K are initial absolute permeability and local absolute permeability, respectively. The exponent value of the power-law relationship was a matter of interest between researchers. Reis and Acok proposed value 5 for sandstone rocks. Lawal et al proposed a range of 2-10 for most rocks, moreover, the dependency of the exponent to the intrinsic flow parameter is stated.

2.4.6. Review on the Modelling Studies of COA systems

There are two ways to implement the simulation, using commercial reservoir simulators or developing a computer program. COA studies based on both approaches are reviewed in the following parts.

- **Studies based on commercial software**

Iwere et al utilized the laboratory data to simulate the asphaltene precipitation in fractured reservoirs using the Eclipse100 simulator. Results obtained from both experiments and representative models showed that asphaltene precipitation rigorously depends on the type of lithology and pore throat size which both form the porosity-permeability combination. So, as the pore throat gets smaller the tendency of the precipitated asphaltene for blockage gets more. Permeability decreases with pressure reduction because of the asphaltene precipitation but the important result was that the same amount of asphaltene for two crude oils did not have the same permeability reduction due to the different pore architecture. Also, it is proven that acidizing which is used for the means of fracturing, chemically reacts with carbonates rock and produces carbon dioxide which ends to the asphaltene precipitation enhancement [98].

Bagherzadeh et al used Eclipse simulator to assess the permeability reduction of sandstone and carbonate rocks using the following power-law expression:

$$\frac{K}{K_o} = \left(1 - \frac{\mathcal{E}}{\varphi_o}\right)^\delta \quad (42)$$

Where K , K_o , φ_o , \mathcal{E} and δ are permeability at time t , initial permeability, initial porosity, the volume fraction of asphaltene deposits and exponent which is different for each experimental data. Both simulated results of sandstone and carbonate rocks matched the experimental data only in the final stages of the injected pore volume. This difference is related to considering the adsorption and plugging coefficient in simulation which may not exist at first. Moreover, in carbonate analysis, the entrainment mechanism just resists the more permeability reduction and cannot improve permeability in contrast with experimental data. Sensitivity analysis showed that adsorption and plugging are governing asphaltene deposition mechanisms at a low injection rate, on the other hand, the entrainment mechanism is determinant at higher injection rates [102].

Khamehchi et al used Intelligent Proxy Simulator (IPS) which is based on Artificial Neural Network (ANN) and Adaptive Neural Fuzzy Inference System (ANFIS) to find asphaltene precipitation onset and bubble point pressure during miscible CO₂ injection. After defining the inputs, adjusting the weight of the neuron using PSO-ANN and BP-ANN algorithms, a sigmoid transfer function is used for output calculation. To verify the accuracy of results obtained by IPS, Khamehchi and his coworkers used the Solid model of CMG simulator to calculate asphaltene onset pressure, moreover, the Standing correlation for bubble point pressure determination is used. The comparison showed a high accuracy of IPS due to its extrapolation capability, a large number of hidden layers and optimized algorithms [99].

Mohebbinia et al used the UTCOMP simulator to study the asphaltene precipitation and deposition in COA system. After generating Asphaltene Precipitation Envelope (APE) by PC-SAFT EOS, the asphaltene precipitation is modeled in LLE ($P > P_b$) and VLLE ($P < P_b$) states. Asphaltene adsorption and mechanical entrapment are modeled using Langmuir-isotherm and Gruesbeck and Collins equations, respectively. Results showed that CO₂ injection expands the APE which leads to an increase in asphaltene precipitation. Formation damage results revealed that around production well, the effect of pressure depletion is more than CO₂ injection in permeability reduction. Furthermore, change in wettability reduces the deliverability at early production times, this trend continues to a point at which the wettability alteration increases productivity due to the mobility reduction of the oil phase. Mohebbinia and her coworkers came up with an idea to decrease the computational time of PC-SAFT by changing the root-finding algorithm and using the analytical methods for some derivative calculations [142].

A three-dimensional simulation of the Oil/Asphaltene system during primary, water flooding and CO₂ injection was made by Al-Qasim [100] using CMG/GEM simulator along with a solid model. The effect of pressure on asphaltene precipitation was as same as previous studies which shows a bell-shape figure with the maximum point around the bubble point pressure. A comparison between asphaltene deposition content during three stages of oil production showed a much higher value for CO₂ injection due to its solubility which causes a change in oil composition. Using WAG process as a supportive force led to a higher asphaltene deposition and lower productivity. Al-Qasim clarified the difference between CMG, UTCOMP and ECLIPSE simulators by implementing 1-D modeling of asphaltene issue as exhibited in Table 2-5.

Table 2- 5: Comparison of the simulators

Simulator	Total Asphaltene Precipitation	Porosity	Permeability Reduction Model	Reference Fugacity
CMG	The adsorbed portion that deposits+ flowing portion remain in the oil phase	Remains constant	Resistance Factor Relationship	Input
ECLIPSE	The adsorbed portion that deposits+ flowing portion remain in the oil phase	Changes due to deposition	Parametrized Power-law Relationship	Calculated automatically
UTCOMP	Precipitated asphaltene deposits and does not flow with the oil phase	Changes due to deposition	Parametrized Power-law Relationship	Calculated automatically

- Studies based on developed computer programs

Vafaie and Mousavi [101] proposed a deposition model with fewer parameters and simulated the miscible COA system by adding an association term to PR-EOS. After dividing the asphaltene into a number of sub-fractions using Analytical Chain Association Theory (ACAT), phase stability analysis for each subfraction is assessed:

$$f_i(T, P, Z_i) - f_{ipure}(T, P) \geq 0 \quad (43)$$

The turning point of this study, is a statement that says” asphaltene decomposes at high temperatures so calculating the critical temperature and critical pressure which are needed for CEOS parameters, will be impossible”, instead Vafaie and Mousavi defined EOS parameters a and b as a function of asphaltene molecular weight:

$$a = r_i^2 a_i \quad (i = 1, 2, \dots, n) \quad (44)$$

$$b = r_i b_i \quad (i = 1, 2, \dots, n) \quad (45)$$

Where a_i and b_i are EOS parameters of all components before considering the association and r_i is association number:

$$r_i = \frac{Mw_i^{aggregate-i}}{Mw_i^{monomer}} \quad (46)$$

Where $MW_i^{aggregate-i}$ and $MW_i^{monomer}$ are the molecular weight of i-th subfraction and asphaltene monomer molecular weight, respectively. The results of this simulation showed that the increase in CO₂ mole fraction leads to an increase in asphaltene deposition, moreover, the more the resin amount, the lower the asphaltene deposition. All results were in good agreement with experimental data and studies based on AEOS theory, Pan and Firoozabadi, and Victorov and Firoozabadi [80].

Gonzalez et al used PC-SAFT EOS to study the asphaltene phase behavior in live oils and dead oils during CO₂, N₂ and methane injection. The PC-SAFT parameters of each component and binary interactions are calculated through correlations with average molecular weight and fitting binary VLE experimental data, respectively. PC-SAFT precisely gave the same behavior as the experimental results and correlated the bubble point pressure and temperature effect curves. Results of gas injection to dead oil revealed that, for N₂ and methane, the more the pressure, the more stable the asphaltene is. On the other hand, for CO₂ injection to dead oil, the lower the temperature, the more stable the asphaltene. For live oil, the PC-SAFT predicted a slope change (at 200 °F) in the P-T diagram of the sample which is the so-called crossover point. At temperatures below the crossover point, increasing CO₂ concentration led to increasing in asphaltene stability, on the other hand, at temperatures above the crossover point, CO₂ concentration enhancement decreases asphaltene stability. The injection of the other two gases increases the asphaltene instability and the dual effect is not reported. This different behavior of injected gases is attributed to the solubility parameters of gases and oil at different temperatures [44].

Mirzabozorg et al, developed a modeling approach to investigate the effect of asphaltene deposition during primary pressure reduction on the permeability of fractured reservoirs. Several models are used to define the solid phase behavior. At the first step, they used a solid model to study the asphaltene precipitation. Asphaltene fluctuations are modeled by defining a chemical reaction and analyzing the corresponding reaction rate to find the reversibility of particles. Wang and Civan's model is utilized to calculate the deposition rate. Results revealed that permeability reduction in fractures is more than matrix due to the high contribution of fractures in fluid transports. Also it is concluded that static and dynamic asphaltene parameters are key factors for increasing the accuracy of the model [106].

Lei et al, simulate the COA system using Association Equation Of State (AEOS). The compression factor of the association compound is introduced to the calculations to define the non-ideal behavior of precipitated asphaltene, then the three-phase flash calculation procedure is presented. Results showed that at constant injection pressure, the asphaltene precipitation first increases by CO₂ mole fraction, then a decrease in the amount of precipitated asphaltene is reported. Moreover, pressure drop and incrementing injection pressure lead to an increase in precipitated asphaltene content [107].

Zendehboudi et al, employed an optimized Artificial Neural Network (ANN) with two algorithms which are the Imperialist Competitive Algorithm (ICA) and Particle Swarm Optimization (PSO) to evaluate the asphaltene phenomena precisely in a proper time period. ANN is a smart information process system which provides a relationship between the inputs and outputs of highly nonlinear systems such as asphaltene precipitation and deposition in oil processes. Results of this smart predictive tool showed a good agreement with the experimental data and it is observed that for the asphaltene precipitation, the pressure and temperature are determinant factors and for asphaltene deposition, the temperature and pressure drop are key variables. Moreover, it is shown that ICA-ANN is a more effective method than other ANN techniques in terms of convergence rate, accuracy, and reproducibility. The recommendation of linking the ICA-ANN technique with another asphaltene phenomena simulator is mentioned to lower the errors and increase the accuracy and efficiency [40].

Ju et al developed a numerical simulator to study the effect of considering the asphaltene precipitation in the convergence rate, CPU time and cost of simulators. At first, multiphase flow equations, the Convection-Diffusion equation and proposed continuum equation by Ju et al are used to express the asphaltene precipitation and deposition rate, respectively. Finite difference method preconditioned conjugate gradient algorithm and explicit methods are utilized to linearize the governing equations, solve the pressure-saturation equations and solve the asphaltene precipitation and deposition equations respectively. Formation damage results revealed that the permeability reduction intense before 1 PV injection of CO₂ is much more than after 1 PV CO₂ injection which is owing to low residual oil in the pores after 1 PV CO₂ injection. The computational effects of asphaltene precipitation consideration showed that the convergence rate, CPU time and simulator cost in the case of asphaltene consideration are 2, 5.5 and 4.5 times higher than the case without asphaltene precipitation [67].

Zanganeh et al developed a model to simulate the COA system using a solid model along with PR EOS. Twu, Lee-Kesler and Riazi correlations are utilized for calculating the critical properties of each component. Results were in an acceptable agreement with experimental data. Furthermore, the Twu correlation is chosen as an appropriate approach for heavy components such as asphaltene [96].

Nasrabadi et al used CPA-EOS to describe the phase behavior of the asphaltene during CO₂ injection. After developing a mathematical model, the mixed finite element method and the discontinuous Galerkin method are used to solve the pressure and mass balance equation, respectively. Moreover, a new algorithm based on the combination of Newton-Bisection methods is utilized to improve the root-finding approach for the compressibility factor and reduce the computational time and cost. Results revealed that increasing CO₂ mole fraction increases the asphaltene precipitation until the time in which the gas phase

appears. At that time, further increment in CO₂ mole fraction leads to a decrease in asphaltene precipitation. Results of the asphaltene extent around injection well and production well showed that the asphaltene saturation increases with CO₂ mole fraction and reaches a maximum, then stays constant. On the other hand around production well, the asphaltene accumulation is the highest which leads to a need for higher injection pressure. The CPA-EOS model with an improved numerical algorithm showed an excellent agreement with experimental data and is verified as an accurate model in terms of computational time and cost with the conventional cubic EOS [68].

Alay et al developed a modeling approach to foresee the CO₂ injection effect on asphaltene precipitation onset condition using SRK, SRK+HV and CPA equation of states. The comparison between different results of different EOS's showed that the SRK is no reliable model for Upper Onset Pressure (UOP) prediction, especially for heavy crudes due to the high dependency of SRK parameters to fluid molecular weight. Moreover, there is no advantage for SRK+HV over regular SRK. On the other hand, the UOP relative deviation for the CPA model from experimental data is the lowest which is attributed to the no sensitivity of the CPA model to asphaltene molecular weight because of association term [69].

One of the recent studies on COA system based on the colloidal model is made by Zhang et al. They presented the P-x phase diagram for the system (MMP= 15 MPa) which expresses the ADE, UOP, LOP curves that can be used to detect the safe range of the CO₂ injection pressure and CO₂ concentration to avoid the asphaltene issue [85]. As can be seen in figure 2-12, when the condition of the system moves from the borderlines to the center, the asphaltene deposition gets more.

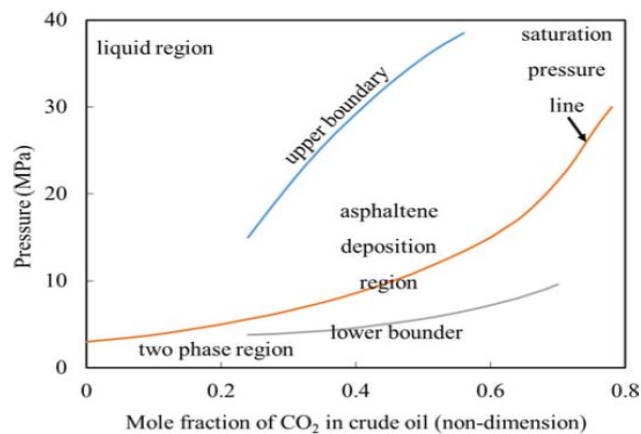


Figure 2- 12: P-X diagram of the asphaltene deposition during CO₂ injection [85]

Tavakkoli et al used LBM to simulate the asphaltene deposition during n-alkane addition. Surface deposition and particle entrainment mechanisms are considered. The deposition profile using LBM is compared with the microfluid experiment which is presented in Figure 2-13.

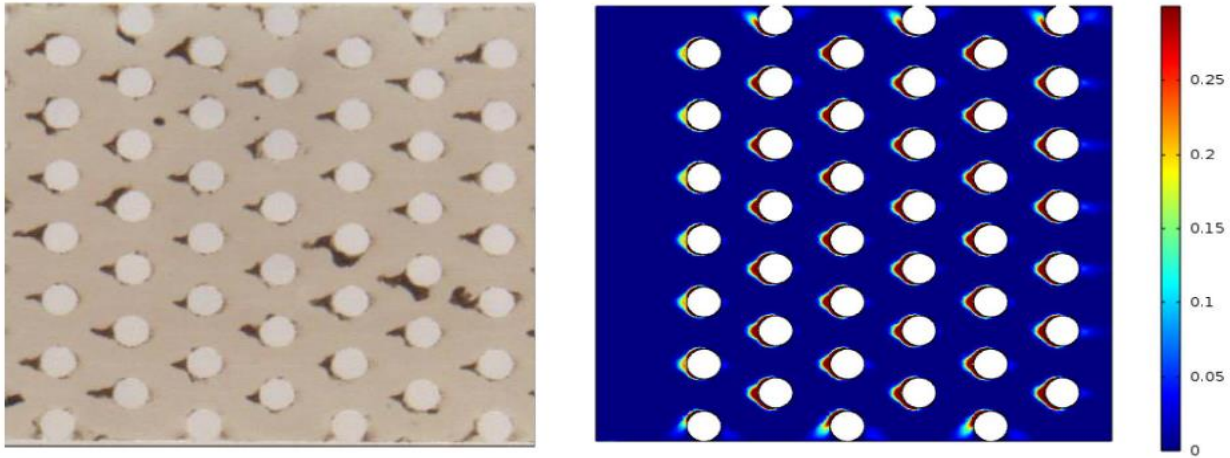


Figure 2- 13: Deposition profile from a micromodel experiment (left), LBM (right): white points are obstacles, dark points are deposited asphaltene [92]

Tavakoli and his coworkers calculated the permeability reduction using Gruesbeck and Collins correlation as follows:

$$\frac{K}{K_0} = \exp(-Y\varphi^4) \quad (47)$$

Where K , K_0 , φ and Y are permeability after deposition, permeability before deposition, the volume fraction of deposited asphaltene to the pore volume and characteristic constant of porous media, respectively. Results of simulation based on LBM were in excellent agreement with experimental data [93].

Mahmoudi et al studied the effect of pore structure and capillary number on the relative permeability curves of immiscible CO₂-Oil systems using a multi-component multiphase Shan-Chen model in two different pore structures and different capillary numbers. Two used pore structures are illustrated in figure 2-14.

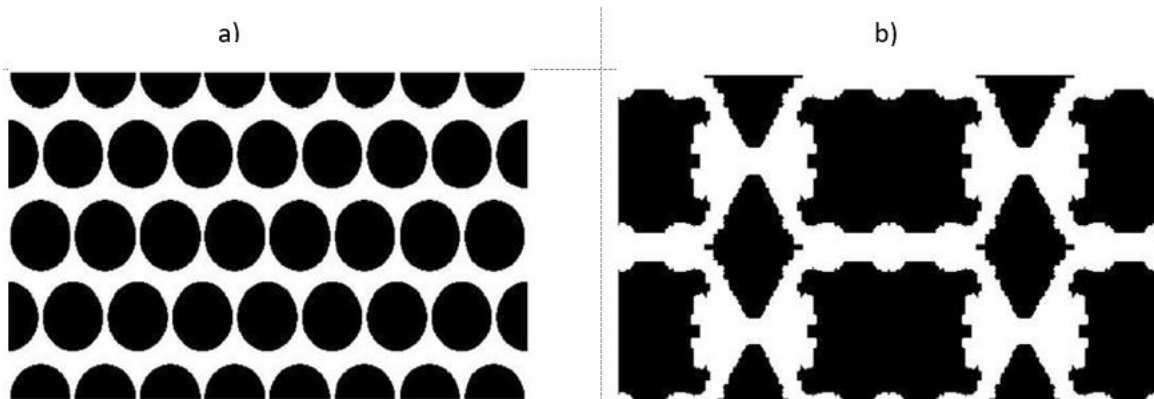


Figure 2- 14: Pore structure (38% porosity): a) ideal sphere pack, b) simplified structure [39]

Results of relative permeability for the wetting phase (oil) and non-wetting phase (CO₂) under different capillary numbers and pore structures are presented in figure 2-15. As can be seen, the increase in the

surface area leads to a decrease in CO₂ relative permeability, on the other hand, there was not a considerable change in the oil relative permeability. The capillary number affects both oil and CO₂ relative permeability.

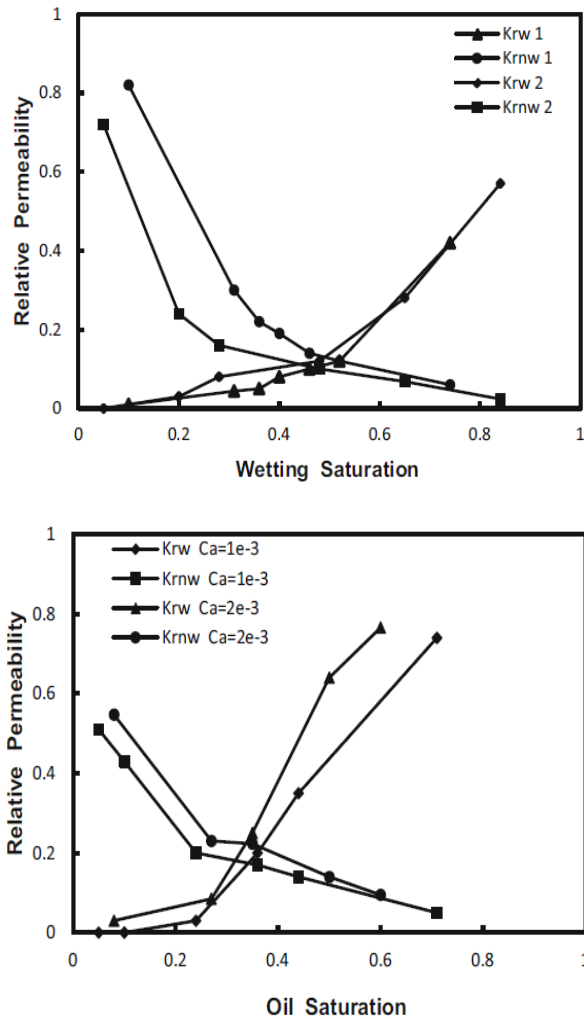


Figure 2- 15: Relative permeability curves of oil (k_{rw}) and CO₂ (k_{rnw}) under different: capillary number (Top), pore structure (Bottom) (1: simple, 2: ideal sphere pack) [39]

Mahmoudi and his coworkers compared the results of their model to the experimental data and found the acceptable agreement for relative permeability predictions which is illustrated in figure 2-16 [39].

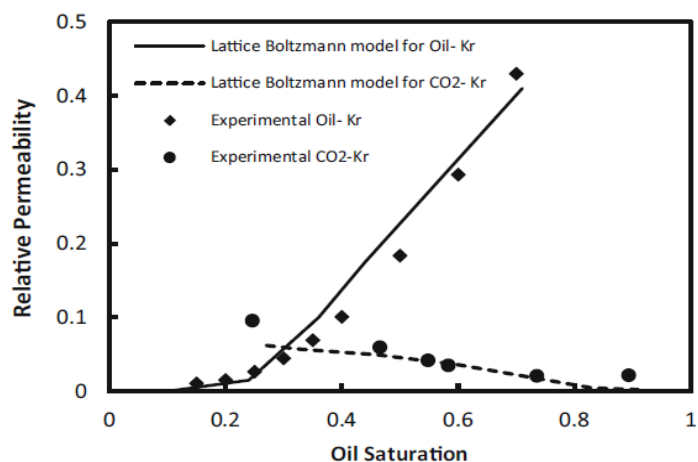


Figure 2- 16: The comparison between the relative permeability obtained from LBM and experimental study [39]

There are a few studies on modeling COA systems using LBM. Okabe et al [105] used a D3Q19 velocity model by imposing bounce-back and periodic boundary conditions to assess the asphaltene deposition effect on permeability reduction during CO₂ injection. At the same time, EOS-based asphaltene precipitation modeling was conducted to compare the results of these two approaches. Both LBM and EOS-based simulations showed an acceptable trend of permeability reduction by asphaltene saturation increase, however, the EOS-based results were inaccurate in high asphaltene saturation amount. The high accuracy of LBM in predicting the permeability reduction in the high range of asphaltene saturation is attributed to using image processed pore structure which gives detailed information of medium as presented in Figure 2-17.

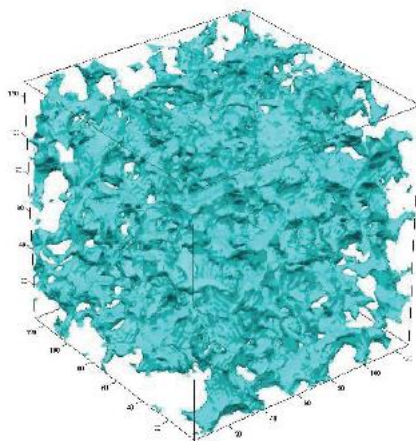


Figure 2- 17: The 3D pore structure of medium used in LBM modeling [105]

LBM results showed a different asphaltene deposition profile for near miscible and miscible CO₂/Oil systems. More permeability reduction is seen during miscible condition which mostly occurred near producer rather than injectors. This behavior is owing to more dissolution of CO₂ in the oil phase during miscible condition which can be extracted from the CO₂ distribution figure in the oil phase in figure 2-18[105].

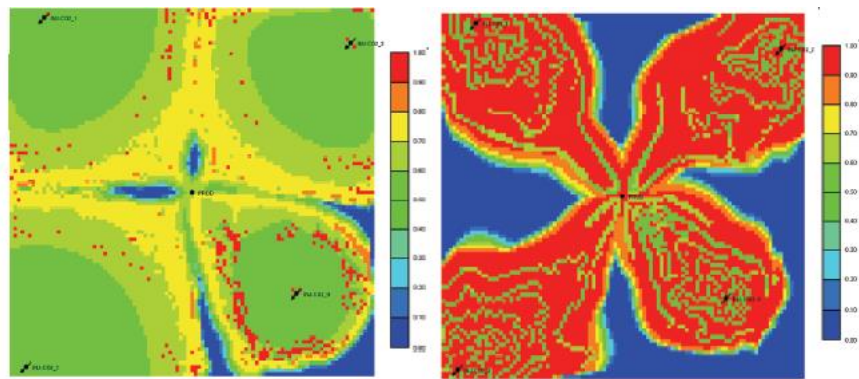


Figure 2- 18: Distribution of CO2 in oil using LBM: near miscible condition (left), miscible condition (right) [105]

Table 2-6 provides a summary of modeling studies on COA systems.

Table 2- 6: Summary of modeling studies on COA systems

Year	System	Technique	Objective	Highlights	Ref
2006	Miscible CO ₂ injection	Association Theory	Determining the reliability of an association model in predicting asphaltene deposition	<ul style="list-style-type: none"> Increasing CO₂ mole% leads to an increase in asphaltene deposition The higher amount of resin in crude oil leads to a decrease in asphaltene deposition The proposed model has fewer parameters EOS parameters (a,b) are functions of asphaltene molecular weight This model is accurate and reliable in modeling heavy organics deposition 	[101]
2007	CO ₂ Injection Live Oil and Dead Oil	PC-SAFT EOS model	Determining the effect of temperature, pressure and CO ₂ concentration on asphaltene stability and evaluating the PC-SAFT validity	<ul style="list-style-type: none"> Dead Oil/ N₂: Increase in P leads to increase in asphaltene stability Dead Oil/ CO₂: Decrease in T leads to increase in asphaltene stability Live Oil/ N₂: Increase in injected N₂ concentration leads to a decrease in asphaltene stability Live Oil/ CO₂: There is a turning point T in P-T diagram at which, above this point, increasing CO₂ leads to decrease in asphaltene stability and below this point, increasing CO₂ leads to increase in asphaltene stability PC-SAFT EOS is an accurate and reliable model in determining the asphaltene phase behavior 	[44]
2010	CO ₂ Injection	Association Equation of State (AEOS)	Determining the effect of CO ₂ mole fraction, injection pressure and pressure drop on asphaltene precipitation	<ul style="list-style-type: none"> Asphaltene precipitation content increases by increasing in CO₂ mole fraction reaches the maximum and then decreases by a further increase in CO₂ mole fraction Asphaltene precipitation content increases with an increase in injection pressure Asphaltene precipitation increases with a pressure drop 	[107]
2011	CO ₂ Injection	CMG.UTCOMP, ECLIPSE/ Solid Model	Comparison between asphaltene precipitation during three stages of oil production and comparing different simulators	<ul style="list-style-type: none"> The P-Asphaltene deposition curve shows a bell-shape figure Maximum asphaltene precipitation is around bubble point pressure The asphaltene precipitation during CO₂ injection is much higher than primary and water flooding stages Using the WAG process increases the asphaltene precipitation 	[100]
2013	Natural Depletion	ANN joined with ICA and PSO	Determining the effect of	<ul style="list-style-type: none"> For asphaltene precipitation, temperature and pressure are determinant factors 	[40]

	CO ₂ Injection		temperature, pressure, pressure drop, dilution ratio and mixture composition on asphaltene precipitation and deposition	<ul style="list-style-type: none"> For asphaltene deposition, temperature and pressure drop are key factors ICA-ANN is a more effective method in terms of convergence rate, accuracy, and reproducibility 	
2013	Miscible CO ₂ Injection	IPS	Evaluating the accuracy of IPS simulator in UOP and P _b determination	<ul style="list-style-type: none"> PSO-ANN and BP-ANN algorithms along with sigmoid transfer function are used Accuracy of IPS is more than Solid model of CMG in UOP determination Accuracy of IPS is more than Standing correlation in P_b determination IPS simulator has extrapolation ability, a large number of hidden layers and optimized algorithm which make it a powerful tool 	[99]
2013	CO ₂ Injection	Finite Difference Method, Preconditioned conjugate gradient algorithm	Determining the effect of CO ₂ injection on permeability reduction and effect of asphaltene consideration on computational aspects of simulators	<ul style="list-style-type: none"> the permeability reduction intense before 1 PV injection of CO₂ is much more than after 1 PV CO₂ injection the convergence rate, CPU time and simulator cost in the case of asphaltene consideration are 2, 5.5 and 4.5 times higher than the case without asphaltene precipitation. 	[67]
2014	CO ₂ Injection	UTCOMP Simulator/PCSAFT EOS	Evaluating CO ₂ injection effect on APE and wettability alteration on the productivity index	<ul style="list-style-type: none"> CO₂ injection expands the APE and increases the asphaltene precipitation Wettability alteration first decreases productivity, then due to lower mobility of the oil phase and lower mechanical entrapment, the productivity slightly increases The computational time of PC-SAFT was reduced using the new root-finding algorithm and using analytical methods for some parts 	[142]
2015	CO ₂ Injection	Solid Model, PR EOS	Determining the effect of pressure, temperature and CO ₂ mole fraction on asphaltene particle size and deposition content	<ul style="list-style-type: none"> Increasing P leads to increase in asphaltene molecule size and more plugging Increasing T leads to more asphaltene aggregation and bigger particles Increasing CO₂ mole fraction from 5 to 20% leads to a 56% increase in asphaltene deposition content Two Correlation is the best choice for calculation of critical properties of heavy components in comparison with Lee-Kesler and Riazi correlations 	[96]
2016	CO ₂ Injection	CPA-EOS, Finite Element+Galerkin method, Newton+Bisection method	Determining the asphaltene behavior around injection and production wells and reducing the computational time and cost of CPA-EOS by implementing a new algorithm	<ul style="list-style-type: none"> At injection well, the asphaltene saturation increases with CO₂ mole fraction and reaches the maximum, then stays constant At production well, the asphaltene accumulation is the highest which leads to needing higher injection pressure The CPA-EOS model with the improved numerical algorithm is an accurate model in terms of computational time and cost with conventional cubic EOS 	[68]
2017	CO ₂ Injection	SRK, SRK+HV, CPA	Comparing the SRK, SRK+HV and CPA performance in UOP prediction during CO ₂ injection	<ul style="list-style-type: none"> SRK is not reliable especially for heavy crudes due to high dependency of SR parameters to asphaltene molecular weight SRK+HV does not have any merit over regular SRK and it is not reliable CPA has the lowest UOP relative deviation from experimental data, which is attributed to association term and low dependency to molecular weight 	[69]

Chapter 3: Methodology

3.1. General Assumptions

Assumptions that are made in the modeling of the fluid flow:

- The two-dimensional model is in x, y (length, width) coordinates and assumes no gravity force
- The porous media is heterogeneously generated model
- The porous media is initially saturated with oil (with known composition)
- There is no water in pores

- The CO₂ is injected to recover the oil from the pores
- Initially, two phases of oil and CO₂ and ultimately three phases of oil, CO₂, and Asphaltene are considered
- The oil is multi-component with thermodynamically known properties
- Oil and rock (grain) are considered incompressible
- CO₂ is considered compressible
- Fluid flow follows Darcy's law (Reynold number is very low 0.09)
- The fluid phase behavior is modeled using the Peng-Robinson equation of state (PR EOS) assuming instantaneous thermodynamic equilibrium within each time step
- The solid asphaltene with a cubic equation of the state is assumed as a liquid-dense phase
- The detailed asphaltene composition is unknown, but depending on the pressure and temperature condition can be categorized in a stable or unstable condition
- Asphaltene deposition affects relative permeabilities
- The flow is isothermal and the temperature of the CO₂ is close to the porous medium's fluid temperature
- It is assumed that there is no chemical reaction between CO₂ and the grain phase in the porous media
- One mechanism is considered for the asphaltene deposition which is a surface deposition
- In this study, a few unique parameters in a two-dimensional medium are defined that are listed below:

Pore Area: is the total area of occupied or unoccupied pore areas in porous media $[L]^2$

Injected Area: fluid injection velocity $\frac{[L]}{[T]}$ multiplied by the width $[L]$ of the entered area $\frac{[L]^2}{[T]}$

Injected Pore Area (IPA): the dimensionless ratio of injected area to pore area at each time step

The newly defined parameters are to avoid the error caused by the assumed minor height for the two-dimensional studies to meet the requirements to estimate pore volume. This assumption is expected to not only positively impact systematic error but introduce a new methodology in two-dimensional simulations.

3.2. Simulation Modules

In this study, there is one main engine which is LBM based fluid flow simulator and the other modules that play a side code program role. Figure 3-1 shows the implemented simulator.

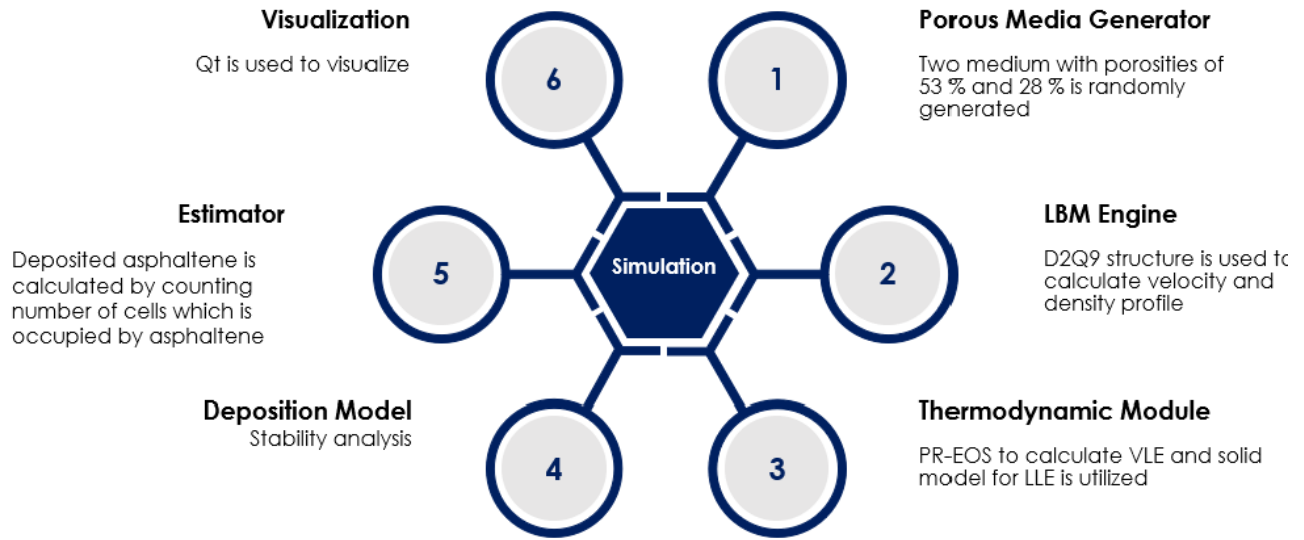


Figure 3- 1: Simulator engine

3.2.1. Porous Medium Generator

To model fluid flow and transport phenomena at the pore-scale using Lattice Boltzmann Method (LBM), a two-dimensional porous medium is needed to be generated. The first step is to set out the geometric properties, including porosity, particle or pore shape, distribution, and pore connectivity to address all the designated factors to study. In this study 2 case studies are considered which are the medium with the porosity of 53% and 28%. Geostatistical methods are used to assure that porous media samples can fairly be described at the pore-scale using mathematical models. The majority of the stochastic reconstruction algorithms are based on the threshold Gaussian field technique.

Gaussian field technique relies on the two-point correlation functions (namely the measure of porosity of a porous medium). The binary image can be represented by an indicator function, $f(r)$ as below to feed the main engine:

$$f(r) = \begin{cases} 1, & \text{if } r \text{ belongs to pore space,} \\ 0, & \text{otherwise} \end{cases} \quad (48)$$

where r denotes the spatial location within the binary image. In order to assure that the medium is randomly generated the developed program in MATLAB is used. Two clusters are enough to differentiate the pore and grain space and determining the porosity. However, in order to assure the quality and certainty of results, twenty clusters are utilized in this program.

In the next step, to have a clear quantified picture from the porous media, the data set of pore spaces are acquired to estimate the Pore Size Distribution (PSD), and Standard Deviation (SD) of the PSD.

Overall absolute permeability (K) is calculated using adjusted Carman-Kozeny equation as follows [178]:

$$K = \frac{\varphi^3}{(1-\varphi)^2} \times \frac{(SD)^2}{48} \quad (49)$$

Where φ is porosity and SD is the standard deviation for each porous medium.

- Case Study 1 ($\varphi=53\%$)

The generated pattern, pore size distribution and geometric properties are presented in Figures 3-2, 3-3 and Table 3-1. respectively. As Figure 3-2 shows, the top and bottom sides of the porous medium are impermeable solid that bounce back rule applies. The CO_2 is injected from the border on the left side and produced from the border on the right end.

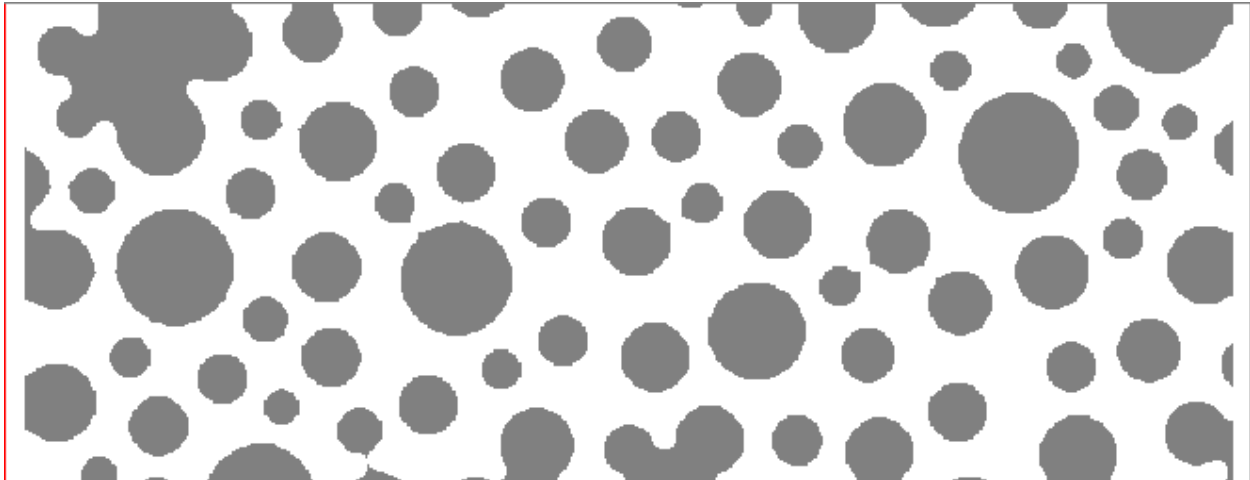


Figure 3- 2: Generated pattern and for case 1 (53% porosity)

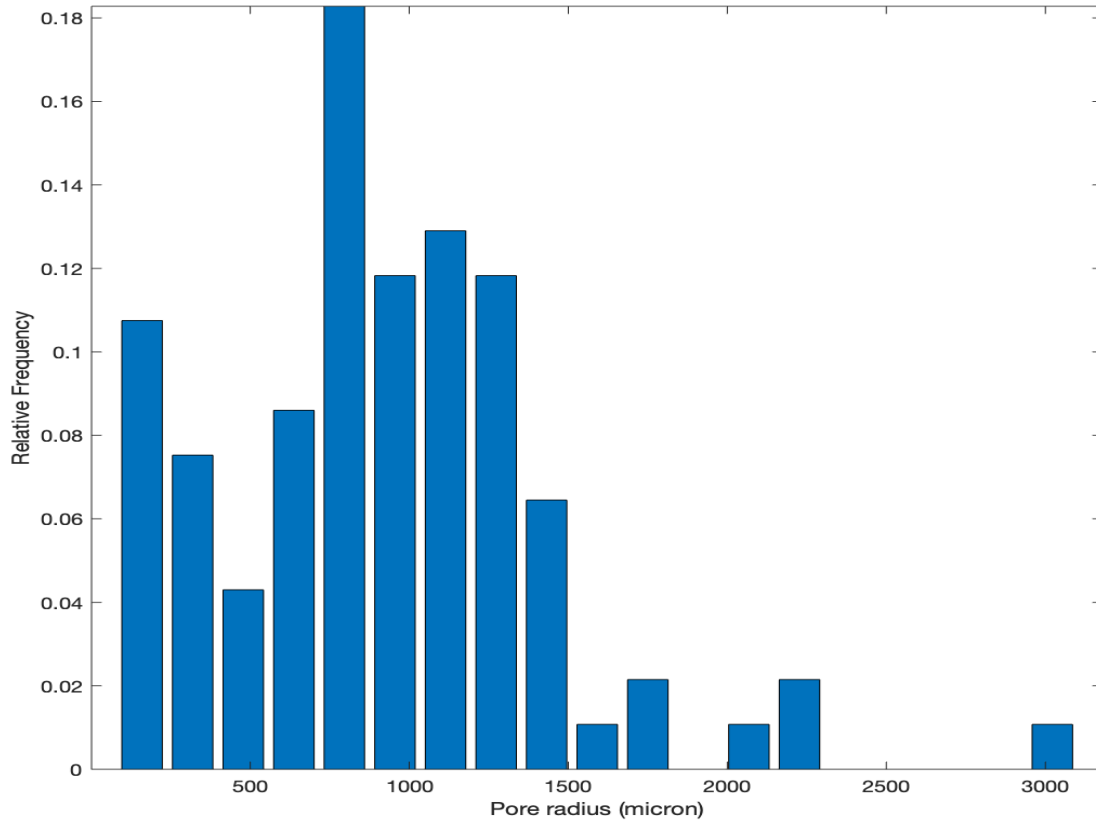


Figure 3- 3: Pore Size Distribution (PSD) for case 1 (53% porosity)

Table 3- 1: Case 1 Properties

Medium Properties	Value
Porosity	53%
Absolute Permeability	408.4 μm^2
Average Pore Radius	915.5 μm
Standard deviation of Pore Radius	523.8 μm
Width	3 cm
Length	9 cm
Pore Area	14.31 cm^2

- Case Study 2 ($\phi=28\%$)

The generated pattern, pore size distribution and geometric properties are presented in Figures 3-4, 3-5 and Table 3-2, respectively. As figure 3-4 shows, the top and bottom sides of the porous medium are impermeable solid that bounce back rule applies. The CO₂ is injected from the border on the left side and produced from the border on the right end.

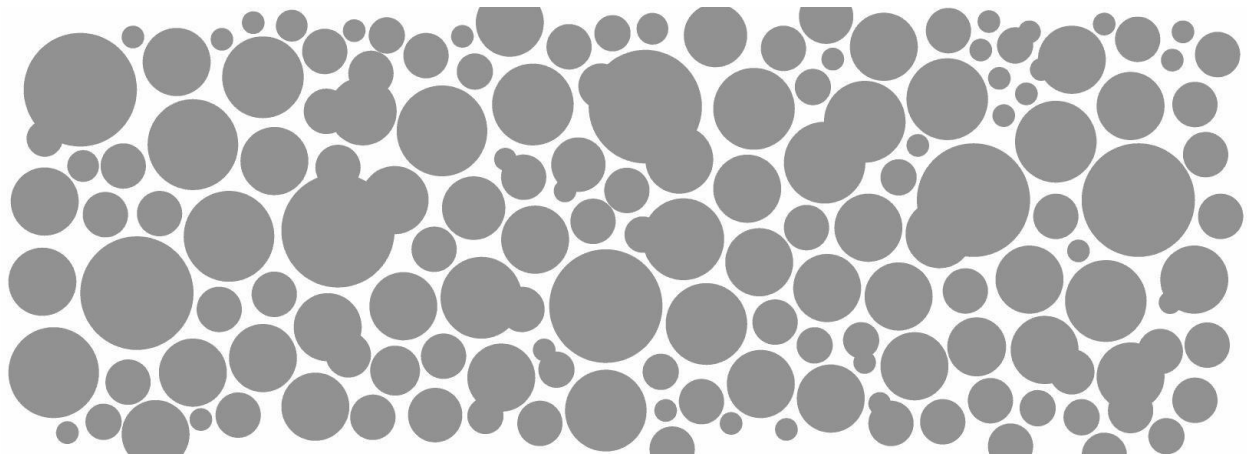


Figure 3- 4: Generated pattern and for case 2, 28% porosity

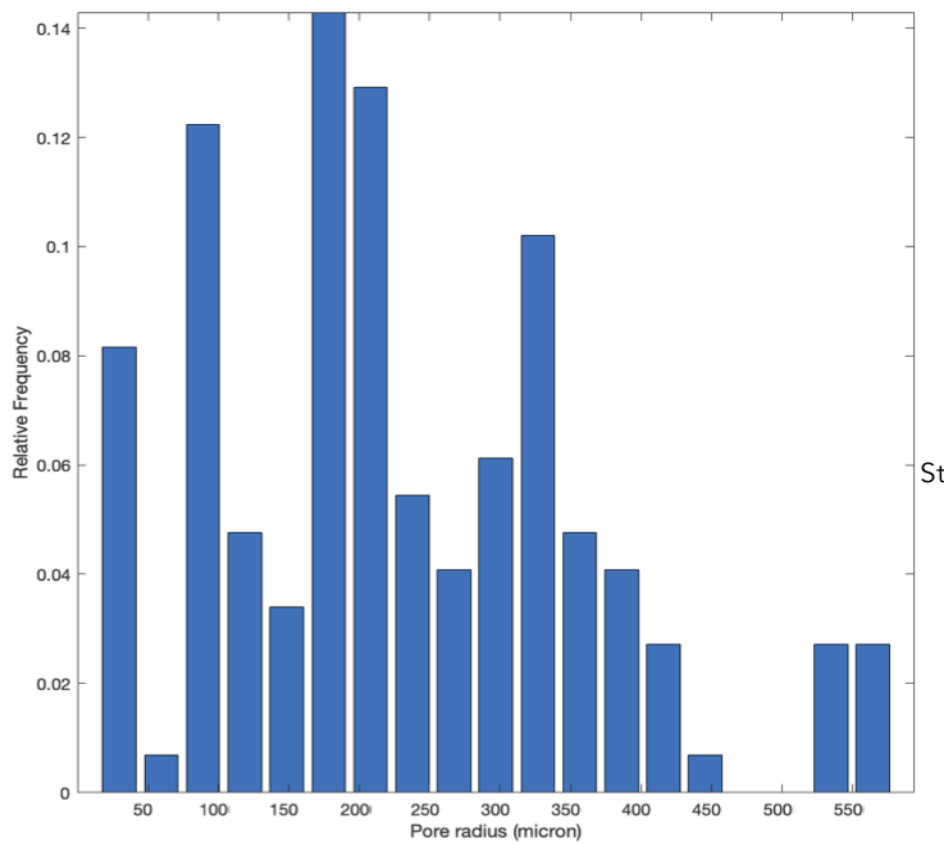


Figure 3- 5: Pore Size Distribution (PSD) for case 2 (28% porosity)

Table 3- 2: Case 2 properties

Medium Properties	Value
Porosity	28%
Absolute Permeability	$14.7 \mu\text{m}^2$
Average Pore Radius	$229.2 \mu\text{m}$
Standard deviation of Pore Radius	$129.1 \mu\text{m}$
Width	3 cm
Length	9 cm
Pore Area	7.56cm^2

When it comes to the modeling of multiphase-multi component flow through porous media using LBM, the porosity values are typically more than 50% due to several reasons such as reducing the effect of interface thickness and pore structure on simulation, reducing the computational cost and time and increasing the resolution of the medium by reducing the ratio of length scale in physical porous structure to unit length to simulated lattice structure. Consequently, the lower the porosity the harder to have a percolating system [39]. Therefore in case study 2, for a visual result, a Region Of Interest (ROI) is selected as shown in figure 3-6. The gridding of the desired ROI is provided in figure 3-7. As can be seen in figure 3-7, the cell sizes are different and depend on the neighbors' data which indicates one of the main differences between LBM and conventional numerical methods.

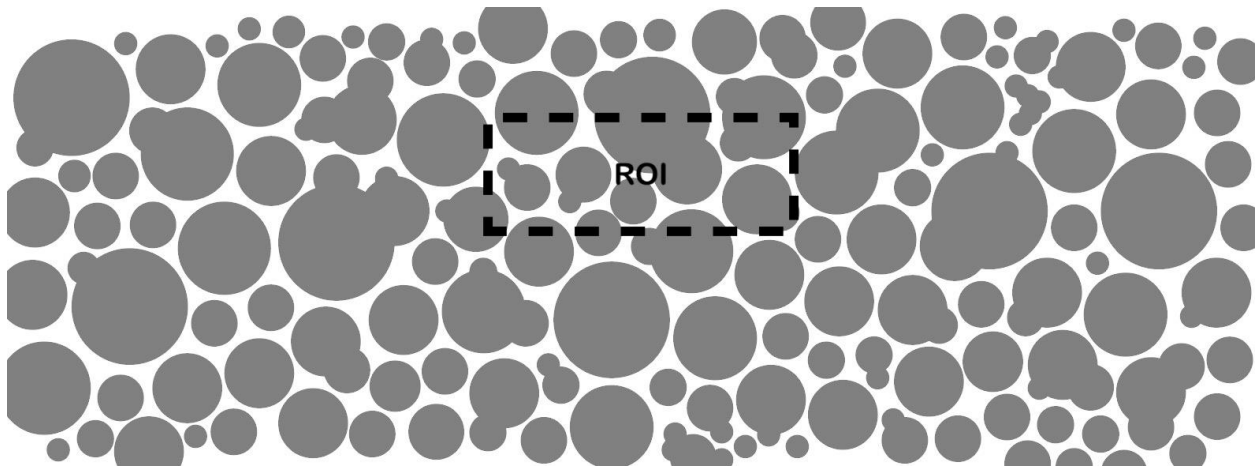


Figure 3- 6: Selected ROI for case 2

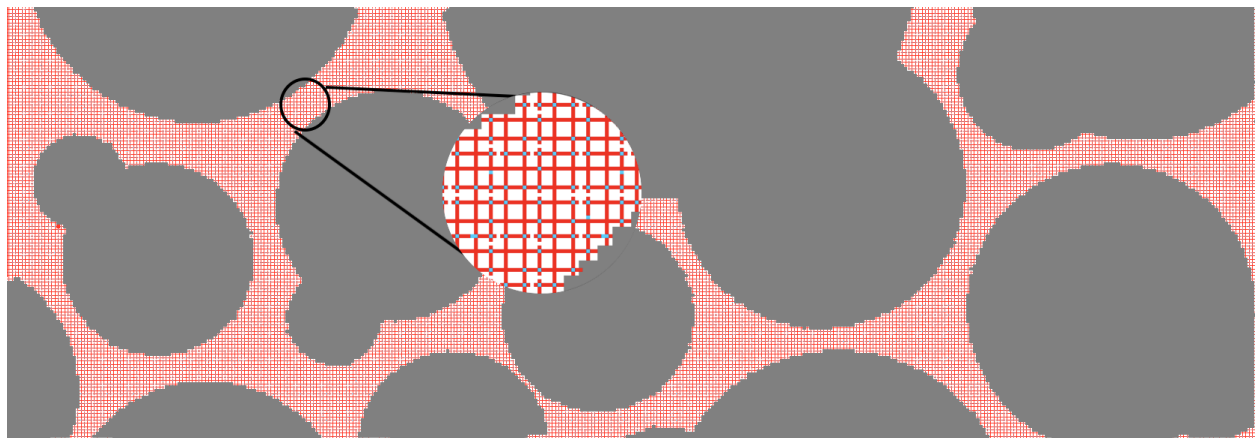


Figure 3- 7: Selected ROI's gridding

3.2.2. Fluid Characterization

The fluid characterization section refers to the chemical analysis of assumed oil that the pattern is initially fully saturated with it. In this study, the oil composition of the sample from Pembina Cardium oilfield in

Alberta, Canada [77] is utilized. The oil composition and determined properties are presented in tables 3-3 and 3-4, respectively.

Table 3- 3: Assumed oil phase composition

Components	Mole (%)
C ₃	0.2
C ₄	1.17
C ₅	3.67
C ₆	5.01
C ₇₊	89.95

Table 3- 4: Assumed oil properties

Oil Properties	Value
Temperature	27 °C
Pressure	940 <i>psi</i>
Density	849 $\frac{g}{cm^3}$
Molecular Weight	212.1 $\frac{g}{mol}$
Viscosity	5.5 <i>cP</i>

3.2.3. Lattice Boltzmann Method Module

All simulation tools can be divided into two groups of deterministic and probabilistic solvers. In deterministic methods the inputs are known and fixed on the other hand, in probabilistic methods, variables change randomly during the simulation. Conventional numerical methods such as Finite Element Method (FEM), Finite Volume Method (FVM) and Finite Difference Method (FDM) are deterministic tools which make them incapable of dealing with complex fluid dynamics. The most promising probabilistic method which has been gained great attention in the last two decades is the Lattice Boltzmann Method (LBM). The main differences of the LBM with conventional methods are programming uniformity and powerful parallelizability in the modeling of complex multi-component fluid and complex boundaries. LBM provides a good approximation to solutions of fluid dynamics problems by redefining the equation and using a parallel and efficient workflow based on the Boltzmann transport equation as follows:

$$f_i(r + dr, t + dt) - f_i(r, t) = \Omega \quad (50)$$

Here, the LBM model describes the fluid dynamics in terms of a particle distribution function $f_i(r, t)$ which denotes the fraction (probability) of fluid particles at a particular position (r) and velocity (u) and Ω is collision operator. Different LBM types for modeling multiphase flow in porous media are published in the last two decades. Gunstensen et al. [72] came up with a color model, Potential model is developed

by Shan-Chen [73], the free energy model is created by Swift et al. [74] and He et al. [75] is the developer of the incompressible-indexed model. In the current study, a multi-component multi-phase Shan-Chen type LBM model is utilized.

There are various equations available to represent the collision operator but the well-known equation is Bhatnagar-Groos-Krook (BGK). Using the BGK equation for collision operator leads to define the streaming (LHS) and collision steps (RHS) of LBM in an equation as follows:

$$f_i(r + dr, t + dt) - f_i(r, t) = \frac{f_i^{eq}(r, t) - f_i(r, t)}{\tau} \quad (51)$$

Based on the above equation, one can assume that the streaming and collision steps compute simultaneously but in the actual simulation, these two steps are computed separately. In equation 4, τ is relaxation time and can either be a constant value or a single relaxation time (SRT) function or a multiple relaxation time (MRT) function. In this study, a single relaxation time function is utilized. This assumption has some defects such as numerical instability and viscosity dependence of boundary locations, especially in under-relaxed situations, that are neglected. In equation 51, $f_i^{eq}(r, t)$ is equilibrium distribution function which can be calculated as follows:

$$f_i^{eq}(r) = w_i \rho(r) \left[1 + 3c_i \cdot u^{eq} + 9(c_i \cdot u^{eq})^2 - \frac{3u^{eq2}}{2} \right] \quad (52)$$

Where w_i are the weight factor of each surrounding points and its value depends on the selected lattice structure for the model. Lattice structures are typically shown as DmQn, where m denotes to the dimension and n expresses the number of velocity directions. D2Q9 and D3Q19 are two highly used structures in LBM. In this study, the D2Q9 model is utilized which is presented in figure 3-8. In accord with lattice structure definition, it can be concluded that after collision each particle on the site can move toward any of different available directions surrounding itself and approach to one of that configurations to get to the equilibrium state, so the weight factor of available velocity directions is as follow:

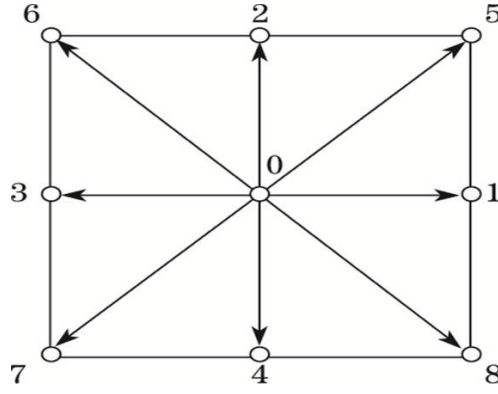


Figure 3- 8: The D2Q9 lattice structure

$$w_i = \frac{4}{9}, i = 0, \quad w_i = \frac{1}{9}, i = 1,2,3,4, \quad w_i = \frac{1}{36}, i = 5,6,7,8 \quad (53)$$

For a multi-component multiphase system (α =phase), the equilibrium velocity (u_α^{eq}) in equation (52), is formulated as follows:

$$u_\alpha^{eq} = U' + \frac{\tau_\alpha \cdot F}{\rho_\alpha} \quad (54)$$

Where F is a total force (in this study only the adsorption forces are considered) and U' is composite velocity which can be calculated using the following equations:

$$U' = \frac{\sum_\alpha \sum_{i=1}^9 \frac{f_i^\alpha \cdot e_i}{\tau_\alpha}}{\sum_\alpha \frac{\rho_\alpha}{\tau_\alpha}} \quad (55)$$

The model properties are presented in table 3-5.

Finally, after each time step, the fluid macroscopic density (ρ) and velocity (U) can be obtained as follows:

$$\rho = \sum_{i=0}^8 f_i \quad (56)$$

$$U = \frac{1}{\rho} \sum_{i=0}^8 f_i \cdot e_i \quad (57)$$

Table 3- 5: Model properties

Model Properties	Value
Relaxation time	1.25
Kinematic viscosity	0.25
G_{ads}	1.1

One of the main factors for a model to be reliable, stable and accurate is the way to apply and deal with the initial and boundary conditions. In this model, the initial condition for the distribution of fluids is a homogeneous saturation of the rock with predefined oil composition, where the saturation at each cell is fixed and determined. In this study, the full-way bounce back boundary is applied to the solid boundary and at the inlet and outlet boundaries the Zou-He velocity and pressure boundary condition is applied. The Zou-He approach is remarkably beneficial for the multi-component scenarios by replacing only unknown particle populations and increases accuracy, especially in two-dimensional models. However, the approach lacks stability for the higher injection velocities in the order of magnitude of $5 \times 10^{-5} \text{ m/s}$. In this simulation, the bounce-back condition is applied to non-equilibrium regions of the particle distributions. This approach is straightforward to implement in the two-dimensional medium.

Figure 3-9 illustrates the procedure of the main simulation engine. In this section, it is assumed that the velocity is known at the inlet, the pressure is known at the outlet, and No-slip effect on the surface of the circular posts. The main engine in the process recognizes the moment that no particles move out from the porous media, the thermodynamic status is stable, and the flow field becomes constant.

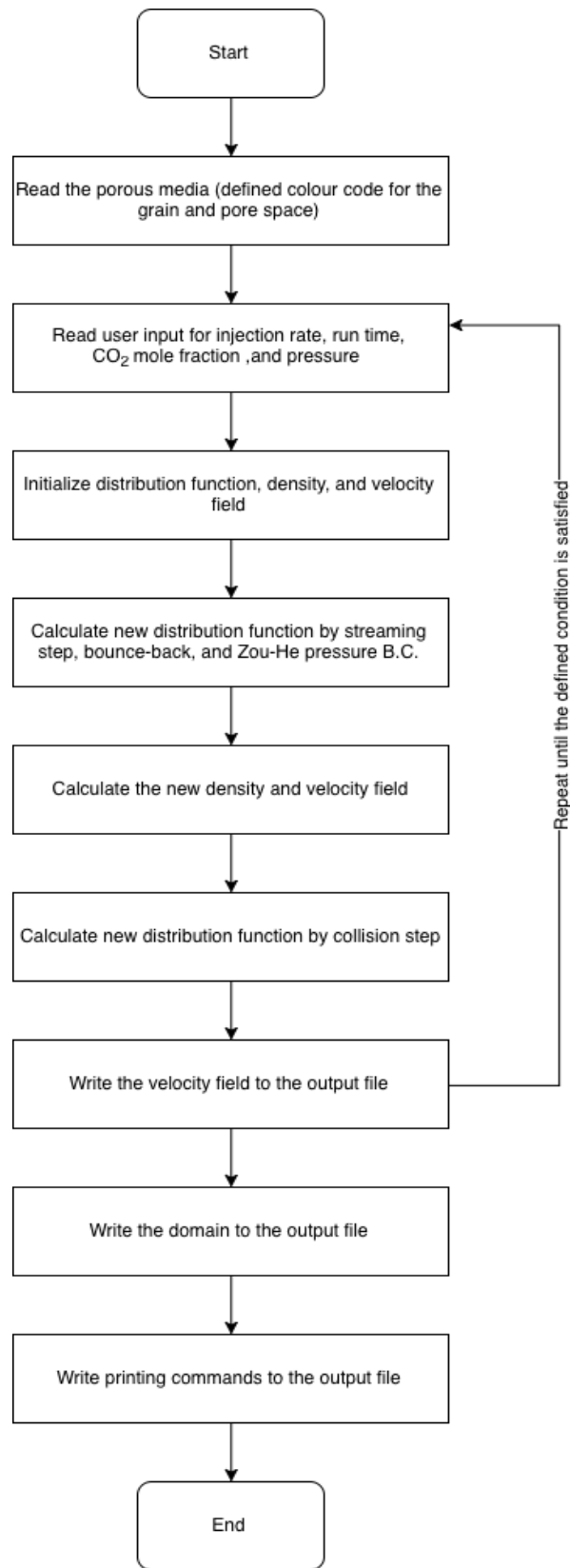


Figure 3- 9: Lattice Boltzmann Method procedure

In this simulation, different types of cells are defined which are:

Source Cell: The inlet of the simulation connected with the boundary abstraction

Open Cell: The outlet of the simulation connected with the boundary abstraction

Null Cell: Represents a cell that doesn't require any computations

Porous Cell: Represents a cell that requires all computations

Wall Cell: The cell that implements the bounce back algorithm

Single-Component Cell (SCC): Represents a cell that contains single-component

Multi-Component Cell (MCC): Represents a cell that contains multi-component

Each cell contains a particle distribution function (PDF). A PDF contains data about the statistical quantity of particles traveling at a determined point (it is a vector) and moment, at a specific direction (vector again, considering $\Delta x = e_i \Delta t$). The D2Q9 structure (nine possible directions: one null, four cardinal and four ordinal) is used and given a PDF, and it is possible to determine the macroscopic velocity (U) and density (ρ) at each point.

3.2.4. Thermodynamic Module

When a system reaches the thermodynamic equilibrium condition at a given temperature and pressure, the chemical potential of each component in all phases is equal. Due to difficulty in chemical potential measurements, the equality of fugacity of each component throughout all co-existing phases indicates the equilibrium condition. The term fugacity can be calculated using a different Equation Of States (EOS). The simplest approach for modeling asphaltene is the single component solid model.

In this study, the heaviest component represents (C_{7+}) the asphaltene. Based on Nghiem's model, the heaviest component is split into non-precipitating (C_{7+np}) and precipitating (C_{7+p}) components with the same critical properties and acentric factors and different interaction coefficients with other components.

In this study, the Peng-Robinson Equation Of State (PR-EOS) is used to construct a gas-liquid-dense liquid (asphaltene) phase equilibrium calculation model during CO_2 injection assuming instantaneous thermodynamic equilibrium within each time step. The fluid properties are calculated using the three-phase (vapor, vapor-liquid, liquid-dense) flash model. For modeling asphaltene precipitation, the conventional liquid/liquid split is used which is described with PR EOS, also the solid asphaltene is modeled with a cubic equation of the state as a liquid-dense phase. In the current model, the solid phase is assumed as a pure asphaltene (one pseudo-component). This assumption is acceptable if the asphaltene is considered as a petroleum fraction insoluble in paraffin solvents. Therefore, all precipitated under these

conditions should be considered as a single asphaltene phase. This assumption simplifies the computation requirements due to neglect of the solubility of other components in the solid phase. In this study, the in-place fluid in the porous media is multi-component oil with known compositions and properties. The thermodynamic module is built to understand the fluid-fluid interaction of the oil in place and CO₂, phase behavior, and the asphaltene precipitation model.

In this module, the fugacity of the pure solid is calculated using Nghiem's model equation as follows:

$$\ln f_s = \ln f_s^* + \frac{V_s(P - P^*)}{RT} \quad (58)$$

Where f_s is solid fugacity, f_s^* is the reference solid fugacity (the threshold), P is pressure, P^* is reference pressure, R is a gas constant coefficient, V_s is solid molar volume, and T is temperature. The fugacity equilibrium equations are solved to obtain the liquid, gas, and dense equilibrium properties. In this module, the interaction coefficients are calculated using equation (59):

$$d_{i-j} = 1 - \left(\frac{2V_{ci}^{\frac{1}{6}}V_{cj}^{\frac{1}{6}}}{V_{ci}^{\frac{1}{3}} + V_{cj}^{\frac{1}{3}}} \right)^{\gamma} \quad (59)$$

where d_{i-j} is the interaction coefficient between component i and j , V_c is the critical volume of component, and γ is an adjustable parameter assumed 0.44 that is reported to provide a good match of the saturation and onset pressure in Y. In this study, the known factors that cause, control and change the asphaltene deposition are assumed to be pressure and composition on the oil.

To add up and show the flash calculation process clearly, the procedure is summarized as below:

- Step 1: Read P and T
- Step 2: Perform stability analysis
- Step 3: Initialize the Gas-Liquid and Liquid-Dense Liquid equilibrium constant values
- Step 4: Calculate the mole fraction and composition for each component at each phase
- Step 5: Use PR-EOS to calculate the fugacities at each phase
- Step 6: Calculate asphaltene fugacity
- Step 7: Perform stability analysis
- Step 8: Show the phase(s) equilibrium

Figure 3-10 shows the stability analysis procedure in detail to determine the number and type of stable phases in equilibrium at each time step.



Figure 3- 10: The stability analysis procedure for each timestep

3.2.5. Deposition Module

- **Recovery Factor Calculation**

In order to calculate the oil recovery at each time step the following procedure has been followed:

- ✓ Considering the watershed Segmentation from the processed medium, count the number of pore block cells N_{pore}
- ✓ Count the number of MC² type block cells that are occupied with oil phase and call it N_{res} (considering the clustered shades of grey).
- ✓ Calculate the ratio of $RF = (1 - \frac{N_{res}}{N_{pore}}) \times 100$

- **Oil Relative Permeability Reduction Calculation**

Using the calculated velocity profiles (that is structured in D2Q9 model), the relative permeabilities of oil is calculated using Yiotis's model [76] as a function of the wetting phase saturation as follows:

$$Yiotis \text{ et al's model: } k_{rw} = \frac{S_w^2}{2} (3 - S_w) \quad (60)$$

The procedure is as follows:

- ✓ Calculate the viscosity ratio in each time step
- ✓ The local velocity within the wetting phase reads
- ✓ Calculate the local velocity for the non-wetting phase
- ✓ Assuming single-phase flow of the wetting phase, the flow area ($[L]^2 [T]$) of the wetting phase is calculated
- ✓ Assuming the single-phase flow of the non-wetting phase, the flow area ($[L]^2 [T]$) of the wetting phase is calculated
- ✓ The relative permeability at known saturation is calculated as a function of the wetting phase saturation from the designated equations developed by Yiotis and et al.

- **Deposited Asphaltene Calculation**

Deposited asphaltene is the area fraction (percentage) of the remained fluid in the medium that is labeled as asphaltene by thermodynamic module and it is calculated as below:

$$✓ \text{ Deposited asphaltene} = \frac{\text{Asphaltene labeled cells}}{\text{Single component cells} + \text{multi component cells} + \text{Asphaltene cells}} \times 100 \quad (61)$$

Chapter 4: Results and

Discussions

4.1. Changing Factors

As mentioned in previous sections, two case studies are considered. In case study 1, the oil recovery, relative permeability reduction, and deposited asphaltene are studied for a medium with the porosity of 53% at an injection velocity of $3 \frac{cm}{h}$. On the other hand, in case study 2, the same factors are studied for a medium with the porosity of 28% at three different injection velocities. In this way, the effect of injection velocity at fixed porosity and the effect of porosity at fixed injection velocity on the system can be reported. Table 4-1 presents the changing factors and studied responses.

Table 4- 1: Changing factors and studied responses

Factor	Studied Responses
Porosity	Oil recovery
CO ₂ injection velocity	Permeability reduction Asphaltene deposition

For case study 2, three levels of CO₂ injection velocity is wisely picked to investigate the thermodynamic and fluid-rock behavior during CO₂ injection. There are three reasons to choose CO₂ injection velocity as a changing factor which are the limited number of studies about this parameter, being very determinative factor for COA systems and when changing CO₂ injection velocity in models based on conventional numerical methods or analytical method the convergence chance is close to zero, but using LBM can overcome this issue. So studying the effect of CO₂ injection velocity on the asphaltene deposition profile is valuable. Table 4-2 exhibits the different levels of applied injection velocity.

Table 4- 2: Designated level for the injection velocity

Level	Injection velocity ($\frac{cm}{h}$)
High	3

Mid	2
Low	1

4.2. Asphaltene deposition

4.2.1. Porous medium properties effect

To study the effect of porosity on the deposited asphaltene ratio, the results of case study 1 and 2 (both at injection velocity of $3\frac{cm}{h}$) are presented in figure 4-1. As can be seen, for case 1 the interval of $0.4 < IPA < 0.6$ and for case 2 the IPA region of 0.2 to 0.4 is critical, at which, 54% and 74% of asphaltene deposition happen in mentioned regions for case 1 and 2, respectively. Also, it is clear that deposited asphaltene for case 2 is almost two times higher than case 1. In case 1, due to higher porosity, uniform pore size distribution and higher absolute permeability, the probability of asphaltene deposition decreases. On the other hand, in case 2, lower porosity and permeability and the higher number of narrower throats provides a condition for more asphaltene deposition according to the results of simulation modules. All in all, higher porosity leads to more pathways and lower particle retention time that causes less deposition, on the other hand, lower porosity and narrower pathways lead to more oil-grain contact and more friction, which consequently cause higher deposition.

Visualization results for deposited asphaltene for the whole medium of case 1 and an ROI of case 2 at the same IPA are presented in figure 4-2. As can be seen, the narrower the throat, the higher the asphaltene deposition is. The CO₂ velocity profile for both cases is shown in figure 4-3. In both cases, the CO₂ phase velocity is higher at pore centers and the closer to the pore surface, the lesser the velocity is. This statement leads to the conclusion that the asphaltene deposition is mostly produced in the near-surface area of the grain domain which is in agreement with the figure 4-2.

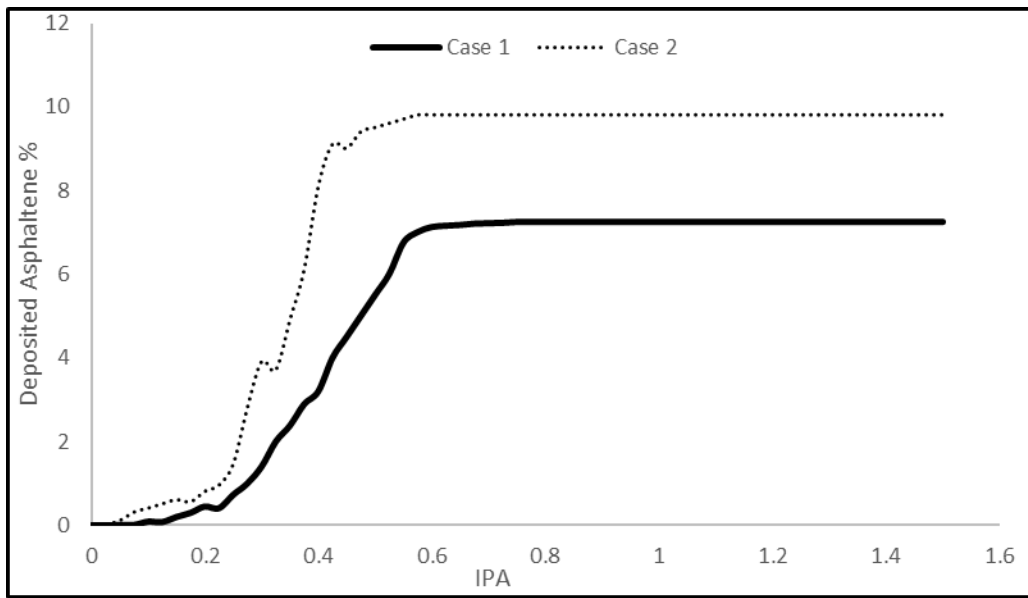


Figure 4- 1: Deposited Asphaltene in case 1 (porosity=53%) and case 2 (porosity=28%), both at the same injection velocity

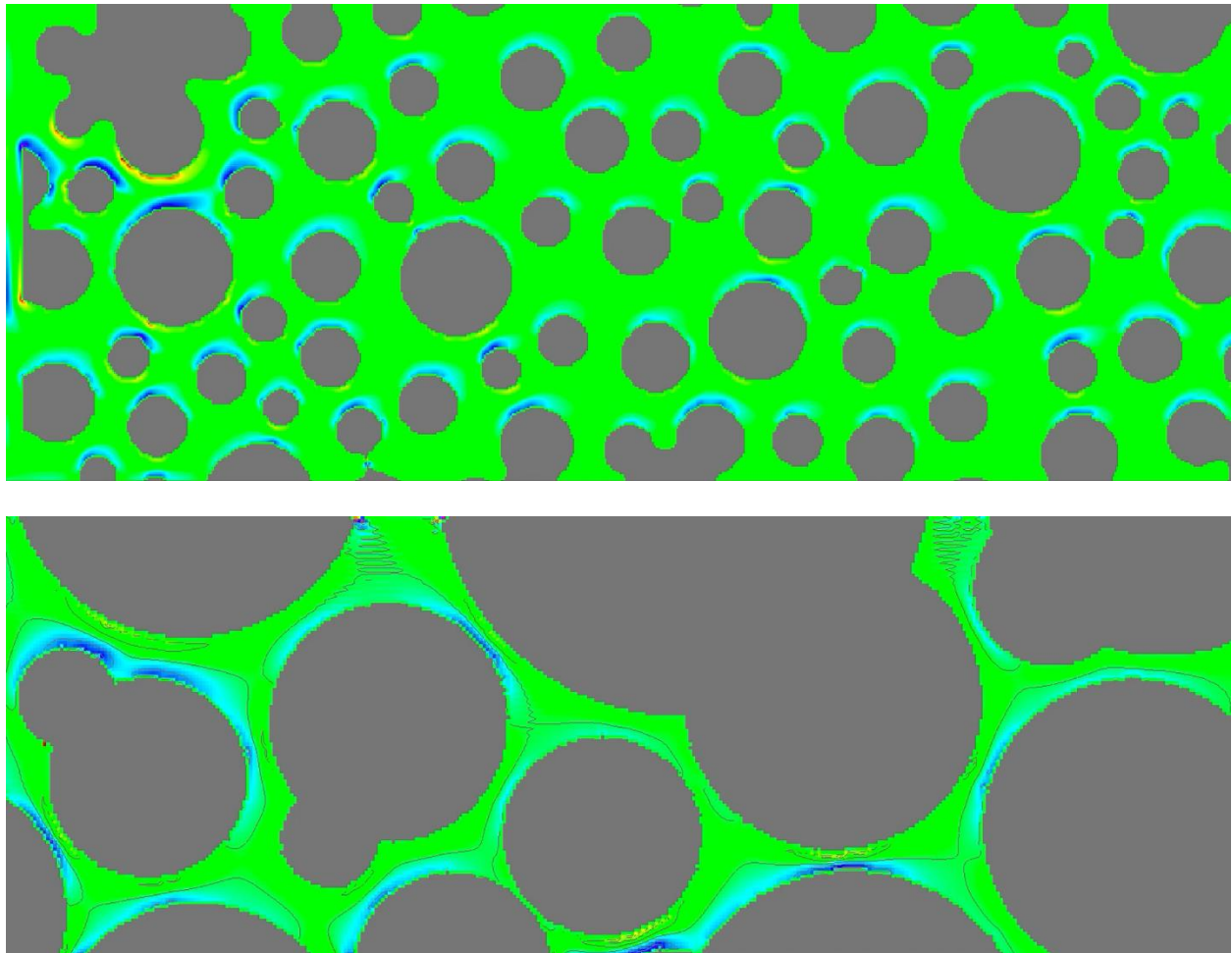


Figure 4- 2: Asphaltene deposition at 3 cm/h injection velocity and 1 IPA, case 1 (Top), ROI in case 2 (bottom), (blue is deposited asphaltene)

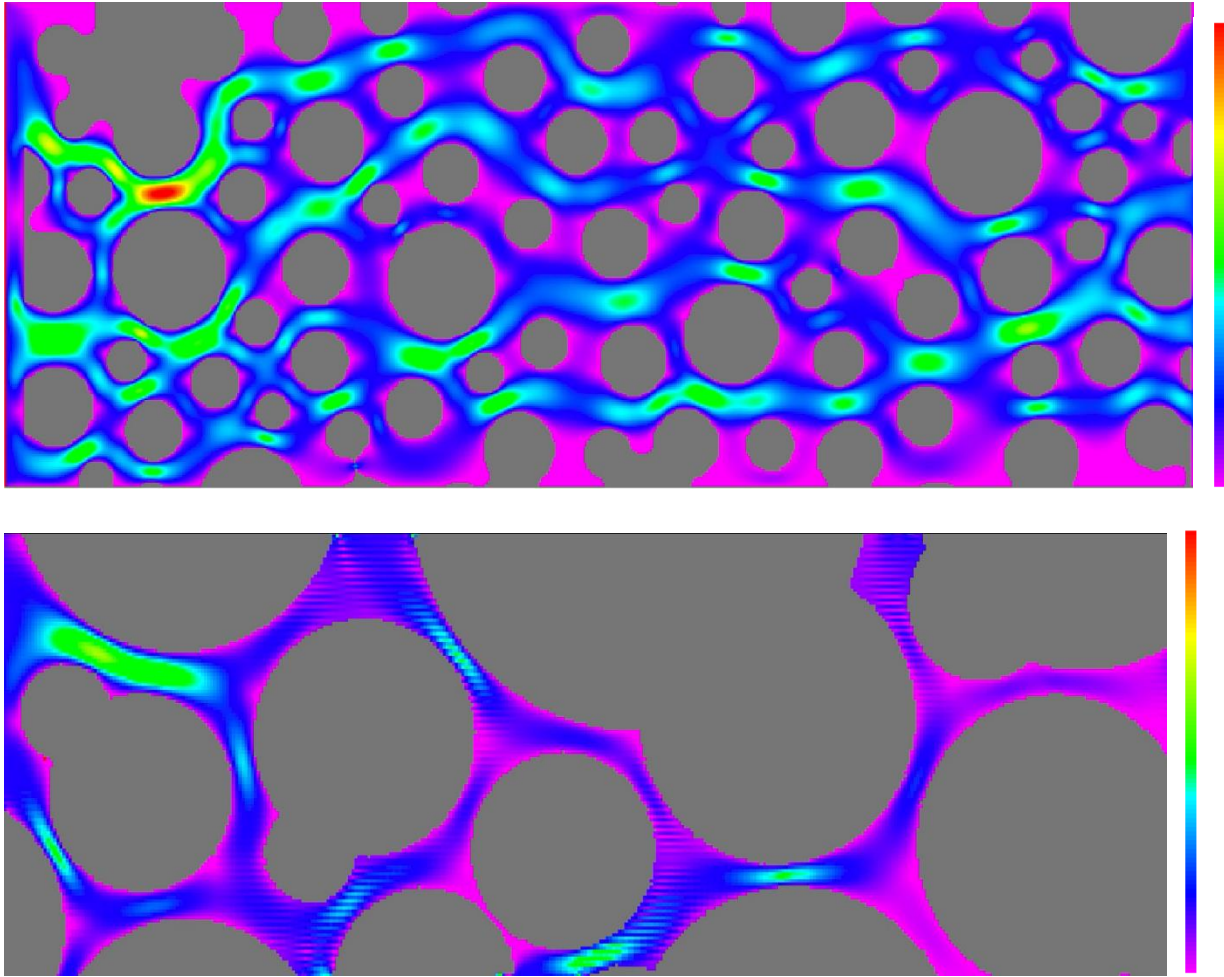


Figure 4- 3: CO₂ velocity profile at 3 cm/h injection velocity an 1 IPA. Case 1 (top), ROI of case 2 (bottom)

4.2.2. CO₂ Injection Velocity Effect

To study the effect of CO₂ injection velocity, three different injection velocities are considered for case 2. During the simulation, the measured equilibrium coefficients for fugacity calculations and interaction between the light components of the oil and CO₂ is reduced. The higher average asphaltene deposition ratio is anticipated at the higher injection velocity because the velocity vectors field impacts the phase behavior calculations and leads more particles to a dense phase in the flash calculations. When the injection velocity increases due to the higher contact time between CO₂ and oil phase, which results to phase change, higher solubility of the CO₂ into the oil phase and oil swelling. Consequently, the lighter components of the oil evaporate and asphaltene starts to precipitate, aggregate and finally deposit. Figure 4-4 illustrates the deposited asphaltene which is the fraction (percentage) of the remained fluid in the medium that is labeled as asphaltene at each IPA at different injection velocities for case 2. Results show

that the asphaltene deposition is sluggish in the beginning and increases over time. By increasing the injection velocity from $1 \frac{cm}{h}$ to $2 \frac{cm}{h}$ and $3 \frac{cm}{h}$, 3.5%, 4.9% and 9.8 % of the remained fluid in the medium are labeled as asphaltene, respectively. It is worth mentioning that, the critical region for the lowest injection velocity is $0.4 < IPA < 0.6$, at which 53% of deposition occurs in this region. On the other hand for injection velocities of $2 \frac{cm}{h}$ and $3 \frac{cm}{h}$, the region $0.2 < IPA < 0.4$ is the most substantial region at which 55% and 74% of deposition happen, respectively. In figure 4-4, the curves experience a minor decrease in some points which is attributed to the redissolution of asphaltene in to the oil phase that causes a reduction in the amount of deposited asphaltene. Furthermore, after a certain IPA (breakthrough) for each injection velocity, the curves enter a steady-state region. Figure 4-5 exhibits the pressure difference between inlet and outlet at each IPA. As can be seen, the ΔP is more for high-velocity scenario which is in agreement with the results of asphaltene deposition.

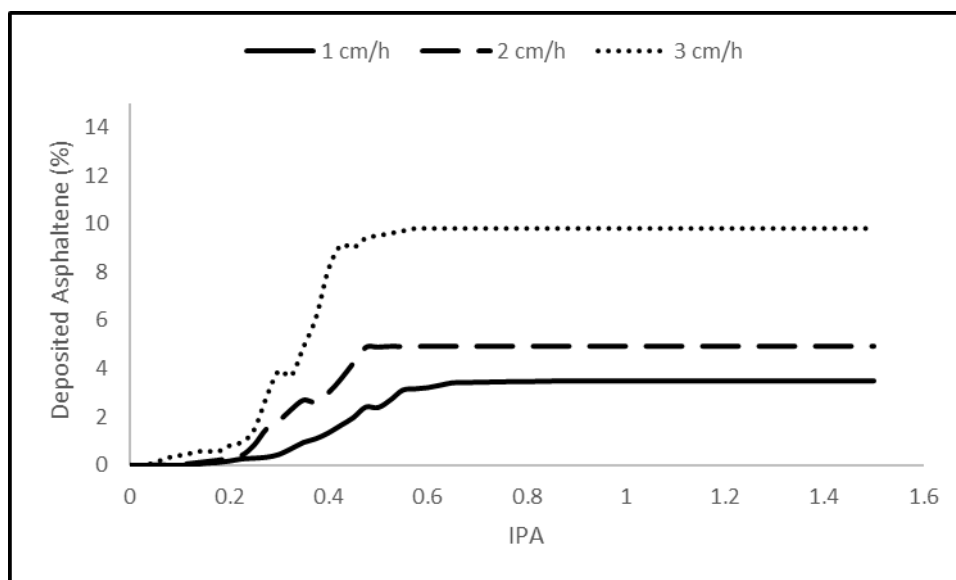


Figure 4- 4: Deposited asphaltene of different injection velocities at different IPA

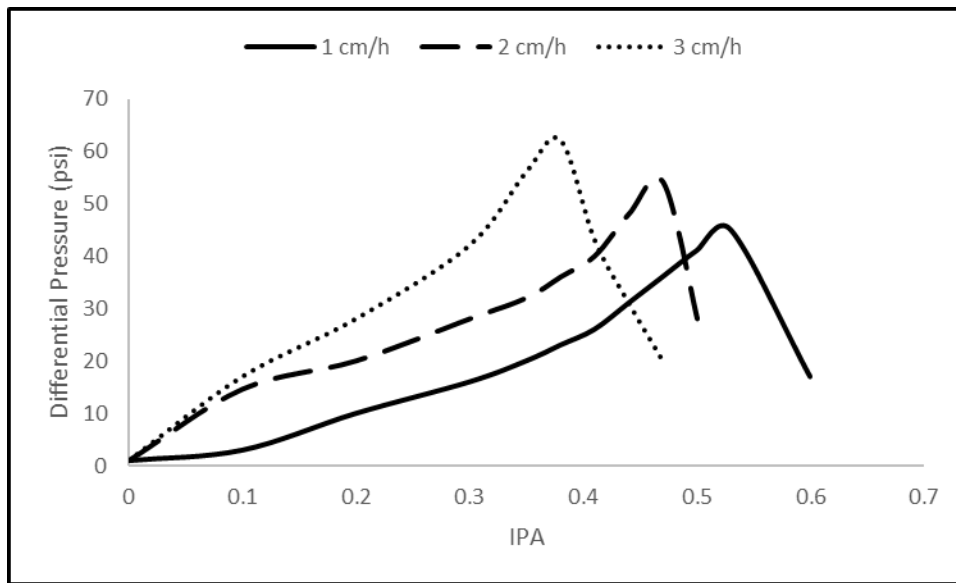


Figure 4- 5: Differential pressure from inlet and outlet at each IPA for different injection velocities

4.3. Recovery Factor

4.3.1. Porous medium properties effect

In this section, the effect of porosity on the recovery factor of case 1 and 2 are studied. As can be seen in figure 4-6, the ultimate recovery factor for case 1 is 22.5% higher than case 2. The reason for this result is in uniform pore size distribution, more porosity and pathways and finally higher permeability of case 1. Moreover, the results of asphaltene deposition show that the amount of deposited asphaltene for case 1 is less than case 2. According to figure 4-6, in the interval of $0 < IPA < 0.2$, 36% and 30% of oil are recovered for cases 1 and 2, respectively. In the next interval $0.2 < IPA < 0.4$ the oil recovery increases slightly for case 2, due to asphaltene deposition, Only 19% and 10% of oil recovery happens in this interval for cases 1 and 2, respectively. As can be seen, the recovery factor enhancement after breakthrough is very low (negligible) for both cases.

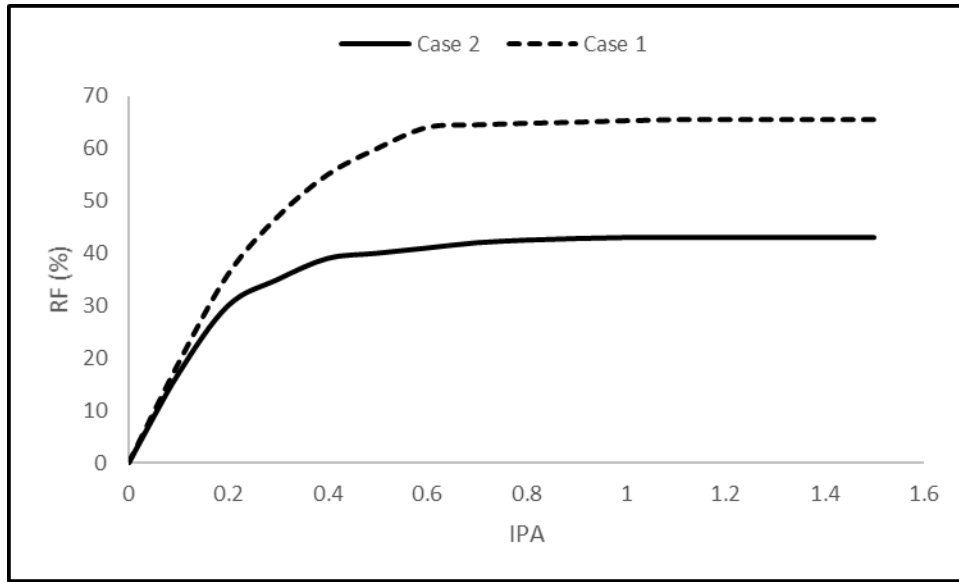


Figure 4- 6: Oil recovery of case 1 and 2 at injection velocity of 3 cm/h.

4.3.2. CO₂ Injection Velocity Effect

The immiscible CO₂ injection is aimed initially at increasing oil recovery from a porous medium. In this section along with applying the same procedure and conditions, the injection velocity is altered to investigate the effect of increasing injection velocity on the ultimate recovery factor. There are two factors that control the recovery factor which is viscosity reduction as a positive factor and permeability reduction as a negative factor. As Figure 4-7 illustrates, increasing the injection velocity from $1 \frac{cm}{h}$ to $2 \frac{cm}{h}$ and then $3 \frac{cm}{h}$ leads to recovery factor of 50.5%, 54.3 % and 43%, respectively. This outcome aligns with the findings for the relative permeability reduction and asphaltene deposition trends. In the first interval, $0 < IPA < 0.2$, the high injection velocity has the highest recovery factor. In this interval, viscosity reduction governs the region and it is more for higher injection velocity. In the second interval, $0.2 < IPA < 0.4$, the asphaltene deposition increases for the high injection velocity which lowers the recovery enhancement. Early breakthrough happens for the high injection velocity which stopped the oil recovery at the end of the second interval. On the other hand, although, the asphaltene deposition is higher and breakthrough happens earlier for mid velocity in comparison with the low velocity, but the viscosity reduction governs the recovery factor in all intervals and leads to higher mobility ratio leading to stronger fluid flow. It can be concluded that there is an optimum scenario at which leads to more recovery and less asphaltene deposition which is injection velocity of $2 \frac{cm}{h}$ in this study. The recovery factor enhancement for all injection velocities slows down after breakthrough which is due to stability of the system

Figures 4-8 is provided to show the number of particles (particle vector distribution) before and after the breakthrough at the injection velocity of $3 \frac{cm}{h}$. As can be seen, the number of particles after breakthrough reduces rigorously which visually indicates the sweep efficiency of the system. Furthermore, before a breakthrough, particles are small vectors that indicate a high vector density of each particle, on the other hand, after breakthrough vectors are bigger which shows a lower density of remained particles. Furthermore, the existence of particles verifies that the simulation is done using LBM.

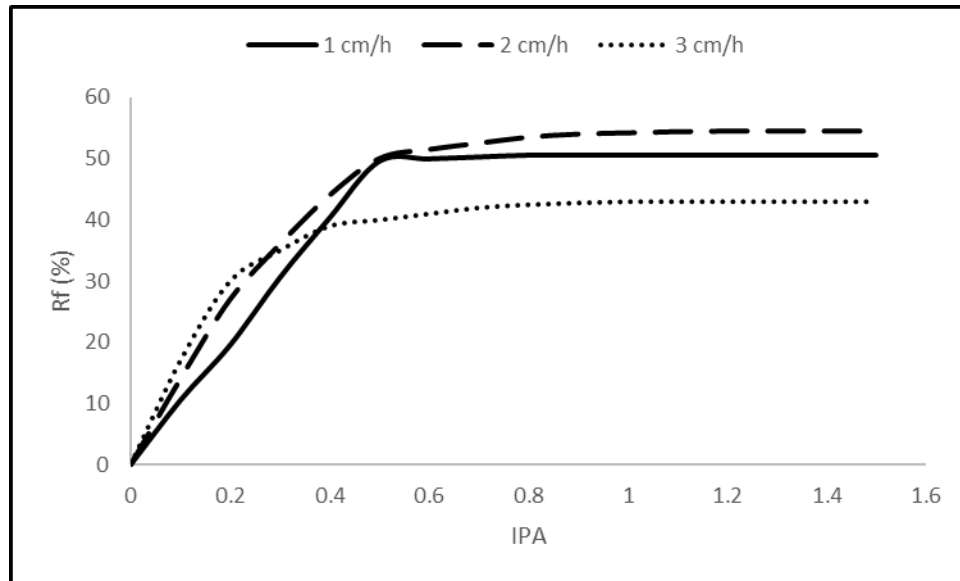
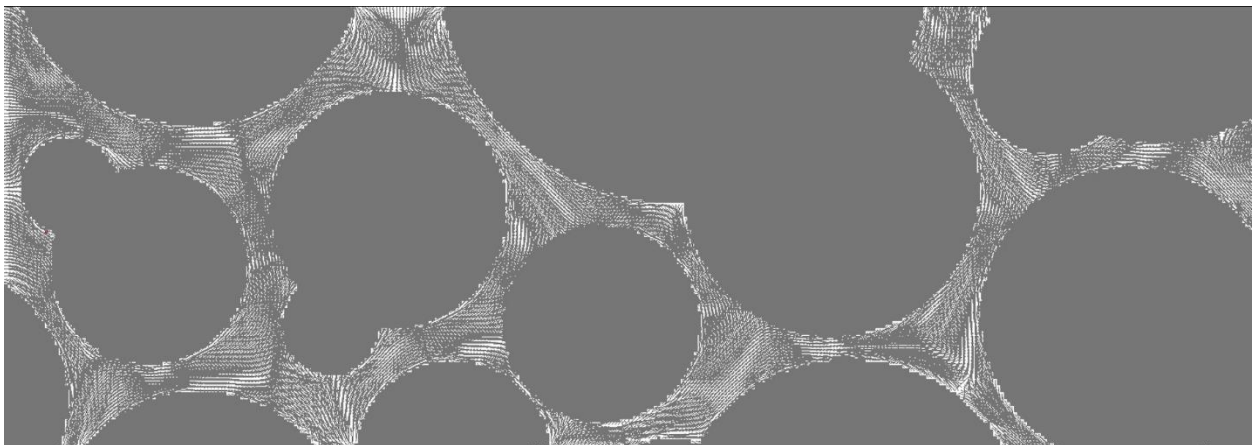


Figure 4- 7: Effect of injection velocity on oil recovery



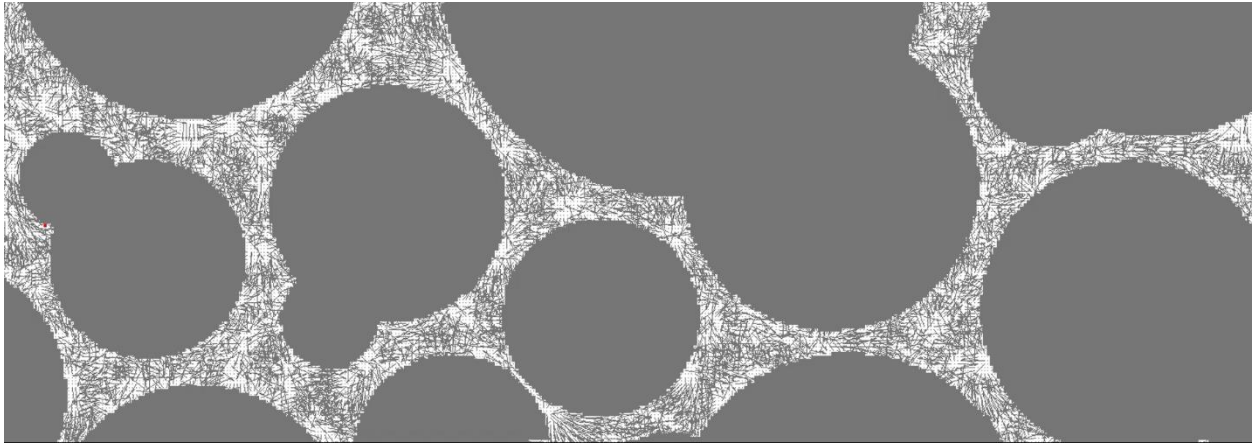


Figure 4- 8: Particles vectors distribution before breakthrough (top) and after breakthrough (bottom) for ROI

4.4. Relative Permeability Reduction

4.4.1. Porous medium properties effect

Any displacement process for sweeping oil from the pores results in an alteration of oil relative permeability. This alteration depends on the applied method and effective parameters. When immiscible CO₂ displacement takes place, oil swelling, and the interfacial tension reduction happens which lower the drag forces in the medium and push the residual oil towards the production port. Meanwhile, the variations in the thermodynamic condition (pressure in this study) and fluid properties (such as variation in composition and viscosity in this study) consequently cause a change in velocity profiles leading to a reduction in effective and relative permeability of the oil phase. Over time the porous media will be a host of different phases, which are: Oil light hydrocarbons, Oil light hydrocarbons mixed with CO₂, pure CO₂, in place original oil composition, and deposited asphaltene (heavier components). Each phase has a fraction of the relative permeability in the medium. When asphaltene deposits on the surfaces of the pores, or where the defined condition is met (following the conditions laid out in the thermodynamic module section) it lowers the pathway probability for the in-place oil that leads to a reduction in relative permeability of oil phase. So by increasing the CO₂ particles and deposited asphaltene, the share of oil in permeability decreases.

In this section, the effect of porosity on oil relative permeability is discussed. As figure 4-9 presents, the oil relative permeability is depicted using Yiotis's model. The oil relative permeability reduction in all IPA regions is more for case 1 which is attributed to the higher recovery factor in case 1. Although the asphaltene deposition is more in case 2, the higher sweep efficiency of case 1 causes a more relative permeability reduction. The calculation shows that 12.6% of the relative permeability reduction for case 2 is due to asphaltene deposition, on the other hand, this value for case 1 is 8.8%.

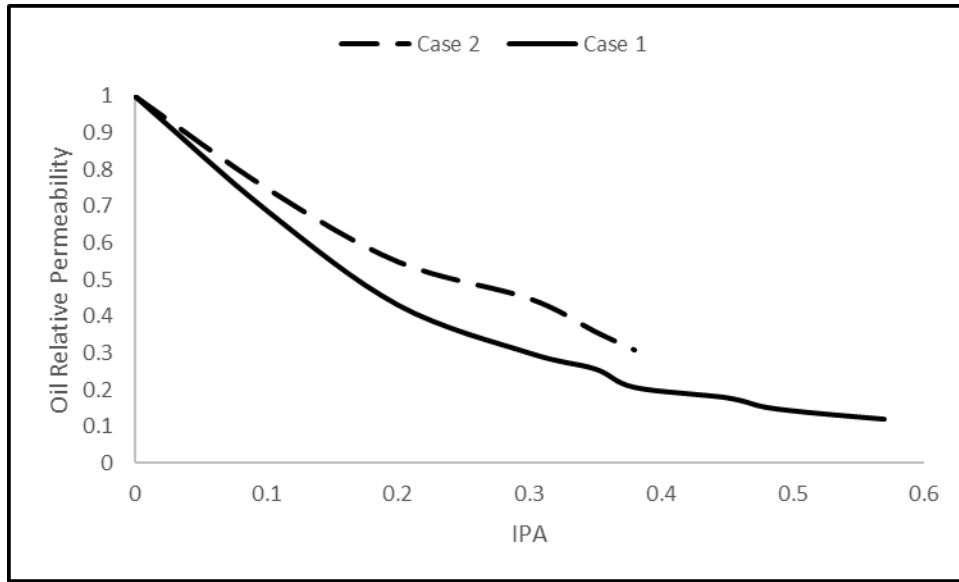


Figure 4- 9: Oil relative permeability using Yiotis's model for case 1 and case 2

4.4.2. CO₂ Injection Velocity Effect

In this section, the effect of injection velocity on the oil relative permeability is studied using Yiotis's model and all stated assumptions before. Figures 4-10 and 4-11, show the oil relative permeability and oil saturation at different IPA's, respectively. As Figure 4-10 shows, the relative permeability reduction for injection velocity of $2 \frac{cm}{h}$ and $3 \frac{cm}{h}$ are very close and higher than $1 \frac{cm}{h}$. The reason for this trend is the higher recovery factor for mid injection velocity and higher asphaltene deposition for high injection velocity. As mentioned before, the relative permeability is the function of oil saturation, at which by oil recovery, the oil saturation in the medium decreases (figure 4-11). Technically speaking, the reasons for the higher permeability reduction at the higher injection velocity is due to the effect of the increasing flow velocity on the updated distribution function in the LBM engine that is affected by the PR EOS module which is resulting in a higher amount of retained particles. On the other side, the lower flow velocity leads to more and closer particle retention that gives ample time to particles to flow along. CO₂ solubility in oil is a critical value that affects the deposition amount and oil viscosity. Another reason for oil relative permeability reduction is flow bypassing which means a higher volume of fluids goes through the same pathways which lead to dead-end zones appearance which happened to occur more in higher injection velocity. Results align with the pressure drop, asphaltene deposition and recovery factor curves. It has been noticed that more than 98% of permeability reduction occurs before breakthrough as the system is stable after breakthrough.

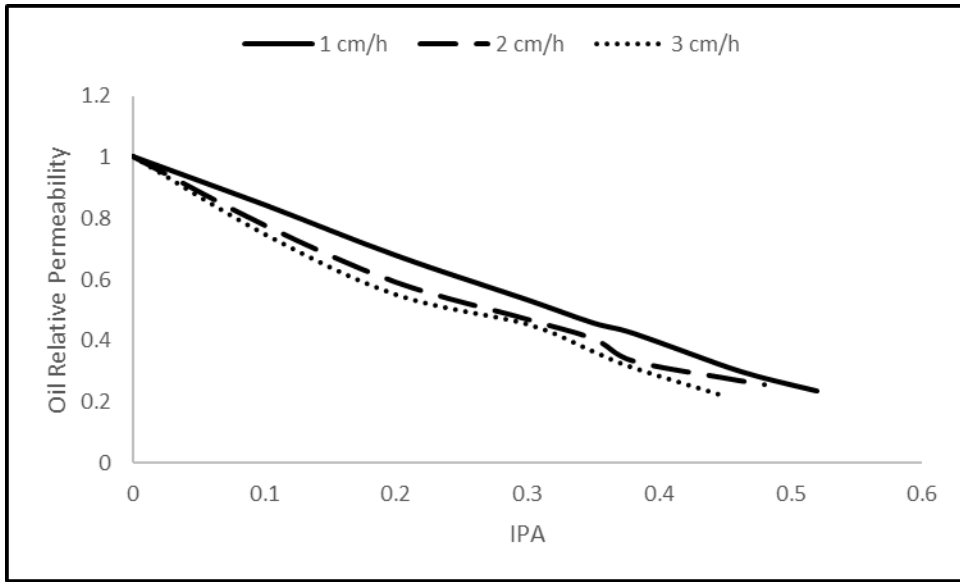


Figure 4- 10: Oil relative permeability using Yiotis’s model for different injection velocities

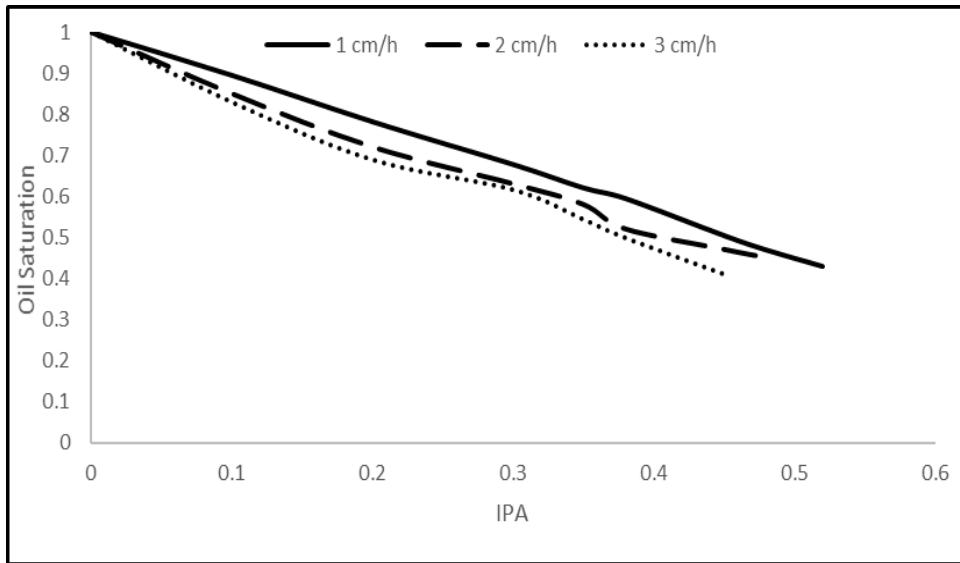


Figure 4- 11: Oil Saturation for different injection velocities

Chapter 5: Conclusion

In this study, the applicability of LBM for asphaltene deposition problems during CO₂ injection is evaluated by considering the injection velocity and porosity as a changing factors which ended with the following results:

- Asphaltene deposition is more potential in near-surface areas due to higher contact time of CO₂ with oil in that area
- Breakthrough for lower injection velocity ($1 \frac{cm}{h}$) occurs at higher IPA (0.53) and for higher injection velocity ($3 \frac{cm}{h}$) occurs at lower IPA (0.38) which is attributed to gas channeling and fingering through high permeability streaks and gas override
- Several factors cause the asphaltene deposition in this study which are pressure drop, CO₂ solubility, viscous forces (friction)
- The recovery factor is 22.5% higher at a more porous medium than the less porous medium.
- Asphaltene deposition is lower in a high porous medium which is attributed to the more uniform pore size distribution and wider throats and more pathways.
- Breakthrough happens earlier for the less porous medium due to gas channeling and fingering phenomena.
- Increasing injection velocity (from $1 \frac{cm}{h}$ to $2 \frac{cm}{h}$) increases the oil recovery from 50% to 55%, further increase in injection velocity ($3 \frac{cm}{h}$) decreases the oil recovery to 43%. It can be concluded that there is an optimum scenario which leads to higher recovery factor and lower asphaltene deposition which is injection velocity of $2 \frac{cm}{h}$ in this study.
- Two elements are dominant in recovery factor analysis, viscosity reduction (positive factor) and oil relative permeability reduction (negative factor), for mid injection velocity, the viscosity reduction dominates
- Asphaltene deposition is 100% and 270% more in $3 \frac{cm}{h}$, in comparison with $2 \frac{cm}{h}$ and $1 \frac{cm}{h}$, respectively.
- Although pressure drop was higher at high injection velocity, but early breakthrough and high asphaltene deposition led to less recovery factor.

- The novelty in this study is added visualization output integrated with the cell level calculation of the parameters and improved parallelizability of the applied methodology
- Defining different modules for the main simulator engine increased the possibility of the model convergence due to parallelable skills of LBM and the capability of LBM in handling the heterogeneous porous medium with complex boundaries is seen

References

- [1] Yarranton H. Asphaltene deposition. SPE; 2000.
- [2] Seifried C M. Asphaltene precipitation and deposition from crude oil with CO₂ and hydrocarbons: experimental investigation and numerical simulation. Ph.D. Thesis; 2016.
- [3] Alboudwarej H, Svrcek W, Yarranton H, Akbarzadeh K. Asphaltene characterization: sensitivity of asphaltene properties to extraction techniques. SPE; 2001.
- [4] Green D W, Willhite G P. Enhanced oil recovery. SPE Richardson TX; 2003.
- [5] Donaldson E C, Chilingarian G V, Yen T F. Enhanced oil recovery, processes, and operations. Elsevier; 1989.
- [6] Nobakht M, Moghadam S, Gu Y. Mutual interactions between crude oil and CO₂ under different pressures. Fluid Phase Equilibria 2008; 265: 94–103.
- [7] Ewing R E. Simulation of multiphase flows in porous media. Transport in Porous media 1991; 6(5):479-499.
- [8] Blazek J. Computational fluid dynamics: Principles and Applications. Elsevier; 2001.
- [9] Wu Y S, Qin G. A generalized numerical approach for modeling multiphase flow and transport in fractured porous media. Communications In Computational Physics 2009; 6: 85-108.
- [10] Leontaritis K J, Mansoori A G. Asphaltene deposition: a survey of field experiences and research approaches. Journal of Petroleum Science and Engineering 1988; 1 (3): 229-239.
- [11] Lin J M. Cell Analysis on Microfluidics. Book 2018.
- [12] Saha A A, Mitra S K . Microfluidics and nanofluidics handbook: chemistry, physics, and life science principles 2012.
- [13] Diallo M S, Cagin T, Faulon J L, Goddard, W A. Thermodynamic Properties of Asphaltenes, A Predictive Approach Based on Computer Assisted Structure Elucidation and Atomistic Simulation, Asphalts and Asphaltenes II, Development in Petroleum Science. 2000.
- [14] Rogel E, Carbognani L. Density Estimation of Asphaltenes Using Molecular Dynamics Simulations. Caracas, Venezuela, Energy & Fuels 2003; 17: 378 – 386.
- [15] API RP 40. Recommended Practices for Core Analysis; 1998.

- [16] Speight J G, Yen T F, Chilingarian G V. *Asphaltenes and asphalts*. Elsevier Science; 1994.
- [17] Santos R G, Loh W, Bannwart A C, Trevisan O V. *An overview of heavy oil properties and its recovery and transportation methods*. SPE Brazil; 2012.
- [18] Speight A G. *The Chemistry and Technology of Petroleum*; 1999.
- [19] Kelland M A. *Production Chemicals for the Oil and Gas Industry*. CRC press 2014.
- [20] Society of Petroleum Evaluation Engineers. *Canadian Oil and Gas Evaluation Handbook*; 2002.
- [21] Yarranton H W, Masliyah J H. Molar mass distribution and solubility modeling of asphaltenes. *AIChE Journal* 1996; 42: 3533-3543.
- [22] Gholoum E F, Oskui G P, Salman M. Investigation of asphaltene precipitation onset conditions for Kuwaiti reservoirs. *SPE* 2003.
- [23] Sadeqimoqadam M, Firoozinia H, Kharrat R, Ghazanfari M H. The Impact of CO₂ Injection and Pressure Changes on Asphaltene Molecular Weight Distribution in a Heavy Crude Oil: An Experimental Study. *Petroleum Science and Technology* 2010; 28:1728–1739.
- [24] Joshi N B, Mullins O C, Jamaluddin A K M, Creek J. Asphaltene Precipitation from Live Crude Oil. *Energy & Fuels* 2001;15: 979-986.
- [25] Buckley J S, Wang J. Crude oil and asphaltene characterization for prediction of wetting alteration. *Petroleum Science and Engineering* 2002; 33:195– 202.
- [26] Ikiensikimama S S, Ogboja O. Evaluation of empirically derived oil viscosity correlations for the Niger Delta crude. *Petroleum Science and Engineering*; 2009.
- [27] Beal C. Viscosity of air, water, natural gas, crude oil and its associated gases at oil-field temperatures and pressures. *Trans. AIME* 1946; 165:94-115.
- [28] Beggs H D, Robinson J R. Estimating the viscosity of crude oil systems. *Pet. Technol* 1975; 27 (9), 1140-1141.
- [29] Labedi R. Improved correlations for predicting the viscosity of light crudes. *Pet. Sci. Eng* 1992; 8 (3), 221-234.
- [30] ECLIPSE Technical Description. *The Asphaltene Option*. 2009; 89 – 102.
- [31] Hildebrand J H. Intermolecular forces in liquids. *Phys Rev* 1929; 34: 984.
- [32] Morrow N R. Wettability and Its Effect on Oil Recovery. *J Pet Technol* 1990; 42 (12): 1476-1484.
- [33] Hildebrand J H, Carter J M. A study of van der waals forces between tetrahalide Molecules. *Am Chem Soc* 1932; 54: 3592.

- [34] Williams L L, Rubin J B, Edwards H W. Calculation of Hansen solubility parameter values for a range of pressure and temperature conditions including supercritical fluid region. *Ind Eng Chem Res* 2004; 43: 4967-4972.
- [35] Allada S R. Solubility parameters of supercritical fluids. *Industrial & Engineering Chemistry Process Design and Development* 1984; 23(2): 344–348.
- [36] Hirschberg A, deJong L N J, Schipper B A, Meijer J G. Influence of Temperature and Pressure on Asphaltene Flocculation. *SPE* 1984; 24: 283- 293.
- [37] Kord Sh, Miri R, Ayatollahi Sh, Escrochi M. Asphaltene Deposition in Carbonate Rocks: Experimental Investigation and Numerical Simulation. *Energy Fuels*, 2012; 26 (10): 6186–6199.
- [38] Mungan N. Carbon dioxide flooding - fundamentals In *Heavy Crude Oil Recovery*. Springer 1984;131–176.
- [39] Mahmoudi S, Mohammadzadeh O, Hashemi A, Kord S. Pore-scale numerical modeling of relative permeability curves for CO₂–oil fluid system with an application in immiscible CO₂ flooding. *Petrol Explor Prod Technol* 2017; 7:235–249.
- [40] Zendehboudi S, Shafiei A, Bahadori A, James L, Elkamel A, Lohi A. Asphaltene precipitation and deposition in oil reservoirs- technical aspects, experimental and hybrid neural network predictive tool. *Chemical Engineering Research and Design*; 2013.
- [41] Sayyad Amin J, Nikkhah S, Zendehboudi S. A new experimental and modeling strategy to determine asphaltene precipitation in crude oil. *chemical engineering research and design* 2017; 128: 162–173.
- [42] Monger T G, Fu J C. The nature of CO₂-induced organic deposition. *SPE* 1987.
- [43] Srivastava R K, Huang S S, Dong M. Asphaltene Deposition During CO₂ Flooding. *SPE*; 1999.
- [44] Gonzalez D L, Ting P D, Hirasaki G J, Chapma W G. Prediction of Asphaltene Instability under Gas Injection with the PC-SAFT Equation of State†. *Energy & Fuels* 2005; 19 (4): 1230-1234.
- [45] Burke N E, Hobbs R E, Kashou S F. Measurement and modeling of asphaltene precipitation. *JPT, Journal of Petroleum Technology* 1990; 42: 1440- 1446.
- [46] Leontaritis K J. The asphaltene and wax deposition envelopes. *Fuel Science and Technology International* 1996; 14: 13–39.
- [47] Hu Y F, Guo T M. Effect of temperature and molecular weight of nalkane precipitants on asphaltene precipitation. *Fluid Phase Equilibria* 2001. 192:13–25.
- [48] Thomas F B, Bennion D B, Bennion D W, Hunter B E. Experimental And Theoretical Studies Of Solids Precipitation From Reservoir Fluid. *Journal of Canadian Petroleum Technology* 1992; 31.

- [49] Cao M, Gu Y. Temperature effects on the phase behaviour, mutual interactions and oil recovery of a light crude oil–CO₂ system. *Fluid Phase Equilibria* 2013; 356: 78– 89.
- [50] Mohammadi S, Rashidi F, Ghazanfari M H, Mousavi-Dehghani S A. Kinetics of asphaltene aggregation phenomena in live oils. *Molecular Liquids* 2016; 222: 359–369.
- [51] Wang Z, Xu J, Liu H, Hou J, Zhang Y. Effect of pressure, Temperature, and mass fraction of CO₂ on the stability of the asphaltene constituents in crude oil. *Petroleum Science and Technology* 2017; 35:2109-2114.
- [52] Zekri A Y, Shedid S A, Almehaideb R A. An experimental investigation of interactions between supercritical CO₂, asphaltenic crude oil, and reservoir brine in carbonate cores. *SPE* 2007.
- [53] Mansoori G A. Modeling of asphaltene and other heavy organic depositions. *J. Pet. Sci. & Eng.* 1997; 17:101–111.
- [54] Gharbi Kh, Benyounes Kh, Khodja M. Removal and prevention of asphaltene deposition during oil production: A literature review. *Petroleum Science and Engineering* 2017; 158: 351–360.
- [55] Leontaritis K J, Amaefule J O, Charles R E. A systematic approach for the prevention and treatment of formation damage caused by asphaltene deposition. *SPE* 1994; 157–164.
- [56] Collins S H, Melrose J C. Adsorption of Asphaltenes and Water on Reservoir Rock Minerals. *SPE* 1983.
- [57] Clementz D M. Alteration of Rock Properties by Adsorption of Petroleum Heavy Ends: Implications for Enhanced Oil Recovery. *SPE* 1982.
- [58] Li Z, Firoozabadi A. Cubic-plus-association equation of state for asphaltene precipitation in live oils. *Energy & Fuels* 2010; 24 (5): 2956-2963.
- [59] Crocker M E, Marchin L M. Wettability and Adsorption Characteristics of Crude-Oil Asphaltene and Polar Fractions. *J Pet Technol* 1988; 40: 470-474.
- [60] Huang E T S, Holm L W. Effect of WAG Injection and Rock Wettability on Oil Recovery During CO₂ Flooding. *SPE* 1988; 3 (1): 119-129.
- [61] Al-Maamari R S H, Buckley J S. Asphaltene Precipitation and Alteration of Wetting: Can Wettability Change during Oil Production. *SPE/DOE, Tulsa*.
- [62] Blauch M, Weaver J, Parker M, Todd B. New Insights into Proppant- Pack Damage Due to Infiltration of Formation Fines. *SPE* 1999.
- [63] Lu T, Li Z, Fan W, Zhang X, Lv Q. Nanoparticles for Inhibition of Asphaltenes Deposition during CO₂ Flooding. *Ind Eng Chem Res* 2016; 55: 6723–6733.

- [64] Civan F. A Multi-Phase Mud Filtrate Invasion and Well Bore Filter Cake Formation Model. SPE 1994.
- [65] Civan F. Modeling and Simulation of Formation Damage by Organic Deposition. Proceedings of the First International Symposium on Colloid Chemistry in Oil Production: Asphaltene and Wax Deposition 1995.
- [66] Civan F. Reservoir Formation Damage-Fundamentals, Modeling, Assessment, and Mitigation. Gulf Publish Company 2000.
- [67] Ju B, Fan T, Jiang Z. Modeling asphaltene precipitation and flow behavior in the processes of CO₂ flood for enhanced oil recovery. Petroleum Science and Engineering 2013; 109: 144–154.
- [68] Nasrabadi H, Moortgat, Firoozabad A. New Three-Phase Multicomponent Compositional Model for Asphaltene Precipitation during CO₂ Injection Using CPA-EOS. American Chemical Society; 2016.
- [69] Alay A, Xiaodong L, Nicolas V S, Georgios K. Prediction of Gas Injection Effect on Asphaltene Precipitation Onset Using the Cubic and Cubic-Plus-Association Equations of State. Energy and Fuels, 31(3): 3313-3328.
- [70] Sanchez N L, Repsol Y. A general approach for asphaltene modelling. SPE; 2007.
- [71] Ali M A, Islam M R. The Effect of Asphaltene precipitation on Carbonate Rock Permeability: An Experimental and Numerical Approach. SPE Production & Facilities 1998; 13(3): 178-183.
- [72] Gunstensen A K, Rothman D. Lattice Boltzmann model of immiscible fluids. Phys 1991; A43: 4320–4327.
- [73] Shan X, Chen H. Lattice Boltzmann model for simulating flows with multiple phases and components, Phys 1993; 47 (3): 1815–1819.
- [74] Swift M R, Osborn W R, Yeomans J M. Lattice Boltzmann simulation of nonideal fluids, Phys. Rev. Lett. 1995; 75 (5): 830–833.
- [75] He X, Luo L Sh. Lattice Boltzmann Model for the Incompressible Navier-Stokes Equation. Statistical Physics 1997.
- [76] Yiotis, Andreas, Psihogios, John, Kainourgiakis, M, Papaioannou, Aggelos, K. Stubos, thanassios. (2007). A lattice Boltzmann study of viscous coupling effects in immiscible two-phase flow in porous media. Colloids and Surfaces A: Physicochemical and Engineering Aspects.
- [77] Costa A. permeability-porosity relationship: the re-examination of the Kozeny-Carman equation based on a fractal pore-space geometry assumption. American geophysical union. 2005.

- [78] Cruz A A, Amarala M, Santosa D, Palmab A, Franceschia E, Borgesa G R, Coutinhob J A P, Palácioc J, Darivaa C. CO₂ influence on asphaltene precipitation. *The Journal of Supercritical Fluids* 2019;143: 24–31.
- [79] ASTM. Standard test method for determining stability and compatibility of heavy fuel oils and crude oils by heavy fuel oil stability analyzer (optical detection). ASTM D-7112.. West Conshohocken: ASTM International; 2012.
- [80] Victorov A I, Firoozabadi A. Thermodynamic micellization model of asphaltene precipitation from petroleum fluids. *AIChE Journal* 1996; 42 (6): 1753-1764.
- [81] Tavakkoli M, Masihi M, Kharrat R, Ghazanfari M H. Thermodynamic model of asphaltene precipitation for heavy crude: a comparative study of thermodynamic micellization and solid model. *CIPC*; 2009.
- [82] Zhao-xia D, Jun W, Gang L, Mei-qin L, Ming-yuan L. Experimental study on asphaltene precipitation induced by CO₂. *Pet.Sci* 2014;11:174-180.
- [83] Behbahani T J, Ghotbi C, Taghikhani V, Shahrabadi A. Experimental investigation and thermodynamic modeling of asphaltene precipitation. *Scientia Iranica* 2011; 18 (6): 1384-1390.
- [84] Gruesbeck C, Collins R E. Entrainment and Deposition of Fine Particles in Porous Media. *SPE* 1982.
- [85] Wojtanowicz A K, Krilov Z, Langlinais J P. Experimental Determination of Formation Damage Pore Blocking Mechanisms. *Energy Resources Technology* 1988; 110: 34-42.
- [86] Muhammad M, McFadden J, BHPbillition, Creek J. Asphaltene precipitation from reservoir fluids: asphaltene solubility and particle size vs pressure. *SPE*; 2003.
- [87] Wojtanowicz A K, Krilov Z, Langlinais J P. Study on the Effect of Pore Blocking Mechanisms on Formation Damage. *SPE* 1988
- [88] Pang S, Sharma M M. A Model for Injectivity Decline in Water-Injection Wells. *SPE* 1997.
- [89] Ring J N, Wattenbarger R A. Simulation of Paraffin Deposition in Reservoirs. *SPE* 1992.
- [90] Wang S, Civan F. Modeling Formation Damage by Asphaltene Deposition during Primary Oil Recovery. *Journal of Energy Resources Technology* 2005; 127(4): 310-317.
- [91] Riveros L, Jaimes B, Ranaudo M A, Castillo J, Chirinos J. Determination of Asphaltene and Resin Content in Venezuelan Crude Oils by Using Fluorescence Spectroscopy and Partial Least Squares Regression. *Energy & Fuels* 2006; 20: 227-230.
- [92] Aske N, Kallevik H, Johnsen E E, Sjøblom J. Asphaltene Aggregation from Crude Oils and Model Systems Studied by High-Pressure NIR Spectroscopy. *Energy & Fuels* 2002; 16: 1287-1295.

- [93] Tavakkoli M, He P, Lin P H, Rezaee S, Puerto M, Doherty R, Creek J, Wang J, Kusinski G, Gomes J, Chapman W, Biswal S L, Vargas F M. Asphaltene deposition and fouling in reservoirs. Offshore Technology Conference; 2017.
- [94] Tahami S A, Dabir B, Asghari K, Shahvaranfard A. Modeling of asphaltene deposition during miscible CO₂ flooding. *Pet Sci Technol* 2014; 32: 2183–2194.
- [95] Yang Z, Ma C F, Lin X S, Yang J T, Guo T M. Experimental and modeling studies on the asphaltene precipitation in degassed and gas-injected reservoir oils. *Fluid Phase Equilibria* 1999; 157: 143–158.
- [96] Zanganeh P, Ayatollahi Sh, Alamdari A, Zolghadr A, Dashti H, Kord Sh. Asphaltene Deposition during CO₂ Injection and Pressure Depletion: A Visual Study. *Energy Fuels* 2012; 26: 1412–1419.
- [97] Wang S. Simulation of Asphaltene Deposition in Petroleum Reservoirs During Primary Oil Recovery. Ph. D. Dissertation, The University of Oklahoma 2000.
- [98] Iwere F O, Apaydin O G, Moreno J E, Schlumberger, Ventura R L, Garcia J L, Penox E& P. Simulation of asphaltene precipitation inn fractured reservoirs, a case study. SPE; 2002.
- [99] Khomehchi E, Behvandi R, Rashidi F. Prediction of Bubble Point Pressure & Asphaltene Onset Pressure During CO₂ Injection Using ANN & ANFIS Models. *Petroleum Science and Technology* 2011; 1(2): 35-45.
- [100] Al-Qasim A S. Simulation of Asphaltene Deposition During CO₂ Flooding. Thesis; 2011.
- [101] Vafaie-Sefti M, Mousavi-Dehghani S A. Application of association theory to the prediction of asphaltene deposition: Deposition due to natural depletion and miscible gas injection processes in petroleum reservoirs. *Fluid Phase Equilibria* 2006; 247: 182–189.
- [102] Bagherzadeh H, Rashtchian D, Ghazanfari M H, Kharrat R. A Core Scale investigation of Asphaltene Precipitation during Simultaneous Injection of Oil and CO₂: An Experimental and Simulation Study. *Energy Sources, Part A*, 2014; 36:1077–1092.
- [103] Coelho R, Hascakir B. The Pore Scale Description of Carbon Dioxide Storage into High Asphaltene Content Reservoirs. Carbon Management Technology Conference; 2015.
- [104] Liou M F. A Numerical Study of Transport Phenomena in Porous Media. Thesis Submitted in partial fulfillment of the requirements For the degree of Doctor of Philosophy, Department of Mechanical and Aerospace Engineering Case Western Reserve University August; 2005.
- [105] Okabe H, Takahashi S, Mitsuishi H. distribution of asphaltene deposition in the rock samples by gas injection. SPE; 2010.
- [106] Mirzabozorg A, Bagheri M B, Kharrat R, Abedi J, Ghotbi C. Simulation study of permeability impairment due to asphaltene deposition in one of Iranian oil fractured reservoirs. CIPC; 2009.

- [107] Lei H, Pingping Sh, Ying J, Jigen Y, Shi L, Aifang B. Prediction of asphaltene precipitation during CO₂ injection. *Petrol. Explor. Develop* 2010; 37(3): 349–353.
- [108] Shirani B, Nikazar M, Mousavi-Dehghani S A. Prediction of asphaltene phase behavior in live oil with CPA equation of state. *Fuel* 2012; 97 (0): 89-96.
- [109] Fayers F J, Foakes A P , Lin C Y. An Improved Three Phase Flow Model Incorporating Compositional Variance. Presented at the SPE/DOE Improved Oil Recovery Symposium. SPE; 2000.
- [110] Mohammed S, Mansoori G A. Effect of CO₂ on the Interfacial and Transport Properties of Water/Binary and Asphaltenic Oils: Insights from Molecular Dynamics. *Energy Fuels* 2018; 32: 5409–5417.
- [111] Afif M, Amaziane B. Numerical simulation of two-phase flow through heterogeneous porous media. *J. Numerical Algorithms* 2003; 34: 117–125.
- [112] Shaw D C, Dawe R A. Averaging Methods for Numerical Simulations of Flows Through Heterogeneous Porous Media', *J. Transport in Porous Media* 1987; 2: 241-267.
- [113] Cuvelier C, Seigal A, van Steenhoven A. Finite element methods and Navier-Stokes equations. *Mathematics and its applications series*, D. Reidel Publishing co; 1986.
- [114] He X, Ren L. A modified multiscale finite element method for well-driven flow problems in heterogeneous porous media', *J. Hydrology* 2006; 329: 674– 684.
- [115] Ma L, Ingham D B, Wen X. A finite volume method for fluid flow in polar cylindrical grids. *j. numer. meth. fluids* 1998; 28: 663–677.
- [116] Deponti A, Pennati V, Biase L D. A fully 3D finite volume method for incompressible Navier–Stokes equations. *J. Numer. Meth. Fluids* 2006; 52:617–638.
- [117] Huber R, Helmig R. Multiphase flow in heterogeneous porous media: A classical finite element method versus IMPES-Based mixed finite element- finite volume approach. *J. Numer. Meth. Fluids* 1999; 29: 899–920.
- [118] Xiong Q, Baychev T G, Jivkov A P. Review of pore network modelling of porous media: experimental characterisations, network constructions and applications to reactive transport. *J. Contaminant Hydrology* 2016; 192: 101–117.
- [119] Mattila K, Hyvaluoma J, Rossi T, Aspнас M, Westerholm J. An efficient swap algorithm for the lattice Boltzmann method, *Computer Physics Communications* 2007; 176 (3): 200–210.
- [120] Succi S. *The lattice boltzmann equation for fluid dynamics and beyond*. Clarendon Press Oxford; 2001.

- [121] Won K W. Continuous Thermodynamics for Solid-Liquid Equilibria: Wax Formation From Heavy Hydrocarbon Mixtures. In A.I.Ch. E. Spring National Meeting, Session 1A, Houston, Texas; 1986.
- [122] Cimino R, Corraera S, Sacomani P A, Carnniani C. In Thermodynamic Modelling for Prediction of Asphaltene Deposition in Live Oils, SPE 28993, Presented at SPE International Symposium on Oilfield Chemistry, 14-17 February, San Antonio, TX; 1995.
- [123] de Boer R B, Leerlooyer K, Eigner M R P, Van Bergen A R D. Screening of Crude Oils for Asphalt Precipitation: Theory, Practice, and the Selection of Inhibitors. SPE 1995; 10: 55-61.
- [124] Novosad Z, Costain T G. Experimental and Modeling Studies of Asphaltene Equilibria for a Reservoir Under CO₂ Injection. In SPE Annual Technical Conference and Exhibition, Society of Petroleum Engineers: New Orleans, Louisiana; 1990.
- [125] Nor-Azlan N, Adewumi M A. Development of Asphaltene Phase Equilibria Predictive Model. In SPE Eastern Regional Meeting, Pittsburgh, Pennsylvania; 1993.
- [126] Rassamdana H, Dabir B, Nematy M, Farhani M, Sahimi M. Asphalt flocculation and deposition: I. The onset of precipitation. AIChE Journal 1996; 42:10-22.
- [127] Mansoori G A, Jiang T S. In Asphaltene Deposition and its Role in Enhanced Oil Recovery Miscible Gas Flooding, Third European Conference on Enhanced Oil Recovery, Rome; 1985.
- [128] Kawanaka S, Park S J, Mansoori G A. Organic Deposition From Reservoir Fluids: A Thermodynamic Predictive Technique. SPE Journal 1991; 6: 185 - 192.
- [129] Nghiem L X, Hassam M S, Nutakki R, George A E D. Efficient Modelling of Asphaltene Precipitation. In SPE Annual Technical Conference and Exhibition,; Society of Petroleum Engineers: Houston, Texas; 1993.
- [130] Lindeloff N, Heidemann R A, Andersen S I., Stenby E H. A thermodynamic mixed-solid asphaltene precipitation model. Petroleum Science and Technology 1998; 16: 307-321.
- [131] Kohse B F, Nghiem L X, Maeda H, Ohno K. Modelling Phase Behaviour Including the Effect of Pressure and Temperature on Asphaltene Precipitation. In SPE Asia Pacific Oil and Gas Conference and Exhibition, 16-18 October; Society of Petroleum Engineers: Brisbane, Australia; 2000.
- [132] Panuganti S R, Vargas F M, Gonzalez D L, Kurup A S, Chapman W G. PC-SAFT characterization of crude oils and modeling of asphaltene phase behavior. Fuel 2012; 93: 658-669.
- [133] Du J L, Zhang D. A Thermodynamic Model for the Prediction of Asphaltene Precipitation. Petroleum Science and Technology 2004; 22 (7-8): 1023-1033.

- [134] Sabbagh O, Akbarzadeh K, Badamchi-Zadeh A, Svrcek W Y, Yarranton H W. Applying the PR-EoS to Asphaltene Precipitation from n-Alkane Diluted Heavy Oils and Bitumens. *Energy & Fuels* 2006; 20 (2): 625-634.
- [135] Wertheim M S. Thermodynamic perturbation theory of polymerization. *The Journal of Chemical Physics* 1987; 87 (12): 7323-7331.
- [136] Chapman W G, Jackson G, Gubbins K E. Phase equilibria of associating fluids. *Molecular Physics* 1988; 65 (5): 1057-1079.
- [137] Ting P D, Gonzalez D, Hirasaki G, Chapman W. Application of the PCSAFT Equation of State to Asphaltene Phase Behavior. In *Asphaltenes, Heavy Oils, and Petroleomics*, Springer New York 2007; 301-327.
- [138] Kraska T, Gubbins K E. Phase Equilibria Calculations with a Modified SAFT Equation of State. 1. Pure Alkanes, Alkanols, and Water. *Industrial & Engineering Chemistry Research* 1996; 35 (12): 4727-4737.
- [139] Huang S H, Radosz M. Equation of state for small, large, polydisperse, and associating molecules. *Industrial & Engineering Chemistry Research* 1990; 29 (11): 2284-2294.
- [140] Gil-Villegas A, Galindo A, Whitehead P J, Mills S J, Jackson G, Burgess A N. Statistical associating fluid theory for chain molecules with attractive potentials of variable range. *The Journal of Chemical Physics* 1997; 106 (10): 4168-4186.
- [141] Gross J, Sadowski G. Perturbed-Chain SAFT: An Equation of State Based on a Perturbation Theory for Chain Molecules. *Industrial & Engineering Chemistry Research* 2001; 40 (4): 1244-1260.
- [142] Mohebbinia S, Sepehrnoori K, Korrani A K N, Johns R T. Simulation of asphaltene precipitation during gas injection using PC-SAFT EOS. *SPE*; 2014.
- [143] Punnapala S, Vargas F M. Revisiting the PC-SAFT characterization procedure for an improved asphaltene precipitation prediction. *Fuel* 2013; 108 (0): 417-429.
- [144] Zúñiga-Hinojosa M A, Justo-García D N, Aquino-Olivos M A, Román-Ramírez L A, García-Sánchez F. Modeling of asphaltene precipitation from n-alkane diluted heavy oils and bitumens using the PC-SAFT equation of state. *Fluid Phase Equilibria* 2014; 376 (0): 210-224.
- [145] Subramanian S, Simon S, Sjöblom J. Asphaltene Precipitation Models: A Review. *Dispersion Science and Technology*; 2015.
- [146] Li Z, Firoozabad A. Modeling Asphaltene Precipitation by n-Alkanes from Heavy Oils and Bitumens Using Cubic-Plus-Association Equation of State. *Energy & Fuels* 2010; 24 (2): 1106-1113.

